2MASS STUDY OF CANDIDATE PRECURSORS TO UCHII REGIONS





A thesis submitted in partial fulfilment of the final requirement for the degree of

Masters in Astronomy

at

Departamento de Matemática Aplicada, Faculdade da Ciências, Universidade do Porto, Portugal.

Candidate Name: Eoin Clerkin

Supervisor: M.S. Nanda Kumar

Abstract

There has been two major efforts in the past 7 years to study UCHII regions (Molinari et al. 1996; Sridharan et al., 2002). They compiled a list of 217 best candidates of the precursors to UCHII regions. We conducted a near IR study into these sources using the 2MASS all sky survey. A method of Nyquist bining stellar counts around these sources revealed the presence of embedded clusters in at least 63 (30%) of the sample. More than 50 of these were previously unknown groupings, 29 are classified as large clusters, 18 as small and the rest as stellar groups. This technique of detection provided stellar density contour maps which allowed us to discuss the morphology of the groupings. We estimated that the ratio of Hierarchical type to central condensed type cluster (H/C = 0.9 \approx 1) which possibly implies both a basic unity of gravity and turbulence but also maybe the decay of the turbulence with time. The positions of the candidate (pre) UCHII regions show a striking preference for the very centre of the clusters.

We statistically calculate the number of cluster members detectable by the 2MASS telescope, and we extend this estimate and the mass to almost the deuterium burning limit with the use of an universal IMF from Muench et al. (2002). We observe a correlation between the relative age of the (pre) UCHII regions and the number of members in the clusters. With the use of cc-diagrams, we obtained the average dust extinction and we discussed the colours of massive protostars. The mass of the dust cloud was available for 15 clusters from Beuther et al. (2002) and so, we estimated the local star formation efficiency.

Contents

1	Intr	oduction	4
	1.1	Precursors to UCHII Regions	4
	1.2	Sample Selection	5
	1.3	2MASS Data	15
		1.3.1 Point Source Catalogue (PSC)	15
		1.3.2 Extended Source Catalogue(XSC)	16
		1.3.3 Comment	17
2	Clu	sters	18
	2.1	Detection of Groups/Clusters	20
	2.2	Data Retrieval and Processing	21
	2.3	Nyquist Sampling and Detection	22
	2.4		26
3	Fur	ther Classification of the Clusters	30
	3.1	The Morphologies of our Stellar Groups	30
	3.2	The Area of the Stellar Groups	33
	3.3	Number of Members	36
4	IR	Colour Analysis on the Cluster sources	4 6
	4.1	Color-Color Diagrams	47
		4.1.1 cc-diagrams of the 63 groupings of stars	49
		4.1.2 A Measurement of the Dust Extinction	57
		4.1.3 The Colours of Massive Protostars	60
	4.2	Color-Magnitude Diagrams	62
5	KL	F, IMF and Mass Estimation	7 6
	5.1	The Initial Mass Function	76
	5.2	The K-Luminosity Function	78
	5.3	Mass Estimation	86
6	Sun	mary & Conclusions	93
Bi	blios	raphy	98

List of Tables

	Candidate precursors to UCHII regions (Sridharan et al. sources)	13
2.1 2.2	Number of stellar cluster detections per source	23 24
3.1 3.2	Total area in pc^2 and morphology of the embedded clusters Richness measure, number estimate and stellar density	35 38
4.1	Measurements of visible and K-band extinction	58
5.1 5.2	Mass estimation	87 89
.i.c1	t of Figures	
2.1	Background count and distance effect on source on detection technique .	26
2.1 2.2	Background count and distance effect on source on detection technique . Dust extinction effect on number of stars observed	27
2.1	Background count and distance effect on source on detection technique .	
2.1 2.2 3.1	Background count and distance effect on source on detection technique . Dust extinction effect on number of stars observed	27 34

Candidate precursors to UCHII regions (Molarini et al. H-type sources)

Candidate precursors to UCHII regions (Molarini et al. L-type sources)

9

11

Chapter 1

Introduction

1.1 Precursors to UCHII Regions

The main processes for the formation of low mass stars is relatively well known. Shu and Adams (1987) summed up these into four principal stages, (i) the formation of slowly rotating cloud cores through the slow leakage of magnetic support, (ii) the dramatic collapse from inside-out, (iii) the bipolar outflow phase where outflows break out from the rotational poles of the stellar object and slowly spreads over all 4π steradians, and (iv) the T-tauri star with a surrounding nebular disk. It was first pointed out by Herbig (1962) and later Mezger and Smith (1977) that more massive stars form using separate mechanisms. A notion which became known as bimodal star formation.

Due to added complexities, the stellar confusion and the crapped nature of massive star forming regions, low mass stars were favoured in studies in early years. Observations of high mass star forming regions have proved very difficult for many reasons. For example higher mass stars are much fewer in number and form 10 times faster, typically 10⁵ years in molecular clouds that are more distant than that of their low mass counterparts. In addition, the definition of a protostar dilutes somewhat for stars over $2M_{\odot}$ as the luminosity of the matter accretting onto it becomes comparable to that of the contracting protostellar core and they also do not have an optically visible pre-main-sequence phase (Palla & Stahler, 1993). Massive protostars dominate their surroundings like no low mass star and shortly after their formation they rip to shreads and diffuse their parental molecular cloud, effectively putting a stop to local star formation. As massive protostars are short-lived, they are likely to trace the spiral structure of the galaxy, they inject large amounts of energy and momentum into the ISM and thus effect its evolution significantly. Thus, knowledge of their formation is very important to many different areas and related subjects of Astronomy and still many questions to how a massive protostar forms needs to be answered.

One of the main problems for a massive protostar forming along similar lines to that of low mass stars is that the radiative pressure from the protostar is sufficient to halt and reverse the infall of the gas. Other theories exist, which circumvent this, such as that by Bonnell, Bate & Zinnecker (1998) which suggests that massive protostars may be formed by accretion-induced collisions of low mass members within the very densest

parts of the embedded clusters. Therefore it is important and has been a quest by many to find and observe a massive protostar in its earliest stages of formation. One of the earliest confirmed stages is that of the ultra-compact HII region (UCHII) where intense UV fluxes from the protostar ionises the surrounding gas.

It remains however to find an isolated young stellar object (YSO) in its earliest stage that where the protostar is still in an active stage of the accretion process. Some authors such as Ceseroni et al., (1994, 1997), Shepherd et al., (1998) and Hunter et al., (1998) discovered oddities around existing UCHII regions which showed up in mm observations similar to UCHII regions but hadn't at cm wavelengths. Since HII regions are detectable at radio wavelengths, these are believed by many to be YSO at the end of an active stages of accretion just prior to the development of the UCHII region, but their worth for study is limited as their close proximity to a UCHII region means their properties are confused and contaminated. So this question to find an isolated YSO in an active phase of accretion remains open, but it has been somewhat simplified to the finding of a precursor to a UCHII region. Two studies have compiled a list of candidate precursors to UCHII regions.

1.2 Sample Selection

During the past six years, two major efforts have been underway to study UCHII and identify its precursors which has been amalgamated in a series of more than 5 papers and a host of observational wavelengths from far infrared to mm and cm.

Molinari et al. conducted a 3 paper search for the precursors of a UCHII region. They followed on from the (Palla et al., 1991) paper which searched 260 bright IRAS sources for H_2O maser emissions. H_2O masers are believed to be associated with one of the first stages of massive star formation, (Churchwell et al. 1990). Molinari and colleges expected there to be only a handful of these sources to be true precursors to UCHII. So they adopted a technique of statistical division and subtraction to obtain a richer group of their target pre-UCHII sources. For their first paper they choose all 44 sources with H_2O masers emissions detected and for statistics some without to a total of 163 sources. They used similar logic at each step and each subsequent paper to narrow down the original list. They then used 11 of these best candidate sources sources in a study into the formation of massive protostars (Molinari et al. 2002). The principal 3 papers of this research are as follows.

- \bullet (Molinari et al., 1996 hereafter MolI) observations of NH $_3$ (1,1) and (2,2) lines into 163 sources.
- (Molinari et al., 1998 hereafter MolII) observations of radio continuum emissions using VLA towards a selected sample of 67 sources.

• (Molinari et al., 2000 hereafter MOIIII) - submillimeter and millimeter continuum photometry of a sample of 30 sources.

These sources were chosen to be very luminous ($F_{60} \ge 100 Jy$) and to have no upper limit for fluxes at 25, 60 or 100 μ m. They have far-infrared colours ($0.6 \le [60-25] \le 0.74$ and $0.87 \le [100-60] \le 0.52$) similar to those associated with compact molecular clouds, (Richard et al., 1987). In addition they excluded sources which had a positional coincidence with known HII regions based on a list of optical HII regions by Marsalkava (1974) on the Bonn (Altenhoff et al. 1978) and the Parkes (Haynes et al. 1979) surveys. This ensured that the sample hadnot as yet had time to produce a significant HII region and are thus similar objects to the youngest of UCHII regions.

Furthermore they divided these sources approximately in half (83 to 80) into High- and Low-type sources. High-type sources being defined solely on the higher [25 -12] colour (≤ 0.57) which makes high-type sources satisfy the Wood & Churchwell (1989) colour conditions for UCHII regions. They theorised that high and low type sources are at different evolutionary stages. With 26% of High and only 9% of low detected in H₂O maser emissions (Palla et al., 1991) and as high-type sources have colours similar to UCHII regions, they further theories that low type sources may contain a subgroup of sources in a stage prior to the formation of a UCHII region.

A list of 163 candidate sources from MoII suitably separated into high- and low-types can be seen at the end of this section on tables 1.1 and 1.2 with a distance and luminosity estimate as described below with RA and DEC coordinates for each source.

The luminosity and distance estimates in tables 1.1 and 1.2 are mostly from the MolI paper. MolI computed the FIR luminosities by integrating the IRAS fluxes. The contribution of the longer wavelengths was estimated from a blackbody function peaking at 100μ m and having the same flux as the sources at that wavelength (Cohen 1973).

The luminosities calculated range from 10 to $10^6 L_{\odot}$. These may be due to a single bright source($B8 \to O3$) or the combined total luminosity of many smaller stellar objects. A luminosity of $10^5 L_{\odot}$ may be due to one O5-type star or two 09 or four B0 or indeed one thousand B8 type (proto)stars or any combination of spectral types in between. Considering the relative rareness of higher mass stars it becomes clear that these luminosities must be due to a high to intermediate mass stellar object even with the presence of a significant ($\leq 1000 \star s$) embedded cluster. Molinari et al's papers (MoII, MoIII) acknowledged this as possibly adding to the observed luminosity but did not negate it in its entirety. It remains an open question for our research whether or not clusters of stars are present around these sources.

Errors in the kinematic distance are the single greatest source of errors in all the following research. MolI calculated a distance estimate using NH₃ line velocity by interpolating in the observed galactic velocity field as measured by (Brand & Blitz, 1993) for sources $90^{\circ} \le l \le 270^{\circ}$ and $d \le 5$ kpc and using rotation curve outside this range. For sources not detected in NH₃, the CO line velocity was used from (Woulerloot & Brand, 1989).

The far and near distance ambiguity was resolved for a number of the sources for whose far kinematic distance estimate placed the object over double the height of the molecular disk (70pc as measured by Blitz (1990)). The far distance estimate was therefore excluded in these cases and distance ambiguity resolved. For all but a few other cases, the near distance estimate was assumed. The distance and luminosity was recalculated for a number of sources in MolIII and (Molinari et al., 2002). We also found a number of estimates in the literature. See the luminosity and distance columns of the tables for details. We mostly assume a chronological accuracy in this regard and assumed the more recent paper to be the more accurate.

The second major effort to identify high-mass protostellar candidates was begun by the (Ramesh & Sridharan, 1997) paper. This paper set out a reliable method to identify UCHII regions using their FIR colours (Wood & Churchwell, 1989) as well as radio continuum data and latitude analysis. (Sridharan et al., 2002 hereafter Srid) used these criteria to compile a list of 69 source coordinates from the IRAS point source catalogue. 15 of whom overlapped with the MolI study. These sources were detected in the highdensity gas-tracing CS $J=2 \rightarrow 1$ survey of massive star-forming regions (Bronfman, Nyman & May 1996) and are bright at FIR wavelengths ($F_{60} \ge 90 \text{Jy}$ AND $F_{100} \ge 500 \text{Jy}$). In addition they were not detected in the galaxy wide 5GHz 1987 Green Bank (Gregory & Condon, 1991) and Parkes-MIT-NRAO radio continuum surveys(Griffith et al., 1994; Wright et al., 1994) at flux densities above 25mJy. As HII regions are detected at radio wavelengths, this ensured that the sources could be in a stage earlier than that of the UCHII region. Srid conducted a detailed observational study of these sources for free-free and dust continuum emissions. They searched for H₂O(water), CH₃OOH(methanol) and NH₃ (ammonia) maser emissions. Beuther et al.(2002) (hereafter Beut) mapped all these target coordinates at 1.2mm continuum emissions. They found compact condensations of dust emission around the IRAS sources and they used these as well as CS spectral line observations to estimate many physical parameters of the regions including the dust and gas masses and column densities.

The kinematic distances were derived from CS velocities (Brand & Blitz, 1993). For some sources, those in the inner galaxy there was a distance ambiguity. This was resolved for a number of those sources whose scale heights were greater than 170pc (4 times the average galactic scale height of UCHII regions of 37pc from Bronfman et al. 2000), and so the near distance estimate was adopted. The distances to some objects were found in the literature (see table 1.3) Some 15 of the sources overlapped with the MolI study. Since Srid is more recent paper, we assumed its estimate was the most accurate and we suitably updated tables 1.1 & 1.2. We found some other distance estimate in a scan of the important sources in the literature and these can be seen at the end of each of the tables.

Srid points to the discrepancy of luminosities derived by the centimetre emissions as to that derived in the FIR. They explain this as probably due to centimetre emissions tracing one massive object while FIR luminosities detecting a whole cluster's luminosity. It remained an issue in both studies whether the observed luminosities were due to wholly one massive contracting protostar or to the summed luminosities of many smaller objects

in an embedded cluster. MolIII addressed to a point this possibility by fitting a luminosity to a cluster whose masses were distributed according to a IMF from (Miller & Scalo, 1979). They concluded that 50% of the total luminosity should still be form the most massive object and thus only a small reduction in the calculated mass or spectral-type (e.g. $09 \rightarrow B0 \ 19M_{\odot} \rightarrow 18M_{\odot}$ or $B2 \rightarrow B3 \ 10M_{\odot} \rightarrow 7.6$). But this question of whether or not or what percentage of these UCHII/pre-UCHII regions contain a surrounding cluster of stars remains important not just to explain the observed luminosity but to explain the very nature of the star formation process in these regions (Bonnel, Vine & Bates, 2004). It is not expected that massive protostars form in isolation but it remains a possibility that low mass protostars may play an active role in the formation of the massive protostar.

We have seen the main sample of 217 unique sources separated into three distinct groups Mol-H (table 1.1), Mol-L (table 1.2) and Srid (table 1.3) with 80, 83, 69 sources respectively. Mol-H satisfy many of the conditions for UCHII regions. It was theorised that Mol-L sources may contain a subgroup of pre UCHII regions and Srid the more recent paper used a more elaborate and pre-planned selection process to identify precursors to UCHII regions. We therefore will assume at least statistically that Mol-H followed by Mol-L and then Srid to be the oldest to youngest in that order.

 $Table\ 1.1:$ Molarini et al.s'(1996) list of candidate precursors to UCHII regions (H-type Sources)

IRAS Name	R.A Degrees(J2000)	Dec Degrees(J2000)	Distance Kpc	Luminosity
	2 0 0 0 0 0 0 0 0 0 0 0 0 0 0 0 0 0 0 0	2 0 0 0 0 0 0 0 0 0 0 0 0 0 0 0 0 0 0 0		
00117 + 6412	3.61750	64.480278	1.80	1380
04034 + 5116	61.80000	51.412500	3.98	14200
$04579 + 4703^{c}$	75.41554	47.123082	2.7^c	3910
05168 + 3634	80.06768	36.622527	6.08	24000
$05274 + 3345^c$	82.69125	33.798889	1.90^{c}	4350
$05553 + 1631^s$	89.55791	16.533333	2.5^{s}	6310^{s}
06056 + 2131	92.17083	21.516944	1.50	5830
$06061 + 2151^c$	92.28250	21.844167	0.10	27.8
06063 + 2040	92.34125	20.657778	4.52	79700
06103 + 1523	93.31291	15.376667	4.63	19100
06104 + 1524	93.33837	15.398972	4.68	46800
06105 + 1756	93.36791	17.925000	3.38	33800
06155 + 2319	94.64666	23.303056	0.10	19.7
17417-2851	266.22250	-28.872222	0.10	31.7
17495-2624	268.17458	-26.425556	4.83	19600
17504-2519	268.39667	-25.332222	3.65	9320
17527-2439	268.95458	-24.672222	3.23	15300
17571-2328	270.05958	-23.482500	-	_
18048-2019	271.96458	-20.310000	4.99	29900
$18089 - 1732^{s}$	272.96375	-17.524722	3.48	63300
18134-1942	274.09000	-19.692028	1.62	7620
$18151 \text{-} 1208^s$	274.48792	-12.122778	3.00^{s}	19953^{s}
$18159 \text{-} 1550^s$	274.69708	-15.816083	4.66	31000
18159-1648	274.72292	-16.794167	2.50	29500
18172-1548	275.02500	-15.783333	2.56	85700
18197-1351	275.65333	-13.836389	-	-
18212 - 1320	276.01958	-13.321111	2.18	1780
18236 - 1205	276.60125	-12.063056	2.51	10400
$18247 \text{-} 1147^s$	276.87958	-11.765556	6.7^{s}	100000^{s}
18258-0737	277.14208	-7.591944	2.97	33100
18316-0602	278.58684	-5.995124	3.17	41400
18317-0513	278.60621	-5.180444	3.13	34800
18360-0537	279.66792	-5.585000	6.28	116000
$18372 \text{-} 0541^s$	279.98333	-5.646944	1.87	7180
18408-0348	280.87958	-3.749167	-	-
$18445 - 0222^s$	281.79500	-2.318333	5.3^{s}	158489^{s}
$18488 + 0000^{s}$	282.85333	-0.071944	5.4^{s}	79433^{s}
18507 + 0121	283.32250	1.415278	3.87	48400
$18517 + 0437^s$	283.55750	4.692222	2.9^{s}	12589^{s}
18532 + 0047	283.96083	0.856111	3.96	12700

18551+0302	284.50972	3.221231	3.95	23600
$18566 + 0408^{s}$	284.79125	4.203889	6.70^{s}	63096^{s}
18596+0536	285.52708	5.675833	3.83	6390
19001+0402	285.65083	4.116111	3.55	11500
19002+0454	285.67500	4.980278	4.98	14300
19043 + 0726	286.69875	7.527222	4.36	14300
19045 + 0518	286.74708	5.381944	3.80	10900
19045 + 0813	286.74958	8.311944	1.58	1730
19088+0902	287.81625	9.124167	4.71	29900
19094+0944	287.96667	9.829444	6.11	37300
19198+1423	290.53208	14.488889	5.54	21800
19213+1723	290.90533	17.484056	4.12	28200
$19282 + 1814^{s}$	292.61708	18.348056	2.11	16300
19368+2239	294.74208	22.775556	4.44	8630
19374 + 2352	294.88833	23.998611	4.30	26700
19388 + 2357	295.24750	24.077500	4.27	14800
20050+2720	301.77792	27.481389	0.73	388
20056 + 3350	301.88125	33.994167	1.67	4000
$20062 + 3550^b$	302.04083	35.988889	4.9^{b}	3200^{b}
$20126+4104^{s}$	303.60833	41.225556	1.70^{s}	7943^{s}
20188+3928	305.16375	39.631111	0.31	343
20220 + 3728	305.98208	37.636111	4.49	8090
20227+4154	306.13083	42.071389	0.10	9.14
20286 + 4105	307.61625	41.263333	3.72	3900
20321+4112	308.48357	41.378758	_	-
20444+4629	311.53458	46.678056	2.42	3340
21078 + 5211	317.35500	52.395556	1.49	13400
21202 + 5157	320.49917	52.182470	6.78	68000
21336 + 5333	323.83750	53.786667	8.22	47100
21391 + 5802	325.17650	58.269361	0.75	93.9
$21519 + 5613^b$	328.41167	56.464722	6.30^{b}	10100^{b}
21526 + 5728	328.57667	57.714167	8.11	27400
$22198 + 6336^c$	335.34375	63.853611	0.9^{c}	1240
22267 + 6244	337.12208	62.995556	0.45	110
22272 + 6358	337.21768	64.228753	1.23	1970
$22305 + 5803^b$	338.10125	58.316111	5.10^{b}	7800^{b}
$22506 + 5944^c$	343.16083	60.015556	5.30^{c}	22200
$22551 + 6221^s$	344.27167	62.628889	0.70^{s}	1585^{s}
$22570 + 5912^s$	344.77708	59.474444	5.10^{s}	50119^{s}
$23545 + 6508^{s}$	359.27167	65.419722	0.80^{s}	1000^{s}

 $Table\ 1.2:$ Molarini et al.s'(1996) list of candidate precursors to UCHII regions (L-type Sources)

IRAS Name	R.A Degrees(J2000)	Dec Degrees(J2000)	Distance Kpc	Luminosity
	2000)	2000)	TIPO	
00070 + 6503	2.4308300	65.335833	6.83	21800
$00420 + 5530^b c$	11.240000	55.788333	5.00^{b}	12400^{b}
01420+6401	26.415000	64.266944	10.07	46800
03211 + 5446	51.246250	54.956944	4.54	35400
$05137 + 3919^{abc}$	79.305417	39.370556	11.5^{b}	44600^{b}
$05345 + 3157^b$	84.449167	31.990000	2.6^{b}	4600^{b}
$05373 + 2349^{ab}$	85.101667	23.848333	2.4^{b}	1800^{b}
05382 + 3547	85.405833	35.813611	25.41	544000
06068 + 2030	92.465417	20.501111	4.44	44900
06291 + 0421	97.950417	4.3252780	1.96	3670
06299 + 1011	98.172083	10.159444	0.35	67.1
06303 + 1021	98.268333	10.322500	0.59	147
06308 + 0402	98.379583	4.0019440	2.02	7870
06382 + 0939	100.26125	9.6027780	0.76	163
$06584 - 0852^a$	105.21254	-8.9413610	4.48^{a}	5670^{a}
$17450 - 2742^a$	267.03875	-27.722500	2.00^{a}	3500^{a}
17582-2234	270.32500	-22.582500	18.83	155000
18014-2428	271.12333	-24.479722	2.87	17100
18018-2426	271.22458	-24.444722	1.50	6640
$18024\text{-}2119^a$	271.35583	-21.327778	0.12^{a}	6.4^{a}
18024-2231	271.37750	-22.526667	2.92	5580
18039-2052	271.73625	-20.864167	-	_
18123-1203	273.78042	-12.045000	3.09	7260
$18144 - 1723^a$	274.35167	-17.370278	4.33^{a}	21200^{a}
18156-1343	274.61917	-13.706111	2.45	51400
$18162 \text{-} 1612^a$	274.78125	-16.189167	4.89^{a}	17300^{a}
18167-1614	274.90708	-16.219722	-	=
18256 - 0742	277.08542	-7.6727780	2.90	11100
$18278 - 1009^a$	277.64667	-10.120000	5.70^{a}	11000^{a}
18288-0158	277.86125	-1.9430560	0.51	188
18311-0701	278.47000	-6.9788890	-	_
18355-0550	279.55667	-5.8047220	-	_
18363 - 0554	279.76542	-5.8708330	4.31	13300
18396-0431	280.57833	-4.4769440	6.08	42300
18424-0329	281.26375	-3.4469440	3.36	5140
18463 + 0052	282.21188	0.9321090	-	-
$18511 + 0146^a$	283.40875	1.8408330	3.86^{a}	13000^{a}
$18527 + 0301^a$	283.81875	3.0852780	5.26^{a}	9000^{a}
18537 + 0145	284.06250	1.8175000	-	-
18544 + 0112	284.24917	1.2722220	3.75	22800

$18565 + 0349^a$	284.76417	3.8894440	6.77^{a}	15400^{a}
$18567 + 0700^a$	284.80667	7.0797220	2.16^{a}	4300^{a}
18571+0326	284.91750	3.5080560		-
18571+0349	284.91667	3.8930560	3.89	18300
18586+0106	285.29375	1.1877780	2.71	4810
19012+0505	285.93125	5.1636110	2.89	16600
19023+0538	286.20417	5.7111110	4.06	6440
19077 + 0839	287.54000	8.7363890	4.66	3210
$19092 + 0841^a$	287.90583	8.7750000	4.48^{a}	9200^{a}
19118+0945	288.56125	9.8444440	_	_
19183+1556	290.15833	16.035000	5.41	24700
19295 + 1637	292.96208	16.724722	5.19	13100
19332+2028	293.85958	20.584444	_	_
19343 + 2026	294.12583	20.552222	4.20	27100
19458 + 2442	297.00042	24.837778	_	_
19542+3004	299.05500	30.215556	_	_
20028+2903	301.22208	29.193611	1.55	5270
$20099 + 3640^a$	302.94333	36.826944	8.66^{a}	25100^{a}
$20106 + 3545^b$	303.13042	35.912778	1.7^{b}	1700^{b}
20180 + 3558	304.99167	36.126944	-	-
20217 + 3947	305.88208	39.956389	3.70	7120
20278 + 3521	307.44542	35.527500	5.02	10800
20293 + 4007	307.78292	40.289722	3.41	7180
20333 + 4102	308.78958	41.221667	0.10	45.7
20406 + 4555	310.59071	46.098139	11.92	125000
21406 + 5110	316.56792	51.370278	0.59	257
21080 + 4758	317.44375	48.183056	7.75	29100
$21307 + 5049^{ab}$	323.13125	51.039444	3.6^{b}	4000^{b}
21548 + 5747	329.12375	58.026389	7.10	23000
22147 + 5948	334.11917	60.063611	7.29	24400
$22172 + 5549^a$	334.78750	56.079167	2.40^{a}	1800^{a}
22187 + 5559	335.14542	56.244167	2.93	7490
22344 + 5909	339.08583	59.415833	7.76	21800
22457 + 5751	341.95655	58.147089	2.28	9910
23026 + 5948	346.19042	60.076389	5.76	17600
$23140 + 6121^b$	349.04875	61.629167	5.20^{b}	10600^{b}
23146 + 5954	349.20375	60.179444	4.43	23000
23152 + 6034	349.35656	60.845372	1.67	1630
23314 + 6033	353.43500	60.841667	2.78	10900
23330+6437	353.84875	64.908611	8.22	34600
$23385 + 6053^{ab}$	355.22167	61.172500	4.90^{b}	16000^{b}
23448 + 6010	356.83375	60.455833	2.02	2530
23507+6230	358.30375	62.783333	4.28	13800

 ${\it Table~1.3:~Sridharan~et~al.s'~(2002)~list~of~candidate~precursors~to~UCHII~regions}$

Name Degrees(J2000) Degrees(J2000) Kpc 05358+3543° 84.793350 35.755300 1.8 3.8 05490+2658 88.053750 26.992500 2.1 3.5 05553+1631 89.557950 16.533300 2.5 3.8 18090+1832 272.96400 -17.524700 13.0 5.6 18090+1832 273.30150 -18.532200 10.0 4.5 18102-1800 273.30150 -17.993100 14.0 5.3 18151-1208 274.69650 -15.816100 11.7 5.0 18182-1433 275.28300 -14.531400 11.8 5.1 18223-1243 276.29550 -12.704700 12.4 5.3 18247-1147 276.87900 -11.765600 9.3 5.0 18264-1152 277.30950 -11.840600 12.5 5.1 18272-1217 277.51050 -12.257500 2.9 4.0 18290-0924 277.93650 -9.3691700 10.5 5.0 18306-0835	IRAS	R.A	Dec	Distance	Luminosity
05490+2658 88.053750 26.992500 2.1 3.5 05553+1631 89.557950 16.533300 2.5 3.8 18090-1832 273.00750 -18.532200 10.0 4.5 18102-1800 273.30150 -17.993100 14.0 5.3 18151-1208 274.48800 -12.122800 3.0 4.3 18159-1550 274.69650 -15.816100 11.7 5.0 18182-1433 275.28300 -14.531400 11.8 5.1 18223-1243 276.29550 -12.704700 12.4 5.3 18247-1147 276.87900 -11.765600 9.3 5.0 18264-1152 277.30950 -11.840600 12.5 5.1 18272-1217 277.51050 -12.257500 2.9 4.0 18306-0835 278.34150 -8.5605600 10.7 4.8 18337-0743 279.12150 -7.6758300 10.4 4.8 18345-0641 279.37050 -6.2375000 9.0 5.1 1	Name	Degrees (J2000)	Degrees (J2000)	Крс	
05490+2658 88.053750 26.992500 2.1 3.5 05553+1631 89.557950 16.533300 2.5 3.8 18090-1832 273.00750 -18.532200 10.0 4.5 18102-1800 273.30150 -17.993100 14.0 5.3 18151-1208 274.48800 -12.122800 3.0 4.3 18159-1550 274.69650 -15.816100 11.7 5.0 18182-1433 275.28300 -14.531400 11.8 5.1 18223-1243 276.29550 -12.704700 12.4 5.3 18247-1147 276.87900 -11.765600 9.3 5.0 18264-1152 277.30950 -11.840600 12.5 5.1 18272-1217 277.51050 -12.257500 2.9 4.0 18306-0835 278.34150 -8.5605600 10.7 4.8 18337-0743 279.12150 -7.6758300 10.4 4.8 18345-0641 279.37050 -6.2375000 9.0 5.1 1	05250 + 25420	24 702250	25 755200	1 0	2 0
05553+1631 89.557950 16.533300 2.5 3.8 18089-1732 272.96400 -17.524700 13.0 5.6 18090-1832 273.00750 -18.532200 10.0 4.5 18102-1800 273.30150 -17.993100 14.0 5.3 18151-1208 274.48800 -12.122800 3.0 4.3 18159-1550 274.69650 -15.816100 11.7 5.0 18182-1433 275.28300 -14.531400 11.8 5.1 18223-1243 276.29550 -12.704700 12.4 5.3 18247-1147 276.87900 -11.765600 9.3 5.0 18264-1152 277.30950 -11.840600 12.5 5.1 18272-1217 277.51050 -12.257500 2.9 4.0 18290-0924 277.93650 -9.3691700 10.5 5.0 18306-0835 278.44650 -8.3930500 10.7 4.8 18337-0743 279.12150 -7.6758300 10.7 4.8 <t< td=""><td></td><td></td><td></td><td></td><td></td></t<>					
18089-1732 272.96400 -17.524700 13.0 5.6 18090-1832 273.00750 -18.532200 10.0 4.5 18102-1800 273.30150 -17.993100 14.0 5.3 18151-1208 274.48800 -12.122800 3.0 4.3 18159-1550 274.69650 -15.816100 11.7 5.0 18182-1433 275.28300 -14.531400 11.8 5.1 18223-1243 276.29550 -12.704700 12.4 5.3 18247-1147 276.87900 -11.765600 9.3 5.0 18264-1152 277.30950 -11.840600 12.5 5.1 18272-1217 277.51050 -12.257500 2.9 4.0 18290-0924 277.93650 -9.3691700 10.5 5.0 18306-0835 278.34150 -8.5605600 10.7 4.9 18310-0825 278.44650 -8.3930500 10.4 4.8 18337-0743 279.12150 -7.6758300 11.5 5.0					
18090-1832 273.00750 -18.532200 10.0 4.5 18102-1800 273.30150 -17.993100 14.0 5.3 18151-1208 274.48800 -12.122800 3.0 4.3 18159-1550 274.69650 -15.816100 11.7 5.0 18182-1433 275.28300 -14.531400 11.8 5.1 18223-1243 276.29550 -12.704700 12.4 5.3 18247-1147 276.87900 -11.765600 9.3 5.0 18264-1152 277.30950 -11.840600 12.5 5.1 18272-1217 277.51050 -12.257500 2.9 4.0 18290-0924 277.93650 -9.3691700 10.5 5.0 18306-0835 278.34150 -8.5605600 10.7 4.8 18308-0841 278.38350 -8.6547200 10.7 4.8 18337-0743 279.12150 -7.6758300 11.5 5.0 18348-0616 279.37050 -6.2375000 9.0 5.1 <					
18102-1800 273.30150 -17.993100 14.0 5.3 18151-1208 274.48800 -12.122800 3.0 4.3 18159-1550 274.69650 -15.816100 11.7 5.0 18182-1433 275.28300 -14.531400 11.8 5.1 18223-1243 276.29550 -12.704700 12.4 5.3 18247-1147 276.87900 -11.765600 9.3 5.0 18264-1152 277.30950 -11.840600 12.5 5.1 18272-1217 277.51050 -12.257500 2.9 4.0 18290-0924 277.93650 -9.3691700 10.5 5.0 18306-0835 278.34150 -8.5605600 10.7 4.8 18308-0841 278.38350 -8.6547200 10.7 4.9 18310-0825 278.44650 -8.3930500 10.4 4.8 18337-0743 279.12150 -7.6758300 11.5 5.0 18348-0616 279.37050 -6.2375000 9.0 5.1 <					
18151-1208 274.48800 -12.122800 3.0 4.3 18159-1550 274.69650 -15.816100 11.7 5.0 18182-1433 275.28300 -14.531400 11.8 5.1 18223-1243 276.29550 -12.704700 12.4 5.3 18247-1147 276.87900 -11.765600 9.3 5.0 18264-1152 277.30950 -11.840600 12.5 5.1 18272-1217 277.51050 -12.257500 2.9 4.0 18290-0924 277.93650 -9.3691700 10.5 5.0 18306-0835 278.34150 -8.5605600 10.7 4.8 18308-0841 278.38350 -8.6547200 10.7 4.9 18310-0825 278.44650 -8.3930500 10.4 4.8 18337-0743 279.12150 -7.6758300 11.5 5.0 18348-0616 279.37050 -6.2375000 9.5 4.6 18348-0512 280.30050 -5.1516700 13.1 5.3 <					
18159-1550 274.69650 -15.816100 11.7 5.0 18182-1433 275.28300 -14.531400 11.8 5.1 18223-1243 276.29550 -12.704700 12.4 5.3 18247-1147 276.87900 -11.765600 9.3 5.0 18264-1152 277.30950 -11.840600 12.5 5.1 18272-1217 277.51050 -12.257500 2.9 4.0 18290-0924 277.93650 -9.3691700 10.5 5.0 18306-0835 278.34150 -8.5605600 10.7 4.8 18308-0841 278.38350 -8.6547200 10.7 4.9 18310-0825 278.44650 -8.3930500 10.4 4.8 18337-0743 279.12150 -7.6758300 11.5 5.0 18348-0616 279.37050 -6.2375000 9.0 5.1 18372-0541 279.98400 -5.6469400 13.4 5.3 18426-0204 281.30400 -2.22200000 13.5 5.0					
18182-1433 275.28300 -14.531400 11.8 5.1 18223-1243 276.29550 -12.704700 12.4 5.3 18247-1147 276.87900 -11.765600 9.3 5.0 18264-1152 277.30950 -11.840600 12.5 5.1 18272-1217 277.51050 -12.257500 2.9 4.0 18290-0924 277.93650 -9.3691700 10.5 5.0 18306-0835 278.34150 -8.5605600 10.7 4.8 18308-0841 278.38350 -8.6547200 10.7 4.9 18310-0825 278.44650 -8.3930500 10.4 4.8 18337-0743 279.12150 -7.6758300 11.5 5.0 18345-0641 279.31950 -6.6422200 9.5 4.6 18348-0616 279.37050 -6.2375000 9.0 5.1 18372-0541 279.98400 -5.6469400 13.4 5.3 18426-0204 281.30400 -2.20200000 13.5 5.0					
18223-1243 276.29550 -12.704700 12.4 5.3 18247-1147 276.87900 -11.765600 9.3 5.0 18264-1152 277.30950 -11.840600 12.5 5.1 18272-1217 277.51050 -12.257500 2.9 4.0 18290-0924 277.93650 -9.3691700 10.5 5.0 18306-0835 278.34150 -8.5605600 10.7 4.8 18308-0841 278.38350 -8.6547200 10.7 4.9 18310-0825 278.44650 -8.3930500 10.4 4.8 18337-0743 279.12150 -7.6758300 11.5 5.0 18348-0616 279.37050 -6.6422200 9.5 4.6 18372-0541 279.98400 -5.6469400 13.4 5.3 18426-0204 281.30400 -2.0200000 13.5 5.0 18437-0216 281.59500 -3.1566700 8.2 4.5 18447-0226 281.84850 -2.2233300 7.3 4.4 <t< td=""><td></td><td></td><td></td><td></td><td></td></t<>					
18247-1147 276.87900 -11.765600 9.3 5.0 18264-1152 277.30950 -11.840600 12.5 5.1 18272-1217 277.51050 -12.257500 2.9 4.0 18290-0924 277.93650 -9.3691700 10.5 5.0 18306-0835 278.34150 -8.5605600 10.7 4.8 18308-0841 278.38350 -8.6547200 10.7 4.9 18310-0825 278.44650 -8.3930500 10.4 4.8 18337-0743 279.12150 -7.6758300 11.5 5.0 18345-0641 279.31950 -6.6422200 9.5 4.6 18348-0616 279.37050 -6.2375000 9.0 5.1 18372-0541 279.98400 -5.6469400 13.4 5.3 1845-0204 281.30400 -2.0200000 13.5 5.0 18431-0312 281.44500 -3.1566700 8.2 4.5 18437-0216 281.59500 -2.223300 7.3 4.4 1					
18264-1152 277.30950 -11.840600 12.5 5.1 18272-1217 277.51050 -12.257500 2.9 4.0 18290-0924 277.93650 -9.3691700 10.5 5.0 18306-0835 278.34150 -8.5605600 10.7 4.8 18308-0841 278.38350 -8.6547200 10.7 4.9 18310-0825 278.44650 -8.3930500 10.4 4.8 18337-0743 279.12150 -7.6758300 11.5 5.0 18345-0641 279.31950 -6.6422200 9.5 4.6 18348-0616 279.37050 -6.2375000 9.0 5.1 18372-0541 279.98400 -5.6469400 13.4 5.3 18426-0204 281.30400 -2.0200000 13.5 5.0 18431-0312 281.44500 -3.1566700 8.2 4.5 18437-0216 281.59500 -2.2233300 7.3 4.4 18440-0148 281.65200 -1.7563900 8.3 4.7 <td< td=""><td></td><td></td><td></td><td></td><td></td></td<>					
18272-1217 277.51050 -12.257500 2.9 4.0 18290-0924 277.93650 -9.3691700 10.5 5.0 18306-0835 278.34150 -8.5605600 10.7 4.8 18308-0841 278.38350 -8.6547200 10.7 4.9 18310-0825 278.44650 -8.3930500 10.4 4.8 18337-0743 279.12150 -7.6758300 11.5 5.0 18345-0641 279.31950 -6.6422200 9.5 4.6 18348-0616 279.37050 -6.2375000 9.0 5.1 18372-0541 279.98400 -5.6469400 13.4 5.3 18385-0512 280.30050 -5.1516700 13.1 5.3 18426-0204 281.30400 -2.0200000 13.5 5.0 18431-0312 281.44500 -3.1566700 8.2 4.5 18437-0216 281.59500 -2.2233300 7.3 4.4 18445-0222 281.79450 -2.3183300 9.4 5.2 <td< td=""><td></td><td></td><td></td><td></td><td></td></td<>					
18290-0924 277.93650 -9.3691700 10.5 5.0 18306-0835 278.34150 -8.5605600 10.7 4.8 18308-0841 278.38350 -8.6547200 10.7 4.9 18310-0825 278.44650 -8.3930500 10.4 4.8 18337-0743 279.12150 -7.6758300 11.5 5.0 18345-0641 279.31950 -6.6422200 9.5 4.6 18348-0616 279.37050 -6.2375000 9.0 5.1 18372-0541 279.98400 -5.6469400 13.4 5.3 18385-0512 280.30050 -5.1516700 13.1 5.3 18426-0204 281.30400 -2.0200000 13.5 5.0 18431-0312 281.44500 -3.1566700 8.2 4.5 18437-0216 281.59500 -2.2233300 7.3 4.4 18440-0148 281.65200 -1.7563900 8.3 4.7 18447-0229 281.84850 -2.4319400 8.2 4.6 <td< td=""><td></td><td></td><td></td><td></td><td></td></td<>					
18306-0835 278.34150 -8.5605600 10.7 4.8 18308-0841 278.38350 -8.6547200 10.7 4.9 18310-0825 278.44650 -8.3930500 10.4 4.8 18337-0743 279.12150 -7.6758300 11.5 5.0 18345-0641 279.31950 -6.6422200 9.5 4.6 18348-0616 279.37050 -6.2375000 9.0 5.1 18372-0541 279.98400 -5.6469400 13.4 5.3 18385-0512 280.30050 -5.1516700 13.1 5.3 18426-0204 281.30400 -2.0200000 13.5 5.0 18431-0312 281.44500 -3.1566700 8.2 4.5 18437-0216 281.59500 -2.2233300 7.3 4.4 18440-0148 281.65200 -1.7563900 8.3 4.7 18445-0222 281.79450 -2.3183300 9.4 5.2 1847-0229 281.84850 -2.4319400 8.2 4.6 18454-0158 282.00600 -1.9136100 5.6 4.3 <td< td=""><td>- '</td><td></td><td></td><td></td><td></td></td<>	- '				
18308-0841 278.38350 -8.6547200 10.7 4.9 18310-0825 278.44650 -8.3930500 10.4 4.8 18337-0743 279.12150 -7.6758300 11.5 5.0 18345-0641 279.31950 -6.6422200 9.5 4.6 18348-0616 279.37050 -6.2375000 9.0 5.1 18372-0541 279.98400 -5.6469400 13.4 5.3 18385-0512 280.30050 -5.1516700 13.1 5.3 18426-0204 281.30400 -2.0200000 13.5 5.0 18431-0312 281.44500 -3.1566700 8.2 4.5 18437-0216 281.59500 -2.2233300 7.3 4.4 18440-0148 281.65200 -1.7563900 8.3 4.7 18445-0222 281.79450 -2.3183300 9.4 5.2 18447-0229 281.84850 -2.4319400 8.2 4.6 18454-0136 282.01500 -1.5563900 11.9 4.8 18460-0307 282.16350 -3.0647200 9.5 4.6 <t< td=""><td></td><td></td><td></td><td></td><td></td></t<>					
18310-0825 278.44650 -8.3930500 10.4 4.8 18337-0743 279.12150 -7.6758300 11.5 5.0 18345-0641 279.31950 -6.6422200 9.5 4.6 18348-0616 279.37050 -6.2375000 9.0 5.1 18372-0541 279.98400 -5.6469400 13.4 5.3 18385-0512 280.30050 -5.1516700 13.1 5.3 18426-0204 281.30400 -2.0200000 13.5 5.0 18431-0312 281.44500 -3.1566700 8.2 4.5 18437-0216 281.59500 -2.2233300 7.3 4.4 18440-0148 281.65200 -1.7563900 8.3 4.7 18447-0222 281.79450 -2.3183300 9.4 5.2 18447-0229 281.84850 -2.4319400 8.2 4.6 18454-0136 282.01500 -1.5563900 11.9 4.8 18460-0307 282.16350 -3.0647200 9.5 4.6 18470-0044 282.40350 -0.6847220 8.2 4.9 <td< td=""><td></td><td></td><td></td><td></td><td></td></td<>					
18337-0743 279.12150 -7.6758300 11.5 5.0 18345-0641 279.31950 -6.6422200 9.5 4.6 18348-0616 279.37050 -6.2375000 9.0 5.1 18372-0541 279.98400 -5.6469400 13.4 5.3 18385-0512 280.30050 -5.1516700 13.1 5.3 18426-0204 281.30400 -2.0200000 13.5 5.0 18431-0312 281.44500 -3.1566700 8.2 4.5 18437-0216 281.59500 -2.2233300 7.3 4.4 18440-0148 281.65200 -1.7563900 8.3 4.7 18445-0222 281.79450 -2.3183300 9.4 5.2 18447-0229 281.84850 -2.4319400 8.2 4.6 18454-0136 282.01500 -1.5563900 11.9 4.8 18460-0307 282.16350 -3.0647200 9.5 4.6 18470-0044 282.40350 -0.6847220 8.2 4.9 18488+0000 282.85350 0.0719444 8.9 4.9 1					
18345-0641 279.31950 -6.6422200 9.5 4.6 18348-0616 279.37050 -6.2375000 9.0 5.1 18372-0541 279.98400 -5.6469400 13.4 5.3 18385-0512 280.30050 -5.1516700 13.1 5.3 18426-0204 281.30400 -2.0200000 13.5 5.0 18431-0312 281.44500 -3.1566700 8.2 4.5 18437-0216 281.59500 -2.2233300 7.3 4.4 18440-0148 281.65200 -1.7563900 8.3 4.7 18445-0222 281.79450 -2.3183300 9.4 5.2 18447-0229 281.84850 -2.4319400 8.2 4.6 18454-0136 282.01500 -1.5563900 11.9 4.8 18454-0158 282.00600 -1.9136100 5.6 4.3 18460-0307 282.16350 -3.0647200 9.5 4.6 18472-0022 282.46200 -0.3191670 11.1 4.9 18488+0000 282.85350 0.0719444 8.9 4.9 1					
18348-0616 279.37050 -6.2375000 9.0 5.1 18372-0541 279.98400 -5.6469400 13.4 5.3 18385-0512 280.30050 -5.1516700 13.1 5.3 18426-0204 281.30400 -2.0200000 13.5 5.0 18431-0312 281.44500 -3.1566700 8.2 4.5 18437-0216 281.59500 -2.2233300 7.3 4.4 18440-0148 281.65200 -1.7563900 8.3 4.7 18445-0222 281.79450 -2.3183300 9.4 5.2 18447-0229 281.84850 -2.4319400 8.2 4.6 18454-0136 282.01500 -1.5563900 11.9 4.8 18454-0158 282.00600 -1.9136100 5.6 4.3 18460-0307 282.16350 -3.0647200 9.5 4.6 18472-0022 282.46200 -0.3191670 11.1 4.9 18488+0000 282.85350 0.0719444 8.9 4.9 18521+0134 283.66950 1.6338900 9.0 4.6 18					
18372-0541 279.98400 -5.6469400 13.4 5.3 18385-0512 280.30050 -5.1516700 13.1 5.3 18426-0204 281.30400 -2.0200000 13.5 5.0 18431-0312 281.44500 -3.1566700 8.2 4.5 18437-0216 281.59500 -2.2233300 7.3 4.4 18440-0148 281.65200 -1.7563900 8.3 4.7 18445-0222 281.79450 -2.3183300 9.4 5.2 18447-0229 281.84850 -2.4319400 8.2 4.6 18454-0136 282.01500 -1.5563900 11.9 4.8 18454-0158 282.00600 -1.9136100 5.6 4.3 18460-0307 282.16350 -3.0647200 9.5 4.6 18472-0022 282.46200 -0.3191670 11.1 4.9 18488+0000 282.85350 0.0719444 8.9 4.9 18517+0437 283.55700 4.6922200 2.9 4.1 18521+0134 283.66950 1.6338900 9.0 4.6 185					
$\begin{array}{cccccccccccccccccccccccccccccccccccc$					
18426-0204 281.30400 -2.0200000 13.5 5.0 18431-0312 281.44500 -3.1566700 8.2 4.5 18437-0216 281.59500 -2.2233300 7.3 4.4 18440-0148 281.65200 -1.7563900 8.3 4.7 18445-0222 281.79450 -2.3183300 9.4 5.2 18447-0229 281.84850 -2.4319400 8.2 4.6 18454-0136 282.01500 -1.5563900 11.9 4.8 18454-0158 282.00600 -1.9136100 5.6 4.3 18460-0307 282.16350 -3.0647200 9.5 4.6 18470-0044 282.40350 -0.6847220 8.2 4.9 18488+0000 282.85350 0.0719444 8.9 4.9 18517+0437 283.55700 4.6922200 2.9 4.1 18521+0134 283.66950 1.6338900 9.0 4.6 18530+0215 283.89300 2.3188900 8.7 5.4 18540+0220 284.14800 2.4150000 10.6 4.9 18553+0					
$\begin{array}{cccccccccccccccccccccccccccccccccccc$					
18437-0216 281.59500 -2.2233300 7.3 4.4 18440-0148 281.65200 -1.7563900 8.3 4.7 18445-0222 281.79450 -2.3183300 9.4 5.2 18447-0229 281.84850 -2.4319400 8.2 4.6 18454-0136 282.01500 -1.5563900 11.9 4.8 18454-0158 282.00600 -1.9136100 5.6 4.3 18460-0307 282.16350 -3.0647200 9.5 4.6 18472-0024 282.40350 -0.6847220 8.2 4.9 18472-0022 282.46200 -0.3191670 11.1 4.9 18488+0000 282.85350 0.0719444 8.9 4.9 18517+0437 283.55700 4.6922200 2.9 4.1 18521+0134 283.66950 1.6338900 9.0 4.6 18530+0215 283.89300 2.3188900 8.7 5.4 18540+0220 284.14800 2.4150000 10.6 4.9 18553+0414 284.47050 4.3016700 12.9 5.1 18566+0					
$\begin{array}{cccccccccccccccccccccccccccccccccccc$					
18517+0437 283.55700 4.6922200 2.9 4.1 18521+0134 283.66950 1.6338900 9.0 4.6 18530+0215 283.89300 2.3188900 8.7 5.4 18540+0220 284.14800 2.4150000 10.6 4.9 18553+0414 284.47050 4.3016700 12.9 5.1 18566+0408 284.79150 4.2038900 6.7 4.8					
18521+0134 283.66950 1.6338900 9.0 4.6 18530+0215 283.89300 2.3188900 8.7 5.4 18540+0220 284.14800 2.4150000 10.6 4.9 18553+0414 284.47050 4.3016700 12.9 5.1 18566+0408 284.79150 4.2038900 6.7 4.8	·				
18530+0215 283.89300 2.3188900 8.7 5.4 18540+0220 284.14800 2.4150000 10.6 4.9 18553+0414 284.47050 4.3016700 12.9 5.1 18566+0408 284.79150 4.2038900 6.7 4.8					
18540+0220 284.14800 2.4150000 10.6 4.9 18553+0414 284.47050 4.3016700 12.9 5.1 18566+0408 284.79150 4.2038900 6.7 4.8	·				
18553+0414 284.47050 4.3016700 12.9 5.1 18566+0408 284.79150 4.2038900 6.7 4.8					
18566 + 0408 284.79150 4.2038900 6.7 4.8					

19035 + 0641	286.50450	6.7763900	2.2	3.9	
19074 + 0752	287.47200	7.9561100	8.9	4.8	
19175 + 1357	289.95450	14.046100	10.6	4.8	
19217 + 1651	290.99550	16.960300	10.5	4.9	
19220 + 1432	291.08250	14.634200	5.5	4.4	
19266 + 1745	292.22550	17.865600	10.0	4.7	
19282 + 1814	292.61700	18.348100	8.2	4.9	
19403 + 2258	295.61400	23.086700	6.3	4.7	
19410 + 2336	295.79700	23.735000	6.4	5.0	
19411 + 2306	295.82550	23.233100	5.8	4.3	
19413 + 2332	295.87050	23.667800	6.8	4.4	
19471 + 2641	297.29100	26.814400	2.4	3.6	
20051 + 3435	301.76550	34.743100	3.7	4.0	
20081 + 2720	302.54850	27.485000	0.7	2.5	
20126 + 4104	303.60900	41.225600	1.7	3.9	
20205 + 3948	305.59050	39.968100	4.5	4.5	
20216 + 4107	305.84850	41.294400	1.7	3.3	
20293 + 3952	307.79400	40.052800	2.0	3.8	
20319 + 3958	308.45550	40.145800	1.6	3.8	
20332 + 4124	308.75250	41.580000	3.9	4.4	
20343 + 4129	309.03000	41.666900	1.4	3.5	
22134 + 5834	333.78750	58.819200	2.6	4.1	
22551 + 6221	344.27100	62.628900	0.7	3.2	
22570 + 5912	344.77650	59.474400	5.1	4.7	
23033 + 5951	346.35750	60.135600	3.5	4.0	
23139 + 5939	349.03800	59.923100	4.8	4.4	
23151 + 5912	349.33800	59.480300	5.7	5.0	
23545+6508	359.27100	65.419700	0.8	3.0	

 $^{^{\}dagger}$ - (Molinari et al., 2002)

^{* -} distance and luminosity ambiguity resolved

^a - Source overlap with Carpenter et al., 1993 study

 $[^]b$ - Source in the MolII study

 $^{^{}c}$ - Source in the MolIII study

 $[^]d$ - Sources overlap with Lada & Lada 2003 embedded source catalogue (LL03)

 $^{^{\}alpha}$ - estimates from the Sridharan et al., 2002 (Srid) paper

 $^{^{\}star}$ - detected at 6cm radio emissions

 $[^]e$ - from Jijina, Myers, & Adams 1999

 $^{^{\}it f}$ - Source of Migenes et al., 1999

 $[^]g$ - Beuther, Schilke & Gueth, 2004

1.3 2MASS Data

The Two Micron All Sky Survey(2MASS) was a joint project by the University of Massachusetts and The Infrared Processing And Analysis Centre(IPAC), Caltech USA. It surveyed the entire sky using two identical 1.3 meter equatorial cassegrain telescopes located at Mt. Hopkins, Tucson, Arizona and Cerro Tololo near La Serra, Chile. Each telescope was connected to a 3-channel camera consisting of 256×256 arrays of HgCdTe detectors capable of simultaneously detecting in the J(1.25 μ m), H(1.65 μ m) and K_s(2.17 μ m) bands with a raw observational pixel size of 2.0". However this is reduced to 1.0" as overlapping images within a tile are made to subsample the pixels.

The 2MASS All-Sky Data Release contains Image & Catalogue data for 99.998% of the Sky. It contains an Image Atlas of 4,121,439 J, H and K_s Fits Images, a Point Source Catalogue(PSC) of 470,992,970 objects and an Extended Source Catalogue(XSC) of 1,647,599 resolved objects.

1.3.1 Point Source Catalogue (PSC)

The PSC is the primary source of data in our research. It contains a composite release of all Level 1 Requirements for the sensitivity, uniformity and reliability and bright stars which saturate for the shortest 2MASS exposures. The second component is a faint extension that contains sources that reach 0.5 to 1.0 magnitudes beyond the completeness limit.

Each point source in the catalogue contains photometric quality and errors, such as read $flag(rd_flag)$, signal to noise $ratio([jhk]_snr)$, detection $statistics(n_det)$, profile-fit reduced chi-squared values($[jhk]_psfchi$) and measurement uncertainties($[jhk]_cmsig$) and others. A full description of these is available from the 2MASS website http://www.ipac.caltech.edu/2mass/releases/second/doc/explsup.html.

All these photometric qualities is summarised into an additional photometric quality flag, ph_qual . This is a three letter string array, each letter corresponding to one band, in which the photometric quality is binned into one of eight categories, A, B, C, D, E, F, U and X. This flag is convenient to use and suffices for our needs for controlling the photometric quality of the selected data.

2MASS data contains several artifacts based on the electronic errors, ghost and persistent images after exposing a bright star. An important flag for eliminating these error is the

contamination and confusion flag, $cc_{-}flg$. Again it is a three string array, it contains six different letters, described below.

 $cc_flg = 0$ - source unaffected by artifact c - confused with nearby bright sources b - confusion during band merging s - electronic stripe p - latent images

d - diffraction spike

For much of our analysis we take point sources with $cc_-flg = 0$ or c in the corresponding band. Although it would be desirable to take only the best quality with $cc_-flg = 0$, our IRAS positions all contain high densities of stars and dust surrounding them. It is therefore expected and indeed observed that a much higher proportion of true point sources with $cc_-flg = c$ are found in high density areas. Therefore we will consider this confusion flag in our selection. Throughout the rest of this thesis when we say a point source is a star of a certain band we mean that it fulfils the requirements of ph_qual = A, B, C or D and cc_flag = 0 or c in that band.

1.3.2 Extended Source Catalogue(XSC)

The 2MASS Extended Source Catalogue database is composed of all sources that are not well fitted by a single point spread function(PSF). It consists, predominantly of galaxies, but also contains nebulae, very close multiple star systems and meteor trails. The sensitivity of the XSC is 1 mag brighter than that of the PSC. It's reliability is also labelled with a confusion flag, $cc_-flag = U \Rightarrow$ unreliable, artifact, false or seriously corrupted source $cc_-flag = 0$ or c having the same meaning as in the PSC. This is a much less used, but important catalogue for our research to deal with sources that may contain very close tightly bound stars or stars with shells, cocoons or associated nebulae.

1.3.3 Comment

At the time of beginning this research the 2nd incremental release the entire 2MASS database was just being released freely to the general public over the Internet through the gator interface. Our sample sources (see section 1.2) already had an abundant quantity of wavelengths from far-infrared to millimeter and centimetre as well as many spectral lines and maser emissions observed. We knew that an addition of a near-infrared study into these regions would only add to our knowledge and understanding of them. Although using the infrared we can see approximately 10 times further than at optical wavelengths in the dust and gas of molecular clouds (Bressel & Brett, 1988), we expected from reading otherworks (Menton & Reid, 1995) that high mass protostars under high extinction would show little or no near-infrared emissions. Initially we had intended to map the regions of high extinction around the sources (areas of dense molecular gas may show up as dark patches of the sky) using 2MASS but we also at the time acknowledged the superior spatial resolution of the 2MASS telescopes (effectively 1") to that of IRAS(a few arcminutes) or others in resolving closely bound point sources or stellar members of an embedded cluster. Or even using the XSC for tightly bound stellar objects that couldnot be resolved into individual point sources. This was a question that had been addressed to a point by both previous studies into these sources, but had remained somewhat open, so we were tempted to begin our research with a search of our sources for embedded clusters.

Chapter 2

Clusters

Physically related stars in the night sky can be grouped together into what one terms as a cluster of stars. They may for example share a common heritage that being they may be born from the same molecular cloud at the same epoch of time and thus share a similar chemical make-up and almost identical age. Also if the cluster of stars is bounded or was recently, they will also share the same distance. A cluster is one of the most basic units of the star formation process. It contains a statistical significant number of members and is the smallest unit were such intrinsic properties as the IMF makes sense.

Clusters have so many positive attributes making them ideal locations for research. Because members share so many properties in common, such as distance, age or chemical composition, we can effectively exclude or cancel them from consideration and just deal with the raw variance of stellar masses between members. Clusters in the past have proved vital to our understanding of the galaxy, as testbeds for gravitational theories and today and in the future is proving invaluable to research into star formation. Although we have been introduced into this topic from massive protostars(chapter 1) they are as important and as fundamental to study of Astronomy in their own right.

Clusters are generally categorised into two main types, globular and open. Globular clusters are massive collections of stars from tens of thousands to one million members or more. Studies into them have help set the scale of the galaxy, the existence of the galactic halo and even the position of the galactic centre itself. But globular clusters are all very old (Gyrs) and the galaxy has ceased its production of them many billion of years ago and thus observation of their formation inside this galaxy is impossible.

On the other-hand, open clusters, the other type of cluster sometimes called galactic clusters are continuously forming in the galactic disk. They can have just a handful to a few thousand members. Now open clusters have been studied for many years and some

haved compiled huge catalogues of them (Lygna, 1985), but it is only recently in tandem with improvements in IR detector technology that we are able to observe open clusters while they are still actively forming deeply embedded in dense molecular clouds. The open cluster catalogue of the past contain very few examples of embedded cluster, they contain mostly exposed classical open clusters, those that have little or no interstellar material between their members and thus were open to optical observations. In the last one or two years there has been a push to identify embedded cluster (Bica et al. (2003)) using infrared all-sky surveys such as 2MASS or DENIS and compile them into an embedded cluster catalogue such as (Bica, Dutra & Barbuy, 2003; Porras et al., 2003; Lada & Lada, 2003 hereafter LL03) so that important statistical properties can be inferred such as the embedded cluster mass function (ECMF). Initial results from these catalogues suggests that any star is as likely to be born in a cluster of 100 M_{\odot} as a cluster 10000 M_{\odot} . That is although a cluster of $10^4~{\rm M}_{\odot}$ contains alot more members, it is also alot rarer and approximately there are hundred more 100 M_{\odot} as there are 10000 M_{\odot} clusters. And Porras et al., (2003) points out that 80% of stars are born in clusters over $100 \mathrm{M}_{\odot}$. It is believed that almost all stars forming today are forming as part of an embedded cluster (Clarke, Bonnell & Hillenbrand, 2000) and only some 4-7% of embedded clusters will survive destructive influences from the galaxy (LL03) and live long enough to emerge from its molecular cloud and form the classical exposed open cluster. Destructive influences could be from tidal disruption by the galaxy or from the effects of passing interstellar clouds. It has been theoretically estimated that a density of greater than $1.0 \rm M_{\odot}~pc^{-3}$ (Bok, 1934; Spitizer, 1958) should be enough to resist these influences.

Furthermore, embedded clusters need 35 members or more for its evaporation time to be greater than the average age of the open clusters in the field (10⁸ Myrs) (Adams & Myers., 2001). In the interest of comparing easily to other studies (Porras et al., 2003) we will define a cluster to have a total number greater than 35 stellar members. A stellar grouping is defined to have 5(from Hodapp (1994b) definition of cluster) to 34 stellar members inclusively. But we will use these terms with a certain amount of interchangeability in the following text and will often use one to mean both.

This short introduction into stellar clusters has tried to emphasise how important the identification of embedded clusters are and how vital they will prove into star formation research for many years to come. Theories into massive star formation like (Bonnell, Vine, & Bate, 2004) have been gaining a certain amount of momentum in recent years. This theory stipulates the importance of an embedded cluster of lower mass member to nurture the formation of massive protostars. In this chapter we test our 217 IRAS sources

for groupings of stars that because these regions are know to be associated with molecular clouds (Beut) have a high probability of being embedded clusters.

2.1 Detection of Groups/Clusters

The near-infrared $K_s(2.2\mu m)$ band allows us to see approximately 10 times deeper into dense molecular cloud than the optical V band (Bressel & Brett, 1988). For this reason, it wasn't really viable until recently with the improvements in IR camera technology to detect deeply embedded clusters. Nevertheless it was over thirty years since Grasdalen, Storm & Storm(1974) detected the first deeply embedded cluster using a single channel infrared photometer.

With today's infrared detectors it has become alot easier. To date there has been alot of different approaches used to detect the presence of clusters or groupings of stars. Some involved case studies of individual star forming regions (Horner, Lada & Lada, 1997) and others have used symmetric surveys of individual molecular cloud complexes (Carpenter, Snell & Schloerb 1995). Our approach and the approach of Hodapp (1994) was to symmetrically survey one of the various signposts of starformation. Hodapp(1994) surveyed sources of known CO molecular outflows and detected a group of stars around approximately $\frac{1}{3}$ of his sample. But probably even more similar to our approach was (Testi, Palla, & Natta, 1998) which looked for clusters around Herbig Ae\Be Stars and Carpenter et al.(1993) who searched for groupings around bright IRAS sources. Indeed the Carpenter and colleges' paper have 7 sources in common with our study.

As well as approaches, techniques of detection also varied between studies. The Testi, Palla & Natta (1998) study counted stellar counts in annular-shaped areas around each Herbig Ae\Be stars with varying radii. This was a good technique and indirectly gave a richness measure to each cluster, but also required a pre-supposed central position of each cluster. For this they assumed the Herbig Ae\Be stars were at the centre. Some otherworks, such as (Carpenter et al., 1993) counted stars for K band detected sources in square boxes around the target (on) field and compared this with a carefully chosen off(control) field. For most studies which had 3 bands available such as we have with 2MASS, they used a visual inspection of the false colour near-infrared images (Bica et al., 2003). They searched for visible clusterings of stars characterised by a reddening in colour which symbolised a heavy extinction. This technique has some advantages, but for us, it mite not be the most ideal, the massive protostars that we expect to be present

may out shine and overshadow the presence of the cluster. It may also make an illusion that they is a cluster when there isn't.

Classifying exactly which star in the sky belongs to a particular group is probably impossible using our 2MASS data alone. Any groupings of stars will be mixed in foreground and background stars that often outnumber them in their own area of the sky, but it is expected that regions with groups of stars will show up in this mixture as areas with higher stellar densities, We make stellar number density contour maps for each of the 217 IRAS sources and determine if a cluster is present around that IRAS source.

To make contour maps for such a large number of sources, we needed an automated system. Human effort would be laborious, biased and prone to errors. All the following research was done by computer code in the IDL language.

2.2 Data Retrieval and Processing

The 1.2mm continuum contour maps of Beuther et al., (2002) show that the dust concentrations spread over a maximum area of 200×200 arcseconds². So, we decided that our contour should cover, at most double its length, an area of 400×400 square arcseconds.

When this research was being done, the GATOR database, which was available on the Internet, had many constraints for data input. It required our IRAS sources names to be converted into J2000 degrees which we did using SIMBAD, as in tables 1.1, 1.2, & 1.3. It also limited the search radius to 1 arcminute for multiple coordinate uploads. Thus to form a complete 400×400 arcsecond² area around each source, we required 49 overlapping circles in accordance with Nyquist Sampling techniques. Due to this, the received file from GATOR contained many multiple entries of point sources. We converted this file into a unique list of point sources by tagging each circle with an IRAS index number, we cropped the data to only RA and DEC and then used the UNIX commands, unique and sort(available in recent versions of IDL) to save indices and backtracked from this to obtain all the previous GATOR data. It was necessary to tag each circle with an IRAS index number as the regions are not isolated, they overlap. Some double entry stars may have been doubled due to two or more of the IRAS sources overlapping(such as in the case of IRAS06103+1523 and IRAS06104+1524) and are not an artifact due to our data retrieval technique. Tagging in this way eliminates this potential problem.

These point sources were then filtered to meet K band photometric and confusion flag quality conditions (see section 1.3.1). We converted the RA and DEC of each star into arcsecond positions from the central IRAS coordinates, adjusting our calculations for the curvature of our metric.

2.3 Nyquist Sampling and Detection

To quantify stellar densities, we Nyquist binned the 400 arcsecond squared areas. This was done using a rigid box, counting the number of stars that fell in it and then moving it half it's length, repeating from left to right, from up to down until the entire 400 arcsec \times 400 arcsec area was sampled. The size of the box for cluster determination was taken as 120 arcseconds in length.

The Nyquist Sampling technique for determining stellar densities was first used by Lada & Lada, (1995) on embedded cluster IC348. This paper used the diagram to examine the stellar structure within the cluster. It is very important to Nyquist sample the area when making stellar contour maps. It does not suffice to simply bin each star in a box. To explain why in a general logistic sense; imagine a boxed area, with a large square matrix of scalars spread internally over the box. For each scalar to represent some quantity measured over the area to each of its four neighbours it must extend as far as them. Imagining stellar densities spread over an area in this way, justifies the use of this technique, but also as a desired by-product, this method has a degree of smoothing rapid changes in star counts. This is the first time that this method has been used as cluster detection technique. The technique created a large matrix of star counts with each indice representing a position of a bin.

We, then used the already written IDL code contour.pro, available in the IDL library files to form contour plots of the stellar densities for each of the 217 sources. To meaningfully choose the contour levels, we needed an estimation of the background and foreground field star density. We did not use a control field, we instead estimated for each of our 400 arcsecond squared areas separately by use of the mode(as defined in the IRAF helpfiles to be 3 times the mean minus 2 times the median). This is a satisfactory estimate for group determination as our stellar groups are expected to be limited to the 200 arcsec sq. dust concentrations (Beut). That is 75% of the sampling area would be off the dust concentration area.

Table 2.1: Cluster Detections in each of the papers, the numbers in square brackets are the overlapping sources.

Paper	Sridharan	Molinari-L	Molinari-H	Total
	(69)	(83)	(80)	(217[15])
Definate Clusters	13	17	21	47[4]
Possible Clusters	2	9	5	16[0]
Total	15	26	26	63[4]
Percentage(%)	22%	31%	33%	29%

For the detection of the groups, we chose the first contour level to be the estimated stellar surface density of the background and foreground field stars plus 3 standard deviations. We then classified each plot into one of the categories

- Y Definite group of stars being revealed in 400 arcsec squared area.
- P Possible group, small contours close to the IRAS coordinates or moderate sized contours far away.
- N No detection, or small contours far from central coordinate.

A list of the sources categorised into definite and possible groups can be seen on table 2.2.

As in table 2.1, we detected a total of 63(approx. 30%) clear groups out of a possible 217 unique IRAS sources. We detected all seven known clusters that overlapped with the (Carpenter et al., 1993) study. We note that there is no clusters detected from -30° to 30° declination despite the fact that there is alot of candidate sources. These are areas of high stellar counts. It is very probable that clusters are present at these declinations but were not detected by our technique as background and foreground stars effectively drowned out any increase in stellar density due to the cluster.

As mentioned in the previous chapter, Srids' candidates to precursor UCHII regions, followed by Mol-L and then Mol-H respectively are the younger. We see a slight but significant increase in our IRAS sources having groups associated with them with age. Mol-L has a large amount classified as possibly clusters and if these percentages are recalculated with a weight of 0.5 attached to possible clusters, these percentages become 20%, 26% and 29% for Srid, Mol-L and Mol-H respectively. This shows a pronounced evolution of age of the precursor UCHII and cluster presence. The difference in ages of the candidate sources between the samples will not be very large and other factors such as background stars will play more heavily on a clusters detection.

If the assumption that Srids' sources are the youngest followed by Mol-L and so forth is correct, then this says as a massive protostar/UCHII region gets older the presence of the cluster is easier to detect and possibly the reason why its easier to detect is that the number of stars in the cluster is increasing. This is not surprising, but it may suggest co-relation between the massive stars and the growth of clusters. Our data is not strong enough to make these arguments exclusive but it is in agreement with others works and theories such as (Bonnell, Vine and Bate, 2004).

Table 2.2: The clusters and groups detected using this technique. Cluster reference contains the type of source along with the Mol number from MolI. Many of the data was undated from the various studies. see footnote

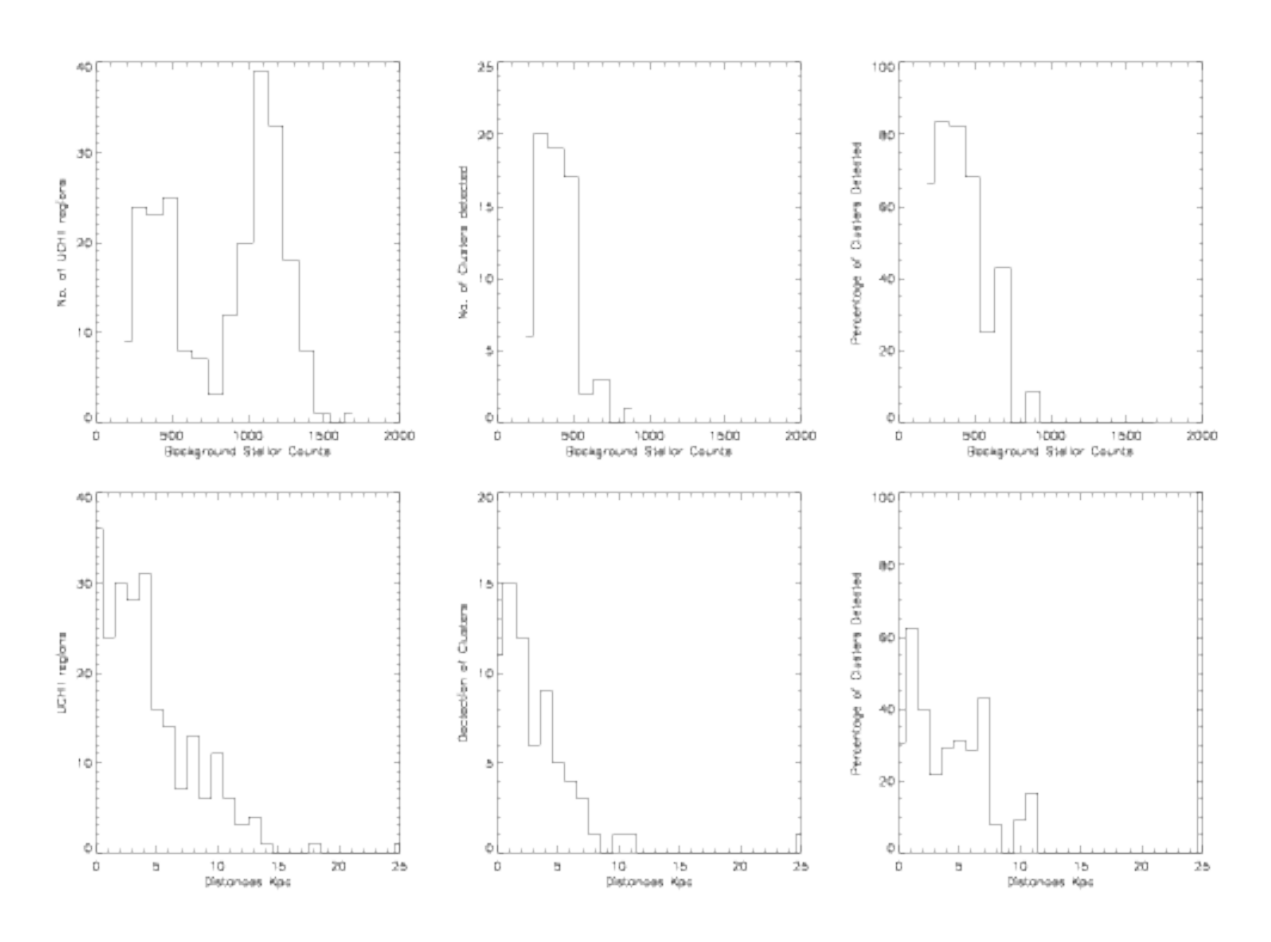
IRAS	Right Ascension	Declination	Cluster	Distance	Luminosity
Name	Degrees(J2000)	Degrees(J2000)	Reference	Kpc	$(Log L_{\odot})$
Groups Detected	l				
00117 + 6412	3.6175000	64.480278	HM2	1.80	3.1
$00420 + 5530^{\dagger f}$	11.240000	55.788333	LM3	4.3^{\dagger}	4.1^{\dagger}
03211 + 5446	51.246250	54.956944	L M5	4.54	4.5
04034 + 5116	61.800000	51.412500	H M6	3.98	4.2
$05137 + 3919^{\dagger bcf}$	79.305417	39.370556	L M8	11.5^{\dagger}	4.6^{\dagger}
$05168 + 3634^{b\star f}$	80.067686	36.622527	H M9	6.08	4.4
$05274 + 3345^a$	82.691250	33.798889	H M10	1.55	3.6
$05345{+}3157^{\dagger b\star c}$	84.449167	31.990000	L 11	2.6^{\dagger}	3.6^{\dagger}
$05358 + 3543^f$	84.793350	35.755300	S	1.8*	3.8^{*}
05382 + 3547	85.405833	35.813611	L M13	25.41	5.7
$05490 + 2658^{\star a}$	88.053750	26.992500	S	2.1^{*}	3.5^{*}
$05553 {+} 1631^{\star a}$	89.557950	16.533300	S, H M14	$2.5^{*\alpha}$	$3.8^{*\alpha}$
$06056 + 2131^a$	92.170833	21.516944	H M15	1.50	3.8
$06061 + 2151^f$	92.282500	21.844167	H M16	0.10	1.4
06063 + 2040	92.341250	20.657778	HM17	4.52	4.9
$06068 + 2030^{ad}$	92.465417	20.501111	L M18	1.50^{d}	4.7
06103 + 1523	93.312917	15.376667	H M19	4.63	4.3
06104 + 1524	93.338375	15.398972	H M20	4.68	4.7
06105 + 1756	93.367917	17.925000	H M21	3.38	4.5
$06155 + 2319^{ad}$	94.646667	23.303056	H M22	1.60^{d}	1.3
06291 + 0421	97.950417	4.3252780	L M23	1.96	3.6
$06308 + 0402^a$	98.379583	4.0019440	L M26	2.02	3.9
06382 + 0939	100.26125	9.6027780	L M27	0.76	2.2
$06584 - 0852^{bc}$	105.21254	-8.9413610	L M28	4.48	3.9
$20050 + 2720^{b\star h}$	301.77792	27.481389	H M114	0.73	2.6
20081 + 2720	302.54850	27.485000	S	0.7^{*}	2.5^{*}

20216 + 4107	305.84850	41.294400	S	1.7^{*}	3.3*
$20293 + 3952^g$	307.79400	40.052800	S	2.0^{g}	3.8
20319 + 3958	308.45550	40.145800	S	1.6^{*}	3.8^{*}
$21078 + 5211^{b\star}$	317.35500	52.395556	H M133	1.49	4.1
21202 + 5157	320.49917	52.182470	H M135	6.78	4.8
21548 + 5747	329.12375	58.026389	L M141	7.10	4.4
$22134 + 5834^{j}$	333.78750	58.819200	S	2.6*	4.1^{*}
$22172 + 5549^b$	334.78750	56.079167	L M143	2.87	3.7
22272 + 6358	337.21768	64.228753	H M147	1.23	3.3
$22305 + 5803^b$	338.10125	58.316111	H M148	5.40	4.1
$22506 + 5944^{b \star f}$	343.16083	60.015556	H M151	5.30^{f}	4.3
22551 + 6221	344.27100	62.628900	S,H~M152	$0.7^{\alpha*}$	$3.2^{\alpha*}$
22570 + 5912	344.77650	59.474400	S,H~M153	$5.1^{\alpha*}$	4.7^{α}
$23026 + 5948^b$	346.19042	60.076389	L M154	5.76	4.2
$23033 + 5951^e$	346.35750	60.135600	\mathbf{S}	3.5^{*e}	4.0^{*e}
23146 + 5954	349.20375	60.179444	L M156	4.43	4.4
23151 + 5912	349.33800	59.480300	\mathbf{S}	5.7^{*}	5.0^{*}
$23314 + 6033^b$	353.43500	60.841667	L M158	2.78	4.0
23448 + 6010	356.83375	60.455833	L M161	2.02	3.4
23507 + 6230	358.30375	62.783333	L M162	4.28	4.1
23545 + 6508	359.27100	65.419700	$_{\mathrm{S,H}}$	$0.8^{*\alpha}$	$3.0^{*\alpha}$
Possible Groups I	Detected				
00070 + 6503	2.4308300	65.335833	L M1	6.83	4.3
$04579 + 4703^b$	75.415547	47.123082	H M7	2.47	3.6
$05373 + 2349^{bc\dagger f}$	85.101667	23.848333	L M12	2.4^{\dagger}	3.3^{\dagger}
06299 + 1011	98.172083	10.159444	L M24	0.35	1.8
20028+2903	301.22208	29.193611	L M113	1.55	3.7
$20188 + 3928^{b\star}$	305.16375	39.631111	H M121	0.31	2.5
20205+3948	305.59050	39.968100	S	4.5^{*}	4.5^{*}
$20286 + 4105^b$	307.61625	41.263333	H M126	3.72	3.6
20293 + 4007	307.78292	40.289722	L M127	3.41	3.9
20343 + 4129	309.03000	41.666900	S	1.4^{*}	3.5^{*}
20406 + 4555	310.59071	46.098139	L M130	11.92	5.1
$20444 + 4629^{b*}$	311.53458	46.678056	H M131	2.42	3.5
21406 + 5110	316.56792	51.370278	L M132	0.59	2.4
21526 + 5728	328.57667	57.714167	H M140	8.11	4.4
22147 + 5948	334.11917	60.063611	L M142	7.29	4.4
$23385 + 6053^{\dagger bc}$	355.22167	61.172500	L M160	6.94	4.8

- † (Molinari et al., 2002)
- * distance and luminosity ambiguity resolved
- ^a Source overlap with Carpenter et al., 1993 study
- ^b Source in the MolII study
- c Source in the MolIII study
- ^d Sources overlap with Lada & Lada 2003 embedded source catalogue (LL03)
- $^{\alpha}$ estimates from the Sridharan et al., 2002 (Srid) paper
- * detected at 6cm radio emissions
- ^e from Jijina, Myers, & Adams 1999
- f Source of Migenes et al., 1999
- ^g Beuther, Schilke & Gueth, 2004
- ^h Chen et al., 1997
- ^j Kumar, Ojha & Davis, 2003
- ^g Porras, Cruz-Gonzalez & Salas, 2003

2.4 The Detection Technique

Figure 2.1: Plots of the (pre)UCHII regions and cluster/groups against a background measure and distance from the combined Srid and MolI studies (see text below)

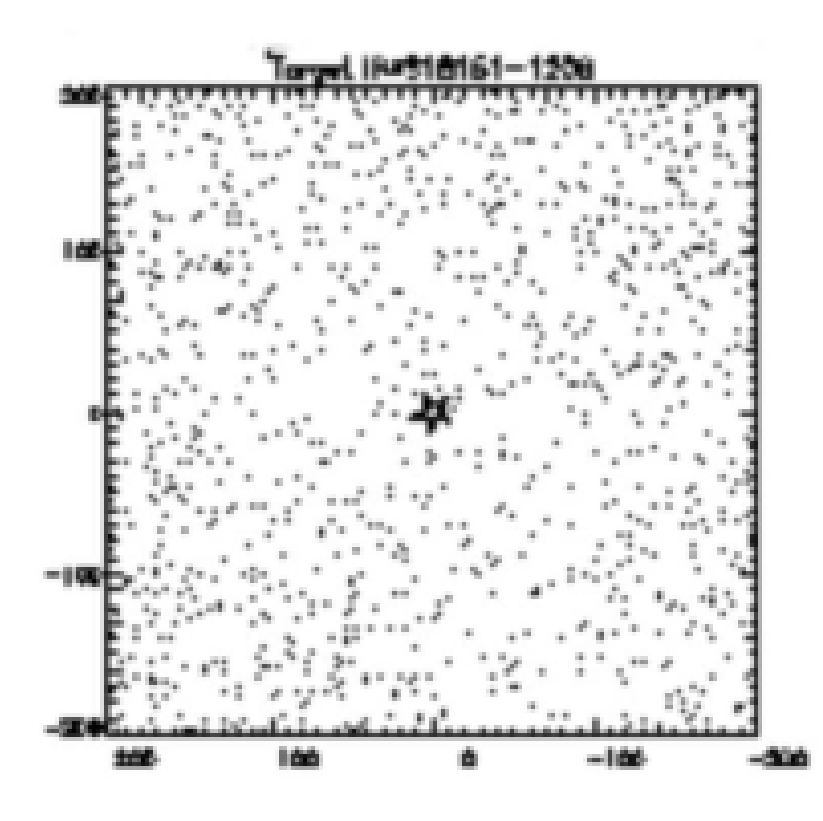


These diagrams (figure 2.1) were created using the unedited data from Srid and MolI.

We can see, bottom-left the exponential fall of (pre)UCHII regions in the two studies with distance and above-left a measure of the K-band stellar background in the all 49 circles(section 2.2). Detection of clusters against their distances can be seen middle-bottom with percentages of UCHII detected with clusters on the right. The bottom-line shows a gradual fall-off of detection with distance. This is expected that the possibility of detecting potential clusters with our technique will decrease with increasing distance. The top-line of the figure shows a dramatic fall of detections for regions of background greater than 700 stellar objects or (approx. $4\times10^{-3}\star$ arcsec⁻²). This demonstrates a heavy weakness of our technique for areas of high background counts, but the sharpness of the cut-off may also be aided to a degree by an apparent dip in candidate (pre) UCHII in the original sample at between 600 - 800 stars(top-left).

This may not be a failure of our technique but rather the very definition of a cluster. Our chose of contour levels at the mode $+ 3\sigma$ may be decreased but this is unlikely to significantly add to our detections. Our only assumption for detecting clusters(section 2.1) is that areas with clusters will show-up against the background as areas of higher stellar density. This may not be so!

Figure 2.2: K-band stars as arcsecond off-set positions from the central IRAS source 18161-1258



On the figure 2.2 we see a plot of stellar positions around the IRAS source 18172-1548(symbolised by open star). We ran our contour program over this region with no detection of a group or cluster of stars. Although it was chosen it may be considered typical of at least a large section of non cluster detected candidate sources and if we examine it more closely we can see a reduction of stars in areas around the IRAS source. What we are possibly seeing is a cloud of gas and dust which may still contain a small cluster of stars blocking from view a sufficient number of background stars to actually lead to an apparent reduction of stellar counts in that area. This will be most endemic in regions of higher stellar background. And as we will see later stellar density per arcsecond squared in our clusters are of the same order of magnitude as our fall-off and it becomes quite conceivable that this process will lead to a significant reduction of detections of clusters around our candidate (pre) UCHII sources.

Although this is a clear failing of our technique, other techniques mentioned 2.1 would not be any better. Visual inspection of the coloured infrared images would show reddened star but it would be totally unclear whether these stars are embedded in a molecular cloud or merely background stars behind it. Hodapp(1994a) was the most prolific study of embedded clusters to date and he detected groupings in 33% of his sources, ours at 30% is not much less. In addition, we have detected all the previously known clusters in our sample (Carpenter et al., 1993; Kumar, Ojha & Davis, 2003 and others see table 2.2). It is however hard to conceive that using 2MASS data alone the existence of method of detecting a cluster whose very presence and the presence of its parental cloud is leading to a reduction of visible stellar objects. Perhaps a method of searching for regions with higher proportions of their stars displaying infrared excess would be more fruitful in areas of high background, but this also may make some undesired assumptions about clusters.

The dip in detections of clusters at very close distances on the bottom middle and right may be due to clusters subtending a smaller angle at larger distances and thus more easily identified via enhanced surface density (Clarke, Bonnel & Hillenbrand, 1999) and also may be due in part to some distance miss-estimates of MolI being droped to 0.1 Kpc. We didnot use the updated distance estimates in this study because the search of the literature focused almost exclusively on sources that had clusters detected. This would of added its own distinctive and somewhat difficult to comprehend errors into the diagrams, while the raw data should be at least statistically hold true.

If one looks once more at the diagrams (fig 2.1) top-left and compare it to its cluster equivalent top-mid, the entire second and larger peak is totally non-existent in the latter.

This could account for a significant, over half of (pre) UCHII regions, being without a cluster detected. This itself poses the questions, what percentage of (pre) UCHII have clusters surrounding them? Our detection of 30% should be treated as a minimum or lower bound to the true percentage.

To in some way strengthen this argument, note that from figure 2.1 background stars start to have a serious influence on cluster detection after $500 \star (3 \times 10^{-3} \star \text{s arcsec}^{-2})$ and distance after 3.0Kpc. There is 28 of the original sample which are less than these two constraints. Twenty-four of these or 86% have clusters detected and all 4 with no clusters detected came from the MolI study where distance miscalculation is a possibility.

In addition to this the selection process of Palla et al., 1991 may of chosen objects that were neither candidate precursors to UCHII regions, a UCHII region itself nor anything what to do with a massive protostar young or old. Therefore it is likely that the true percentage of forming massive protostars associated with an embedded cluster is likely to be even higher, possibly even approaching the 100% mark. And if all massive stars forming today are associated with embedded clusters, it becomes a real likelihood that some processes of massive star forming are dependant of the presence of a cluster environment.

Chapter 3

Further Classification of the Clusters

To further analyse the 63 IRAS sources that displayed groups of stars that were possible clusters, we went back to the GATOR database, and separately obtained point source data within a circle of 8 arcminute radius around each of the sources. This made it possible to increase our Nyquist sampling area to 600 arcseconds squared (max $\sqrt{2}$ R). Which allowed us to better classify structures that were partially outside the previous 400×400 arcsec² area. It gave us a better estimation of the mode(background and foreground stars) and standard deviation and improved many of our later calculations.

To reveal more structures within the clusters, we decreased the binsize to 80", and smoothed the contours with the IDL library function $min_curve_surf.pro$. In our case, the function worked by fitting a minimum curvature spline surface over our data. We already had a degree of smoothing from the Nyquist technique so, we only set it to interpolate once between each of our points. We then plotted the contour diagrams that can be seen at the end of the chapter, figure 3.2, with the contour levels starting at the $mode + 2\sigma$ contour and in integer steps of σ afterwards. Hence the first greyscale is the $mode + 3\sigma$ contour. We over plot the stars locations in the background of each diagram. Although its purpose is primarily cosmetic, we bring the readers attention to the difficulties in detecting groups and their boundaries by human inspection alone.

3.1 The Morphologies of our Stellar Groups

The morphology of an embedded clusters can give important underlying clues to the star formation processes and influences that lead to the creation of the cluster. It was our primary motivation for making stellar density maps to probe into the morphology and star formation process in this way. Although at the small scale all the cluster show structure, generally embedded clusters are classified into two basic structural types.

1. Centrally-Condensed clusters

2. Hierarchical-type clusters

For an ideal case, we define a centrally condensed cluster, as a cluster which contains one clear peak of stellar density at its centre. On the other hand, clusters of hierarchical type are ones which appear to exhibit many separated peaks in stellar density. Our clusters are, of course not ideal, and direct classification into one of these two groups is not always straight forward. Many of our clusters show qualities which belong to both of these types. So, with a certain amount of caution we choose to ignore, for example, small (both spatially and in magnitude) contours around clear circularly symmetric contours, such as IRAS06308+0402 and IRAS06105+1756 and classify it clearly as a centrally condensed cluster. In general, we classify a group as central condensed, if it a proximately ad-hears to a King's model. So, central condensed clusters may have associated closed contours surrounding it, provided that they are clearly decreasing in magnitude from the centre.

A cluster is classified as Hierarchical if it contains more than one peak in stellar density. We made numerous contours maps of varying binsizes for each cluster to classify each stellar group into one of these categories, one of which can be seen at the end of this chapter (figures 3.2). A full list of classifications for each cluster can be seen on table 3.1.

Varying of bin sizes does change the apparent morphology of the cluster. If the binsize is too large, then all structure within the cluster is lost, and the contours appear only as a blob. On the other hand, a very small binsize results in a fragmentation of the entire cluster into separated clumps and then further into individual stars. There is however a clearly correct binsize for each cluster which becomes intuitively evident with the observation of many different binsizes for each individual cluster. There is perhaps a precise exact binsize which will be most ideal for a particular cluster which would probably depend on distance and background counts, but a compromise of binsizes, for the sake of simplicity must be sought, for further classification of these groupings. This may be less than ideal for some clusters, which make them appear fainter then they should when compared to others. A binsize of 80arcseconds was chosen for the clusters at the end of this chapter (figures 3.2).

Thirty of our clusters appear to be Hierarchical compared to thirty-three of a centrally-condensed type. Therefore the ratio of hierarchical to centrally condensed forms is (H/C = $0.9 \approx 1$). One interesting theory to be discussed in relation to the morphology of the

clusters is that from Elmegreen (1993). The theory proposes a scenario of star formation in a turbulent self gravitating cloud where the greatest compression should occur parallel to the magnetic field lines. The initial cloud is stabilised by turbulence and magnetic forces rather than thermal pressure and then any small-scale gravitational collapse must be followed by a sequence of larger scale parallel collapse, so that turbulent compression and dissipation on the large scale to the smaller and smaller scales form denser and denser cores and subcores. Thus the collapse is hierarchical in nature, and the resultant embedded cluster should be hierarchical in form provided the star formation forms faster than an orbit time for the cluster, otherwise its members would become mixed and scattered (Yanaguchi et al., 2002). The scenario above also suggest an intuitive natural equality between gravitational and turbulent energy on the large scale of the clouds, but also this is extended weakly to more the local scale of the embedded cluster. This equality can be seen from the ratios of the hierarchical to centrally condensed types of the clusters in our samples. Also this theory requires on a smaller scale gravitational instability to pump energy into turbulence may be loosely suggested by the slightly weaker hierarchical and more dominant gravity component in our clusters driving the formation of stars(see also (Elmegreen, 2002) for a good detailed discussion on this topic).

Another theory, that could be important to explain the observed morphology of the clusters, but probably should not be considered as a competing one to the above, was an interesting numerical simulation by Bonnell, Bates & Vine (2003). They modelled the fragmentation of a molecular cloud into fragments capable of forming into individual stars. The cloud initially condenses into small subclusters of stars that appear as a hierarchical cluster form. As the simulation progresses the subclusters are attracted by mutual gravitational forces and eventually merge into a central-condensed type of cluster. Interestingly to massive star formation is that, as the subcluster are of a much diminished radii and thereby volume compared to the final centrally condensed cluster, it allows for a high enough density of stars to make stellar interactions a probability in them. Massive protostars may be created by these interactions or their position in these subclusters to allow them to competitively accret more matter than its sibling members. Purely from figure 3.2 at the end of the chapter, $\frac{2}{3}$ of the central IRAS sources (most probable position of a massive protostar) are within the central regions of the contours or the subcluster or main cluster. Only 12% of the central position is outside the contours of a (sub)cluster. It is interesting that our study confirms that massive protostars are forming in the centre of the (sub)clusters. In the case of IRAS06103+1523 and IRAS 06104+1524 which is the same region overlapping. Two bright IRAS sources are forming at the centre of two subclusters of a Hierarchical form cluster which if the simulations

of Bonnell, Bates & Vine are correct will converge to form one centrally condensed cluster and thus will presumably form a cluster with two massive protostars at its centre. Although it somewhat of a leap of faith to suggest that the weak differences in ages of (pre) UCHII regions of the Srid, Mol-L and Mol-H type sources should be anything but less attached to the age of the embedded cluster and hence younger cluster will be more likely appear hierarchical in form then central-condensed. It is worth noting that the hierarchical to central condensed ratio is conserved between the different types of samples.

3.2 The Area of the Stellar Groups

The Area was calculated by manipulating the IDL function contour proto write positional offsets for the mode+ 2σ contour level instead of plotting it. These positions formed a number of closed polygons. The area enclosed by a polygon $(x_1, y_1), (x_2, y_2), \ldots, (x_n, y_n)$ is

$$Area = 1/2 \sum_{i=1}^{n} (x_{i+1}y_i - x_i y_{i+1})$$

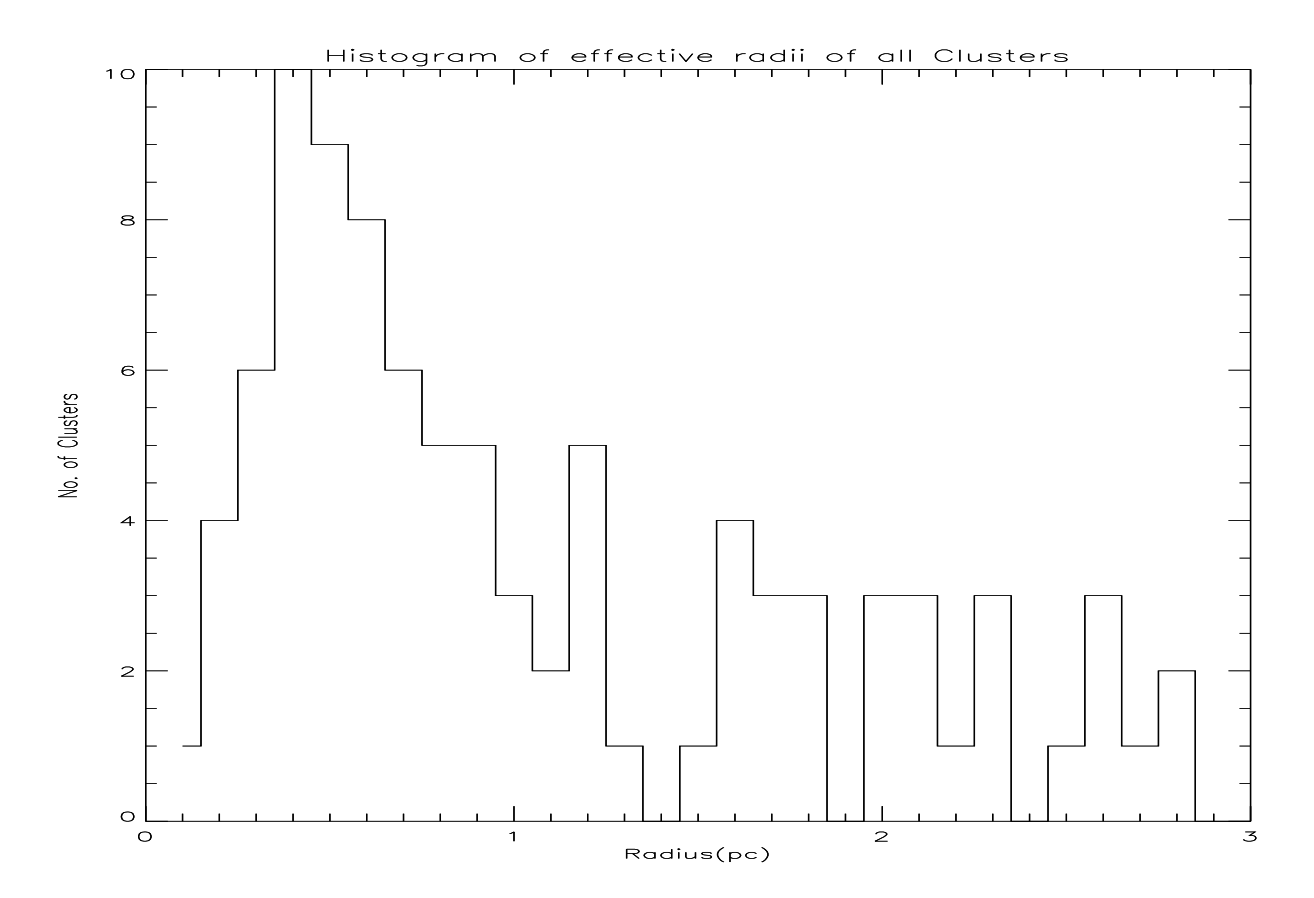
where $(x_{n+1}, y_{n+1}) = (x_1, y_1)$. We then summed the polygon areas for each IRAS source. Our coordinates are in arcsecond, so the Area is in arcseconds².

To convert the arcsecond Area into pc² we needed to have a reliable measure of the distance to the group of stars. The distances to the IRAS sources, which are close to if not at the centre of the group, are available from their respective papers, to varying degrees of accuracy.

The equations to convert the Area into pc² depends on the square of the distance, so any errors in distance estimation would be squared. Note also that for some MolI sources such as IRAS06061+2151 at 0.1kpc and IRAS05382+3547 at 25.41kpc, the distances are highly suspect. Even with a extensive search of the literature, we still failed to obtain a reasonable estimation for these sources. We therefore excluded them from many later calculations. Because of the unreliability of the distance in our analysis we display the area estimation in both arcsec² and pc². Note that for one source 05137+3919, the effective radius was estimated to be 6.5pc. The distance estimate for this source of approximately 11Kpc appeared in close argument in many studies including (Molinari et al., 2002) and is therefore less likely to be in error. The effective size of this grouping of stars is about twice the length of the ONC at 3.8pc (LL03).

Directly from our estimate of the area, for the groups which are close to circular, we calculated the effective radius to be $\sqrt{Area_{arcsec}}/\pi$ and converted it to pc as above.

Figure 3.1: A histogram plot of the effective radii(thus also the Area and Volume) of our embedded clusters(61) and 36 from LL03 catalogue.



see figure 3.1. We then used this effective radius to estimate a volume by assuming a spherical-shape. This is not unreasonable ,relaxed clusters should be approximately spherical (Hillenbrand, 1997). The median effective radius of our clusters is 0.5 pc, thus the median area is 0.79pc^2 and median volume 0.52pc^3 .

The effective radii vary from 0.2 to 2.5 pc (see fig. 3.1 and table 3.1) which is similar to the effective radii collected in the LL03 catalogue. The median effective radius of our study is a little less than 0.5pc across while it combined with the 36 sources of LL03 is approximately 0.4pc. There is a difference in the way that our study and others in this catalogue estimated their sources' radii. We know of no other study that estimated it in a similar fashion as we did. As always the LL03 contains a composite of many method. The most popular of which was to calculate the distance of half the stellar density fall-off from the densest central region(FWHM) to the background (Testi et al., 1998; Muench et al., 2003). It was normal practice then to estimate the area from the effective radii rather than the other way around. Figure 3.1 contains 36 from LL03 and 61 from our study. A complete list of effective radii and areas for each cluster can be seen in the table 3.1.

One possible word of caution with our calculations of the total volume is that we summed the total areas of different subclusters in a region then calculated effective radii and from this the volume. The volume from the combined effective radii will be much greater than if we had calculated the volume from individual effective radii of the subclusters of a hierarchical type cluster. For example an effective radii of 0.5pc split into four subclusters of equal length would produce four volumes of 0.008 pc³ or 0.03 pc³ in total compared to 0.52 pc³ if the effective radii was first summed. Which is 17 times too large. This may account for a diminished stellar density estimate in next section and also in Chapter 5.

Table 3.1: The Area and effective radii of the stellar groupings. The Morphology letter specifies either a hierarchical or centrally-condensed form.

IRAS Name	Morph. letter	$Area$ $arcsec^2$	Eff.Radius arcsec	Dist. Kpc	$\begin{array}{c} {\rm Area} \\ {\rm pc}^2 \end{array}$	Eff.Radius pc	Volume
						_	
00070 + 6503	Н	13070	65	6.83	14.33	2.14	41.05
00117 + 6412	Н	13508	66	1.80	1.028	0.57	0.78
00420 + 5530	С	29066	96	4.30	12.632	2.01	34.02
03211 + 5446	\mathbf{C}	31951	101	4.54	15.478	2.21	45.21
04034 + 5116	С	39641	112	3.98	14.759	2.16	42.21
04579 + 4703	Н	12958	64	2.47	1.86	0.77	1.91
05137 + 3919	Н	42380	116	11.5	131.736	6.48	1139.76
05168 + 3634	Н	41215	115	6.08	35.810	3.37	160.32
05274 + 3345	\mathbf{C}	33282	103	1.55	1.879	0.77	1.91
05345 + 3157	С	49668	126	2.6	7.8927	1.58	16.52
05358 + 3543	С	53004	130	1.80	4.036	1.13	6.04
05373 + 2349	Н	13281	65	2.40	1.798	0.76	1.84
05382 + 3547	Н	72860	152	25.41	_	_	_
05490 + 2658	Н	46575	122	2.10	4.827	1.23	7.79
05553 + 1631	Н	34190	104	2.50	5.022	1.24	7.99
06056 + 2131	\mathbf{C}	54625	132	1.50	2.888	0.95	3.59
06061 + 2151	Н	66163	145	0.10	_	_	_
06063 + 2040	С	45802	121	4.52	21.994	2.64	77.07
06068 + 2030	\mathbf{C}	29076	96	1.50	1.537	0.69	1.38
06103 + 1523	Н	43653	118	4.63	21.995	2.64	77.07
06104 + 1524	Н	48405	124	4.68	24.919	2.81	92.94
06105 + 1756	\mathbf{C}	41012	114	3.38	11.012	1.87	27.39
06155 + 2319	С	54329	132	1.60	3.269	1.02	4.45
06291 + 0421	\mathbf{C}	40003	113	1.96	3.612	1.07	5.13
06299 + 1011	Н	43962	118	0.35	0.127	0.20	0.03
06308 + 0402	\mathbf{C}	28980	96	2.02	2.779	0.94	3.48
06382 + 0939	Н	49323	125	0.76	0.669	0.46	0.41
06584-0852	Н	36371	108	4.48	17.158	2.33	52.98

20028 + 2903	Η	16388	72	1.55	0.925	0.54	0.66
20050 + 2720	\mathbf{C}	34643	105	0.73	0.433	0.37	0.21
20081 + 2720	\mathbf{C}	19106	78	0.70	0.2203	0.26	0.07
20188 + 3928	Η	20717	81	0.31	0.047	0.12	0.01
20205 + 3948	Η	17182	74	4.50	8.178	1.61	17.48
20216 + 4107	Η	29952	98	1.70	2.034	0.80	2.14
20286 + 4105	Η	10405	58	3.72	3.384	1.04	4.71
20293 + 3952	\mathbf{C}	6486	45	2.00	0.609	0.44	0.36
20293 + 4007	\mathbf{C}	34494	105	3.41	9.428	1.73	21.69
20319 + 3958	Η	14692	68	1.60	0.884	0.53	0.62
20343 + 4129	\mathbf{C}	11228	60	1.40	0.517	0.41	0.29
20406 + 4555	Η	2479	28	11.92	8.279	1.62	17.91
20444 + 4629	\mathbf{C}	10232	57	2.42	1.408	0.67	1.26
21078 + 5211	\mathbf{C}	40416	113	1.49	2.109	0.81	2.23
21202 + 5157	\mathbf{C}	22350	84	6.78	24.148	2.77	89.03
21406 + 5110	Η	22864	85	0.59	0.187	0.244	0.06
21526 + 5728	Η	8705	53	8.11	13.46	2.07	37.15
21548 + 5747	\mathbf{C}	4537	38	7.10	5.375	1.30	9.20
22134 + 5834	\mathbf{C}	34003	104	2.60	5.402	1.31	9.41
22147 + 5948	Η	35351	106	7.29	44.158	3.75	220.89
22172 + 5549	Η	49636	126	2.87	9.609	1.74	22.07
22272 + 6358	Η	17141	74	1.23	0.609	0.44	0.36
22305 + 5803	Η	21552	83	5.40	14.771	2.16	42.21
22506 + 5944	\mathbf{C}	26272	91	5.30	17.346	2.35	54.36
22551 + 6221	Η	72837	152	0.70	0.838	0.51	0.56
22570 + 5912	Η	20904	82	5.10	12.779	2.01	34.02
23026 + 5948	\mathbf{C}	23095	86	5.76	18.010	2.39	57.19
23033 + 5951	\mathbf{C}	17422	74	3.50	5.016	1.26	8.38
23146 + 5954	Η	44568	119	4.43	20.558	2.55	69.46
23151 + 5912	\mathbf{C}	29858	97	5.70	22.801	2.69	81.54
23314 + 6033	\mathbf{C}	49775	126	2.78	9.041	1.69	20.22
23385 + 6053	\mathbf{C}	22434	85	6.94	25.397	2.84	95.95
23448 + 6010	\mathbf{C}	24732	89	2.02	2.371	0.86	2.66
23507 + 6230	\mathbf{C}	24167	88	4.28	10.405	1.81	24.84
23545 + 6508	С	66458	145	0.80	0.999	0.56	0.74

3.3 Number of Members

The total number of members in a cluster is one of the most important and fundamental properties of a cluster. With it, one can estimate a total stellar mass and thereby infer star formation efficiency (SFE) and a whole manner of important and nice properties of the cluster, many of which we will see and discuss later. It is not however trivial or even possible sometimes to obtain an exact number of members in a cluster. Determining ex-

act membership of a particular star to a cluster we need data such as the proper motions and accurate distances to each star. This data is not available to us, but with the 2MASS data we have, it is possible to statistically determine the number of members to a good estimation.

Many studies decided to argue that the molecular cloud associated with the embedded cluster will effectively shield from view the background in the region of the cluster. Therefore, the number of stars in the region of the cluster is a mixture of a handful of foreground stars and the members of the embedded cluster. It mite be possible to remove foreground stars by subtracting optically blue detected stars arguing that they are not reddened enough to belong to the embedded cluster, however at least for nearby clusters, the foreground contribution to the total number of stars is likely to be quite minimum. Alot of studies decided to count the total number of stars in a square area around the cluster (Chen et al., 1997), others chose a circular region (Lada & Lada, 1991). We had the out-line of the cluster available to us from the stellar density contour maps (fig 3.2), which should better trace the area of the cluster and so we decided to count all the stars that fell inside the mode $+ 2\sigma$ contour level. We used the polygons formed in the previous section for area estimation and ran a "for" loop to test each K band star, if it fell inside or outside the polygons. This number estimate can be seen column 2 of table 3.2.

For a second number estimate, we assumed that the background and foreground counts did play a large role in the number of stars in the regions of interest. This was done by realising that contour maps are essentially a three dimensional space represented on a two dimensional diagram. Under each of our cluster diagrams, there is a three dimensional mesh surface of stellar counts by arcsecond by arcsecond in the RA and DEC directions. We use this to obtain an statistical number of cluster members to the limiting magnitude of the 2MASS telescopes. We first calculate, by use of a simple Riemann estimate, the total volume ($\star arcsec^{-2}$) under the mesh for the entire arcsecond area. This we set proportional to the total number of stellar counts in our 600 arcsecond squared area. We then calculate the volume of space under the mesh yet above the 'mode + 2σ ' constant stellar count plane. This is proportional to the stellar members in the group and we calculate the number of stars in each cluster, using this method. The results can e seen on table 3.2 column 5.

Due to high levels of extinction by the embedded group/cluster, there will be a reduction in the number of background stars behind the group. If this is the case it will mean that we overestimated the total contribution of the background and foreground stars in the regions. So we expect that our number to be less than the actual number of group members. Carpenter et al. (1993) who also subtracted a total background counts but in a different way argued that this number should be considered a lower bound. Indeed others that used the first method above argued that their number is a maximum or upper-bound of the total detectable members of the embedded cluster to the seeing power of their telescope. We leave both these estimates on table 3.2 as an upper and lower bound to the total number of cluster members in the 2MASS database.

We also estimated stellar densities by using the areas and volume estimates of the last section. Notice that the stellar densities per arcsecond (column 6) range from 0.4 to 1.5×10^{-4} stars per arcsecond squared. This is comparable to the cut-off of cluster detections at 3×10^{-3} stars per arcsecond squared and we are detecting modest increases in stellar density due to the cluster. Table 3.2 also displays stellar densities calculated from the area and volume in parsecs.

Table 3.2: Richness measure, number estimate and stellar density of the 63 groupings

IRAS Name	Number 2σ	$rac{ ext{Area}}{ ext{pc}^2}$	Area arcsec	cluster #	star density 10^{-4} per arcsec^2	stellar density $\star s pc^{-2}$	stellar density $\star s pc^{-3}$
00070 + 6503	120	5.680	13070	15	11.4767	2.64085	0.37
00117 + 6412	104	1.028	13508	16	11.8448	15.5642	20.63
00420 + 5530	75	40.715	29066	28	9.63325	0.687707	0.82
03211 + 5446	112	15.478	31951	33	10.3283	2.13206	0.73
04034 + 5116	60	14.759	39641	23	5.80207	1.55837	0.54
04579 + 4703	78	3.947	12958	12	9.26069	3.04028	6.28
05137 + 3919	104	116.187	42380	17	4.01133	0.146316	0.01
05168 + 3634	72	35.810	41215	14	3.39682	0.390952	0.09
05274 + 3345	87	1.879	33282	32	9.61481	17.0303	16.73
05345 + 3157	116	3.782	49668	38	7.65080	10.0476	2.30
05358 + 3543	74	4.036	53004	24	4.52796	5.94648	3.97
05373 + 2349	40	2.447	13281	7	5.27069	2.86065	3.80
05382 + 3547	104	1105.732	72860	31	4.25474	0.0280357	_
05490 + 2658	110	4.827	46575	36	7.72947	7.45805	4.60
05553 + 1631	63	5.022	34190	14	4.09476	2.78773	1.75
06056 + 2131	147	2.888	54625	57	10.4348	19.7368	15.88
06061 + 2151	124	0.015	66163	39	5.89453	2600.00	_
06063 + 2040	178	21.994	45802	71	15.5015	3.22815	0.92
06068 + 2030	80	1.537	29076	36	12.3813	23.4223	26.09
06103 + 1523	125	21.995	43653	37	8.47593	1.68220	0.48
06104 + 1524	99	24.919	48405	24	4.95817	0.963121	0.26
06105 + 1756	80	11.012	41012	30	7.31493	2.72430	1.10

06155 + 2319	136	3.269	54329	46	8.46693	14.0716	10.34
06291 + 0421	69	3.612	40003	21	5.24961	5.81395	4.09
06299 + 1011	38	3.347	43962	6	1.36482	1.79265	200.00
06308 + 0402	80	2.779	28980	22	7.59144	7.91652	6.32
06382 + 0939	98	0.669	49323	27	5.47412	40.3587	65.85
06584 - 0852	110	17.158	36371	29	7.97339	1.69017	0.55
20028 + 2903	105	5.273	16388	9	5.49182	1.70681	13.64
20050 + 2720	107	0.433	34643	24	6.92781	55.4272	114.28
20081 + 2720	67	0.2203	19106	12	6.28075	54.4712	171.43
20188 + 3928	159	3.043	20717	18	8.68852	5.91522	1800.00
20205 + 3948	77	8.178	17182	10	5.82004	1.22279	0.57
20216 + 4107	57	2.034	29952	7	2.33707	3.44149	3,27
20286 + 4105	55	3.169	10405	6	5.76646	1.89334	1.27
20293 + 3952	96	0.609	6486	15	23.1267	24.6305	41.67
20293 + 4007	94	12.331	34494	12	3.47887	0.973157	0.55
20319 + 3958	107	0.884	14692	22	14.9741	24.8869	35.48
20343 + 4129	48	3.232	11228	8	7.12504	2.47525	27.58
20406 + 4555	89	1.515	2479	8	32.2711	5.28053	0.45
20444 + 4629	73	2.946	10232	6	5.86396	2.03666	4.76
21078 + 5211	152	2.109	40416	40	9.89707	18.9663	17.94
21202 + 5157	73	24.148	22350	13	5.81655	0.538347	0.15
21406 + 5110	101	3.095	22864	15	6.56053	4.84653	250.00
21526 + 5728	115	3.961	8705	9	10.3389	2.27215	0.24
21548 + 5747	38	5.375	4537	3	6.61230	0.558140	0.33
22134 + 5834	91	5.402	34003	30	8.82275	5.55350	3.19
22147 + 5948	92	16.086	35351	17	4.80892	1.05682	0.08
22172 + 5549	240	9.609	49636	37	7.45427	3.85056	1.68
22272 + 6358	55	0.609	17141	10	5.83397	16.4204	27.78
22305 + 5803	77	14.771	21552	10	4.63994	0.677002	0.24
22506 + 5944	143	20.063	26272	28	10.6577	1.39560	0.52
22551 + 6221	275	0.838	72837	44	6.04089	52.5060	78.57
22570 + 5912	95	12.779	20904	18	8.61079	1.40856	0.53
23026 + 5948	59	18.010	23095	16	6.92791	0.888395	0.28
23033 + 5951	50	5.016	17422	9	5.16588	1.79426	1.07
23146 + 5954	122	20.558	44568	28	6.28253	1.36200	0.40
23151 + 5912	72	22.801	29858	12	4.01902	0.526293	0.15
23314 + 6033	144	9.041	49775	35	7.03164	3.87125	1.73
23385 + 6053	26	12.148	22434	2.4	1.06980	0.197563	0.03
23448 + 6010	109	2.371	24732	35	14.1517	14.7617	13.16
23507 + 6230	52	10.405	24167	6	2.48272	0.576646	0.24
23545 + 6508	88	0.999	66458	21	3.15989	21.0210	28.37

The recent embedded cluster catalogues of Lada & Lada, 2003 and Porras et al., 2003 compiled lists from a scan of the literature. Many different studies took various approaches along similar lines of the two main method above, and its not always clear

which method was preferred without going back to the original paper. Most studies had one or two or at most a dozen new clusters, so it was possible for them to make a case by case decision as to which of the above methods (background subtraction or not) was most ideal for them. As we have over 50 new embedded cluster it was not feasible to make a decision for each cluster individually. So with a one size fits all motto, we will be using the background subtracted number for many of the later calculations in chapter 5. The stellar densities of columns 6 to 8 on table 3.2 are from the background subtracted estimate.

Note also that the average number of stars in Srid, Mol-L and Mol-H clusters are 18.8, 20.5 and 25.5 respectively. Once again confirming the hypothesis that these types of sources are at different ages and also suggesting a relationship between the age of the forming massive protostar and the total number of members in the cluster. Notice also that Mol-L sources are consistently closer in value to Srid sources than to Mol-H type source, despite the fact that all overlaps between the MolI study and Srid are with H-type sources (due to the same colour conditions). Thus over 25% of the Srid sources with clusters overlap with the Mol-H sample. The implications to this will be discussed in more detail in the final chapter of this thesis.

Figure 3.2: Stellar contour maps for all 63 groupings of stars. Starting with the last three, same order as appeared in table 2.2

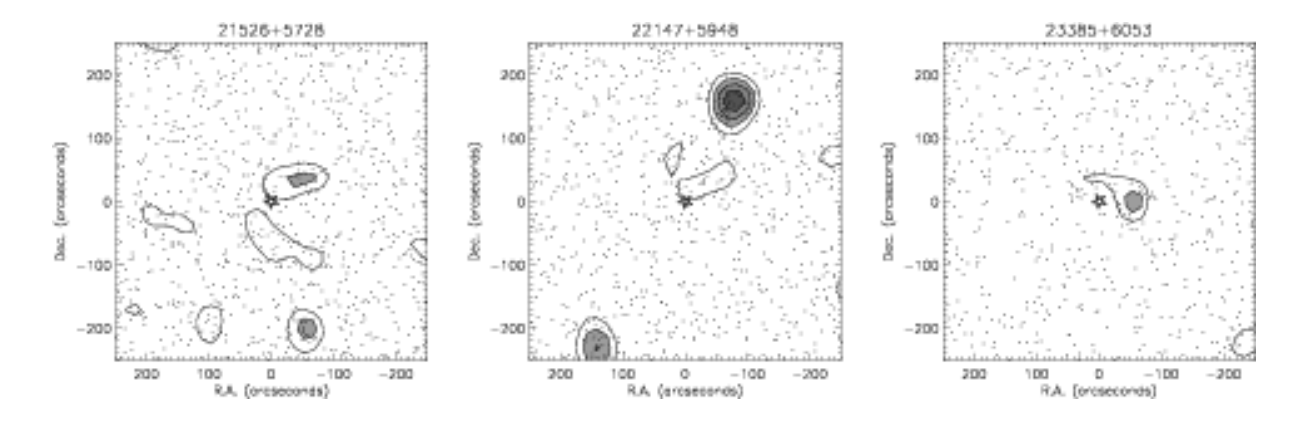


Figure 3.2: figure continued

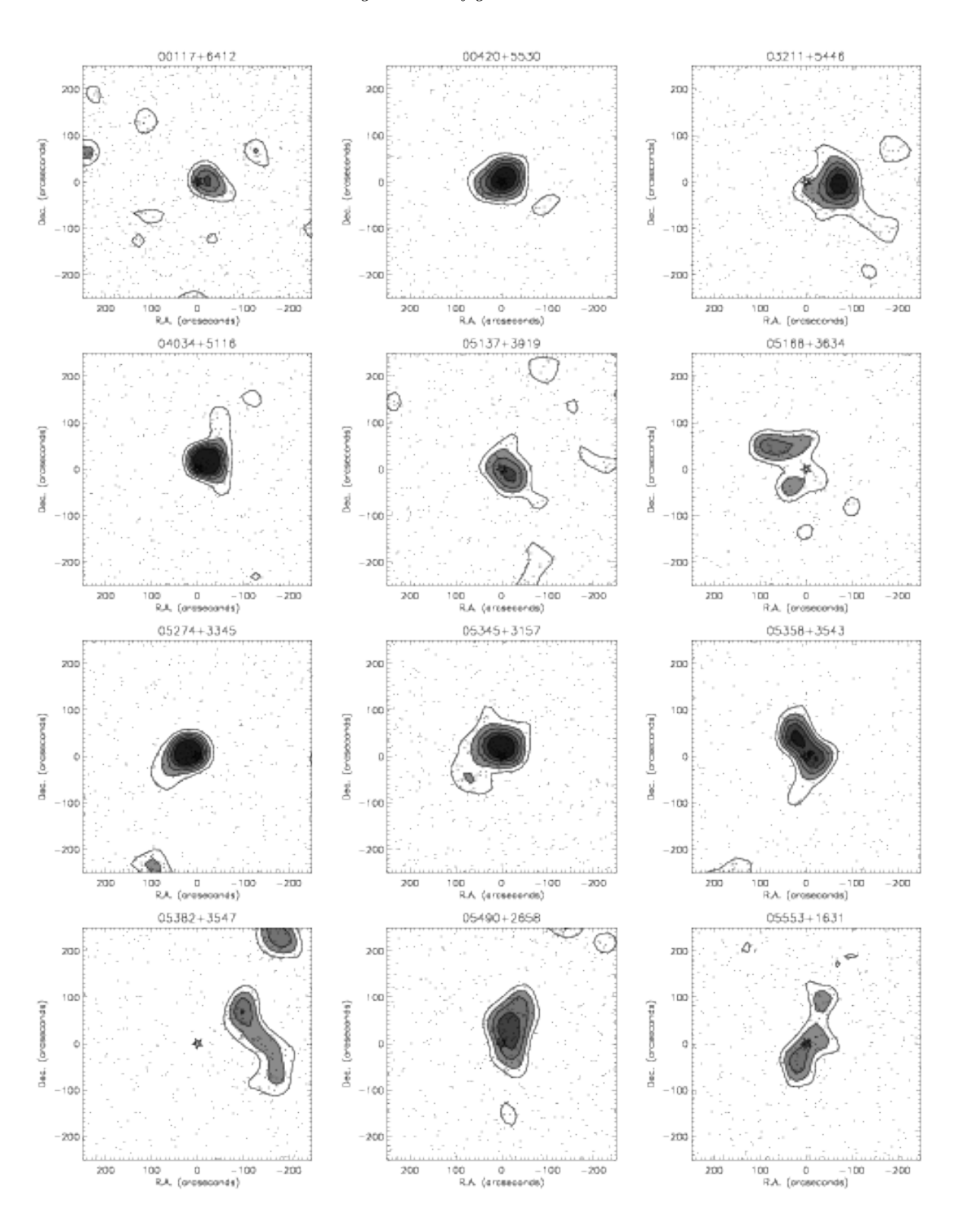


Figure 3.2: figure continued

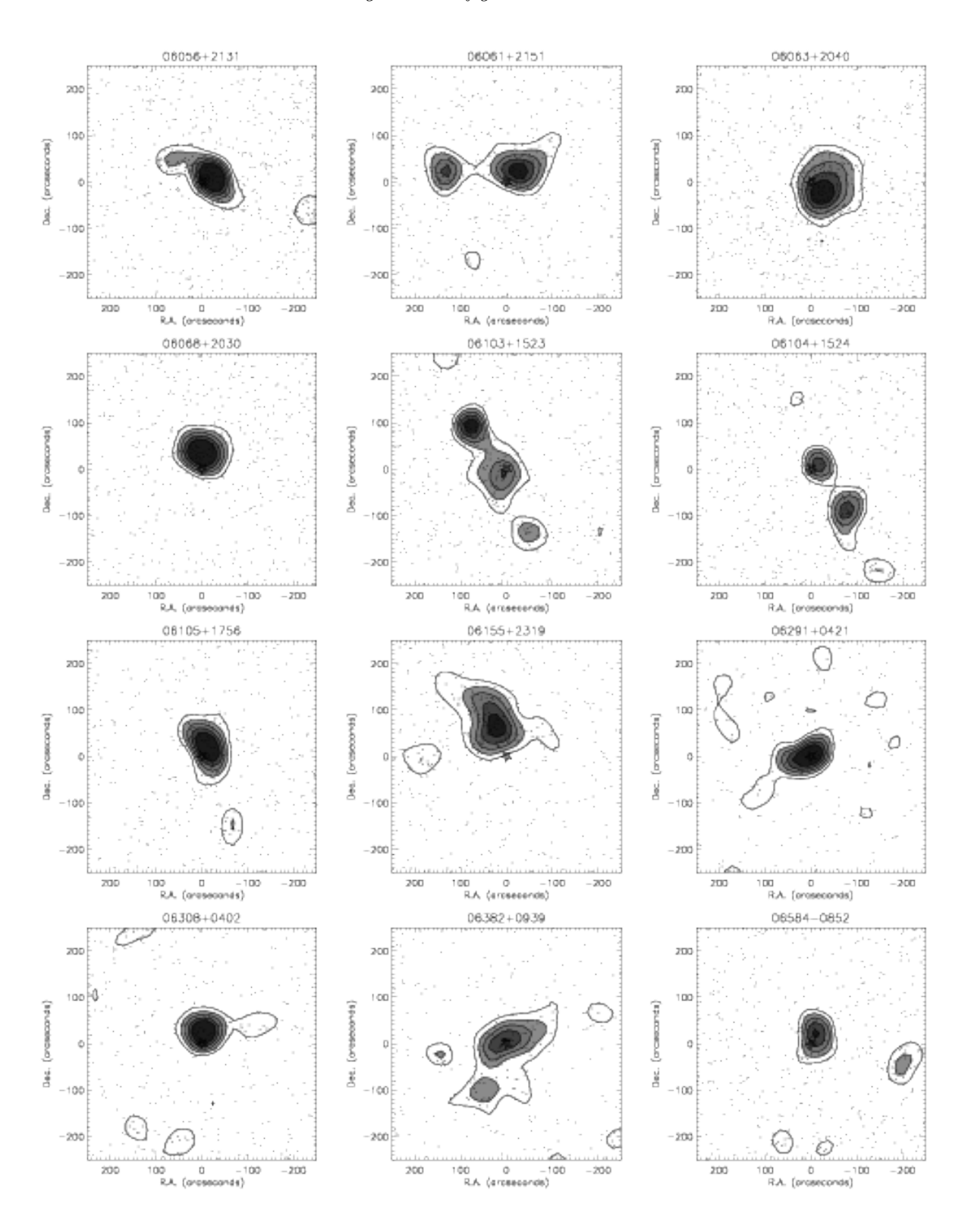


Figure 3.2: figure continued

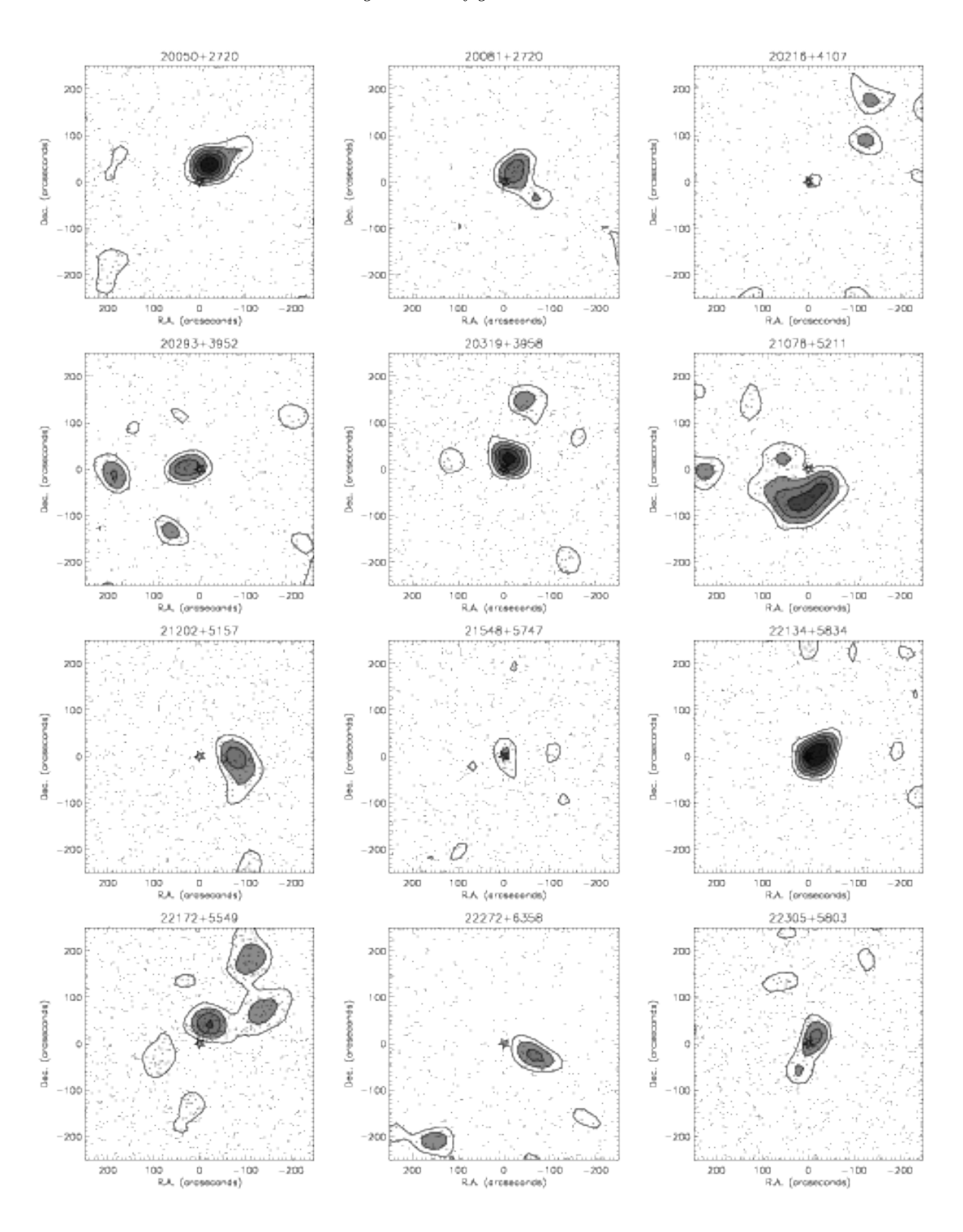


Figure 3.2: figure continued

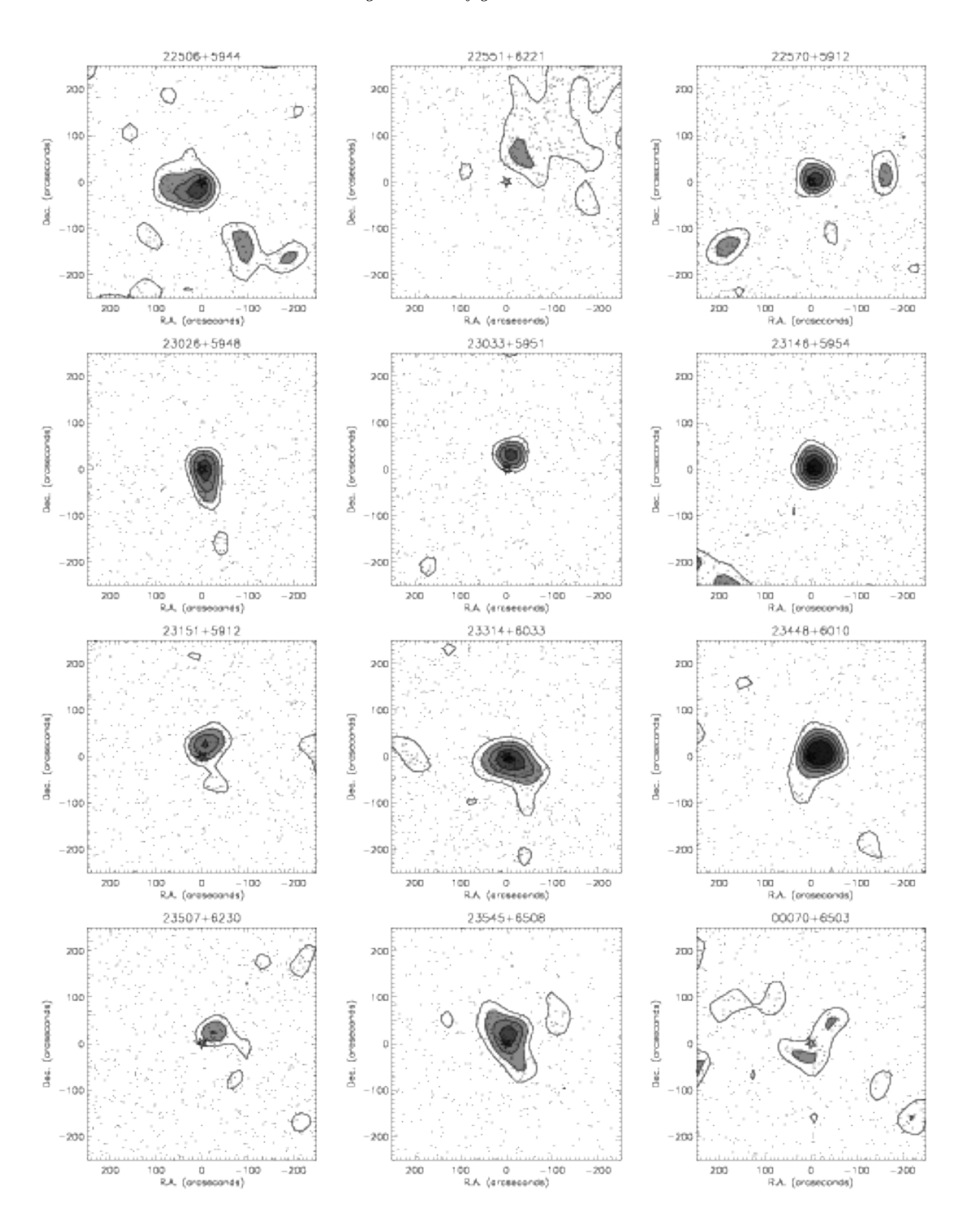
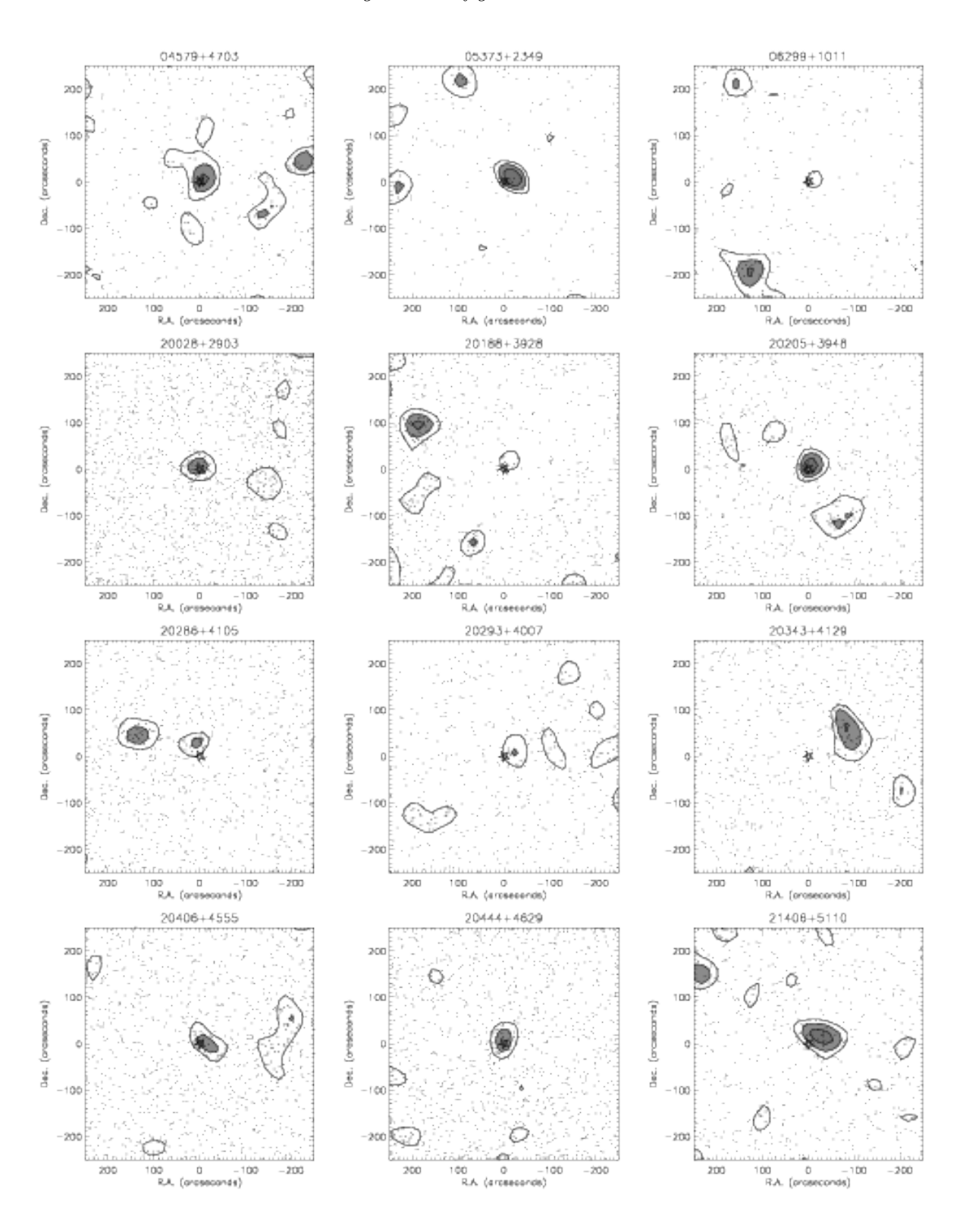


Figure 3.2: figure continued



Chapter 4

IR Colour Analysis on the Cluster sources

Open clusters are an intrinsic part of star formation. Its member are formed from the swirling and contracting clumps of dust and gas within cool dense molecular clouds. Perhaps they competitively accret matter and effect and interact with one another to nurture the growth of its most massive members. Clusters are the ideal locations for study of star formation. As members of the same cluster are born from the same progenitor cloud over a short period of 1 to 2 Myrs, they share identical chemical make-up, similar age and are at almost equal distances. All this means that between members the only major variable is that of mass. They have a statistical significant number of members and are thus the best laboratories for the study of very basic units of star formation processes, such as the star formation efficiencies(SFE) and the initial mass function(IMF).

Traditionally the older exposed open cluster have been preferred over the younger embedded cluster, due primarily to high levels of interstellar dust extinction in the latter that makes both observation and analysis more difficult. However we can learn alot more with studies into embedded clusters. They are regions that are still actively engaged in the star formation processes, or have very recently ceased and therefore these cluster will contain all its original members, before they've had time to evaporate or otherwise be ejected from the cluster. The new IR cameras and multiple wavelength near-infrared analysis can to an extent open the door to highly extincted embedded clusters. Firstly the K-band can penetrate deep into molecular clouds, almost 10 times deeper than that of the optical V band and detect the presence (chapter 2) and coordinates of possible members, while J band better maps the temperature of the photospherical core of the newly forming protostars.

The conceptual idea of colour can be measure in the optical, IR and other wavelengths as a measure of the magnitude differences of the same object seen through different filters. Any contacting protostar will naturally radiate energy at different wavelengths according to its underlying blackbody function and therefore different objects will display different colours. In the optical and IR regimes at least, the interstellar dust and gas between radiating object and camera detector will extinct percentage wise more electromagnetic radiation at shorter wavelengths than at higher. Thus in the NIR, more light at the $J(1.25\mu m)$ wavelengths will be extincted than compared to the $K_s(2.2\mu m)$ wavelength and hence the object under extinction will appear redder than it naturally is. In addition to this, this form of extinction is predictable and objects can be effectively de-reddened. However, the colours of young stellar objects can be complicated further, the surrounding nebular disk which is characteristic of young protostars will extinct and shatter the light, dependant on the angle of the disk to the viewer.

In this chapter, we adopt two well-known colour analysis techniques to probe the grouping detected and massive (pre) UCHII of the sample.

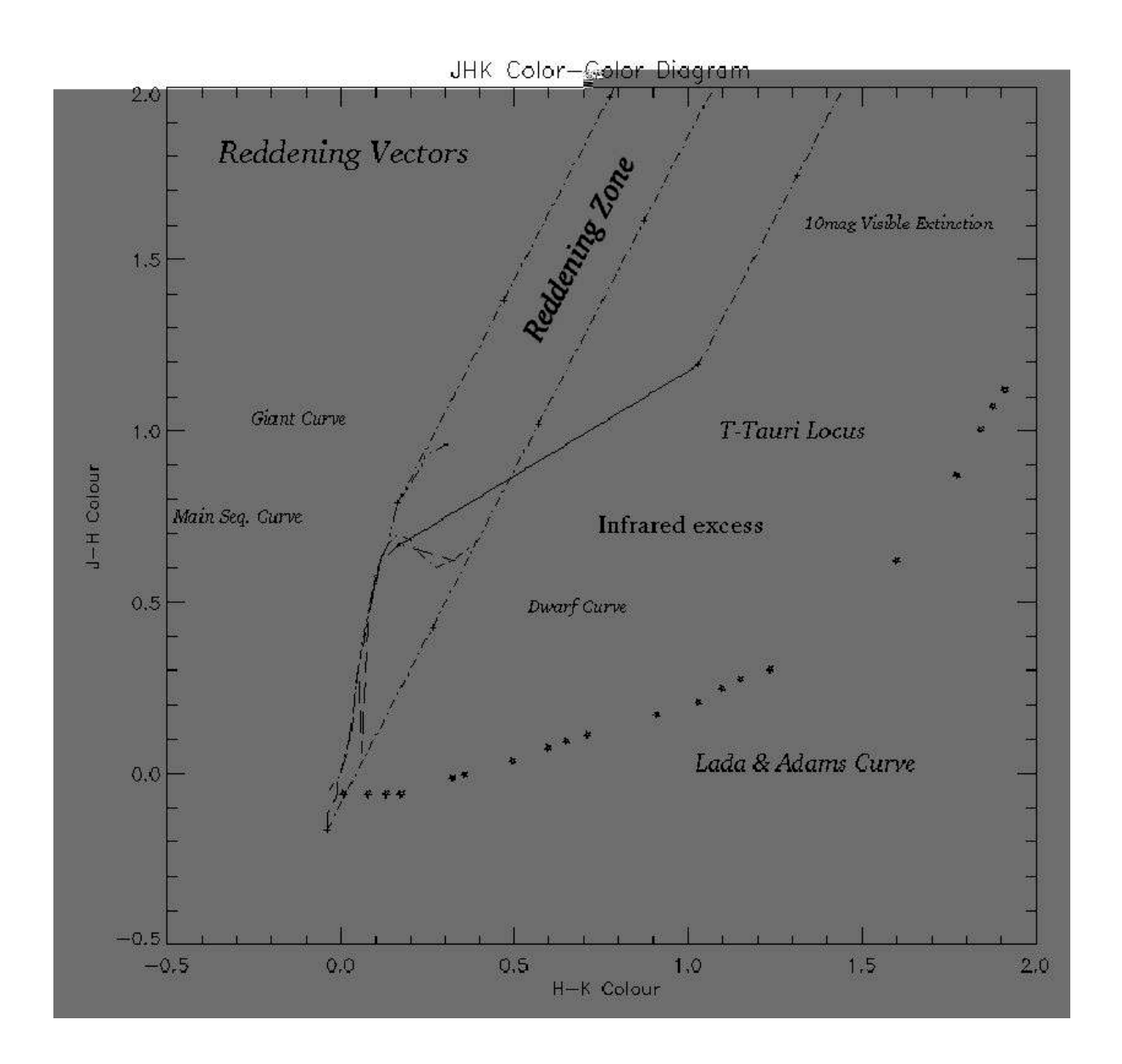
4.1 Color-Color Diagrams

A JHK color-color diagram can be thought of as a plot of the slope of the spectrum of the star at the wavelength position H. However, probably more intuitively, it is just thought of as a simple plot of magnitude differences in the colours (J-H) and (H-K) of stars. Either way, the useful analytic aspect of cc-diagrams is that stars with different basic properties inhabit different locations on the diagram.

There has been considerable theoretical and observational research to interpret the significance of the different regions in a cc-diagram. Bressel & Brett, (1988) estimated the colours of main sequence stars as well as giants and dwarfs of different spectral types. These form three separate but overlapping loci, quadratic in appearance extending from a little below the origin and bounded to less that one in each colour direction. The Bressel & Brett, (1988) paper, henceforth B&B, also calculated a set of linear transformations between colours of several different JHKL systems as well as a list of reddening relations. We decided to use the B&B system, so all data both graphical and 2MASS to be displayed in colour form must be first transformed into the B&B system. The linear transformation between 2MASS and B&B is

$$(H - K)_{BB} = 1.0298 \times (H - K)_{2MASS} - 0.0350$$

Figure 4.1: Different regions on a colour-colour diagram as explained in the text



$$(J-H)_{BB} = 1.0101 \times (J-H)_{2MASS} - 0.0495$$

as found on the 2MASS website

http://www.astro.caltech.edu/~jmc/2mass/v3/transformations/.

Jones and Hyland, (1980), found no evidence for variation in the ratios of colour excess E(J-H)/E(H-K) on the basis of photometry of reddened stars. Using the B&B relations we calculated the slope of the reddening vectors. These were drawn from the two ends of the main sequence curves forming two parallel lines. So, stars which fall between the two lines, i.e in the reddening zone are most probably normal main sequence stars showing the effect of normal interstellar extinction (see fig 4.1). Furthermore, we represented each

five magnitudes of visible extinction along these reddening vectors by a small cross.

The T-tauri locus (Meyers et al., 1997) extends into the area of infrared excess and accounts for the positions for normal T-tauri stars on the cc-diagram. The circumstellar disks that surround T-tauri stars can re-manufacture the radiation from the central protostar to appear abnormal when compared to normal stars in the reddening zone. The effect of the circumstellar disk will depend both on its size and on its viewing angle and therefore the T-tauri locus extends both inside the normal reddening zone (where the circumstellar disk is at a planar angle) and also deep into the area of infrared excess (where the disk is at right angles to the observer). Lada and Adams, (1992) explained the observed positions of AeBe stars on cc-diagrams, by theoretically modelling AeBe stars with centrally holed stellar disks. The Lada and Adams' curve that we have used in our diagrams is that of a 12,000K AeBe star with a 1,000K disk temperature with the size of the central hole as the parameter being varied. The curves for other disks with higher and lower temperatures were of similar curvature but of higher initial slope which made them extend up along the extinction boundary of the T-Tauri region. And thus any stars that lie just above this Lada and Adams' curve are probably AeBe star with a centrally holed stellar disk.

4.1.1 cc-diagrams of the 63 groupings of stars

We wanted to apply cc-diagram analysis to our IRAS sources that showed clear groupings of stars as in chapter 2. We have to deal with the normal problem of possibly having more background and foreground stars than cluster members themselves. We can nevertheless maximise the number of cluster members as well as minimise the number of background stars by plotting only those stars that fall within the mode+ 1σ contour. Although this may have the undesired effect of excluding some cluster members that are at the outer extremities of the cluster, it will have the benefits of taking presumably the densest areas of the cluster. Also, the dust and interstellar extinction is higher in these areas, leading to a reduction in the number of background stars. With this in mind our cc-diagrams will still have a high number of non-members, depending on its internal extinction and distance from the sun(no. of foreground stars).

Other techniques could be used to remove foreground stars, such as removing comparisons with an optical study such as USNO. It can be assumed that optically detected, at least optically blue stars are not reddened enough by interstellar dust and hence not within the embedded clusters and most probably foreground stars. This was done and

 $\label{eq:Figure 4.2:} Figure~4.2:$ Color-Color diagrams of the 63 IRAS sources that displayed clusters.

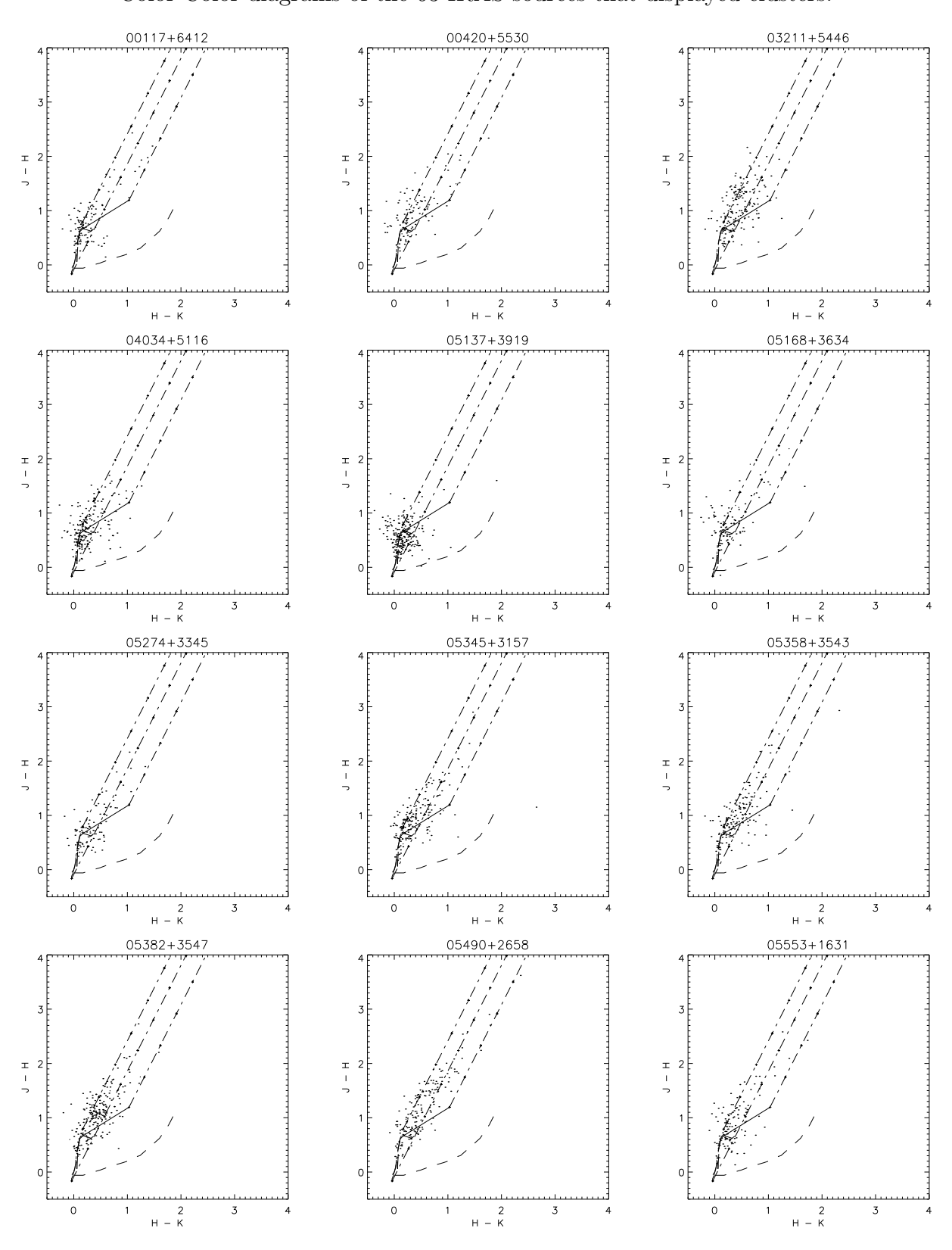


Figure 4.2: figure continued

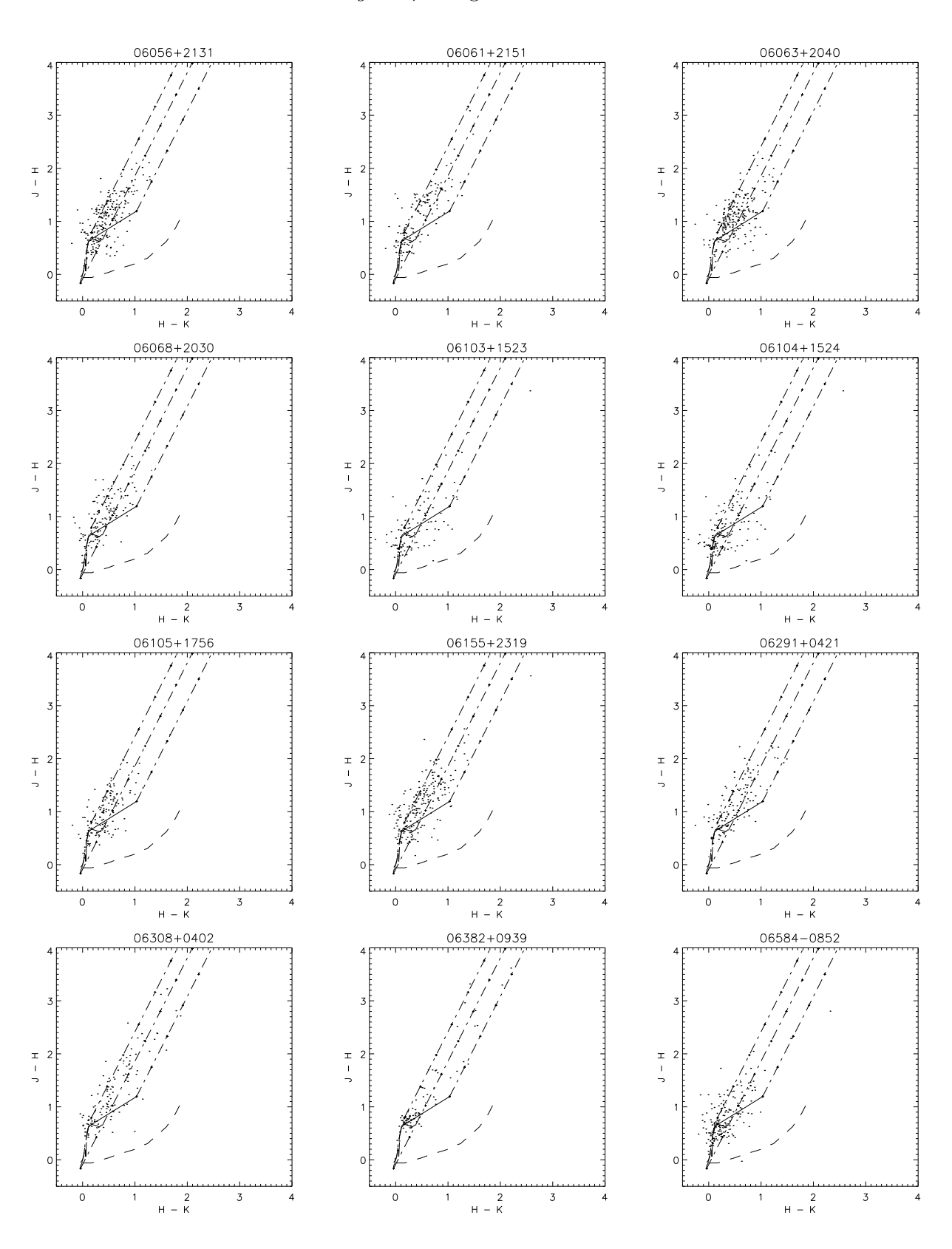


Figure 4.2: figure continued

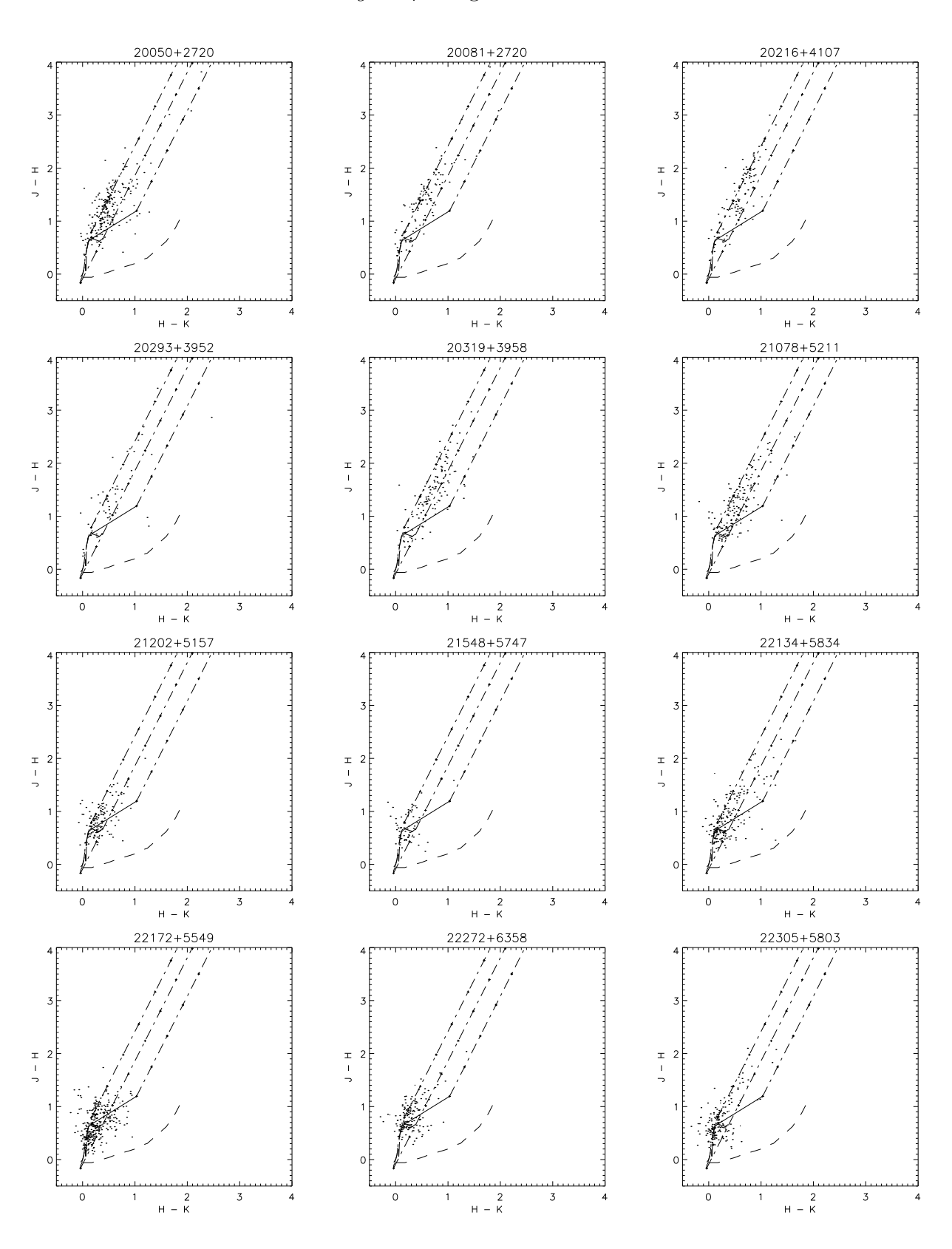


Figure 4.2: figure continued

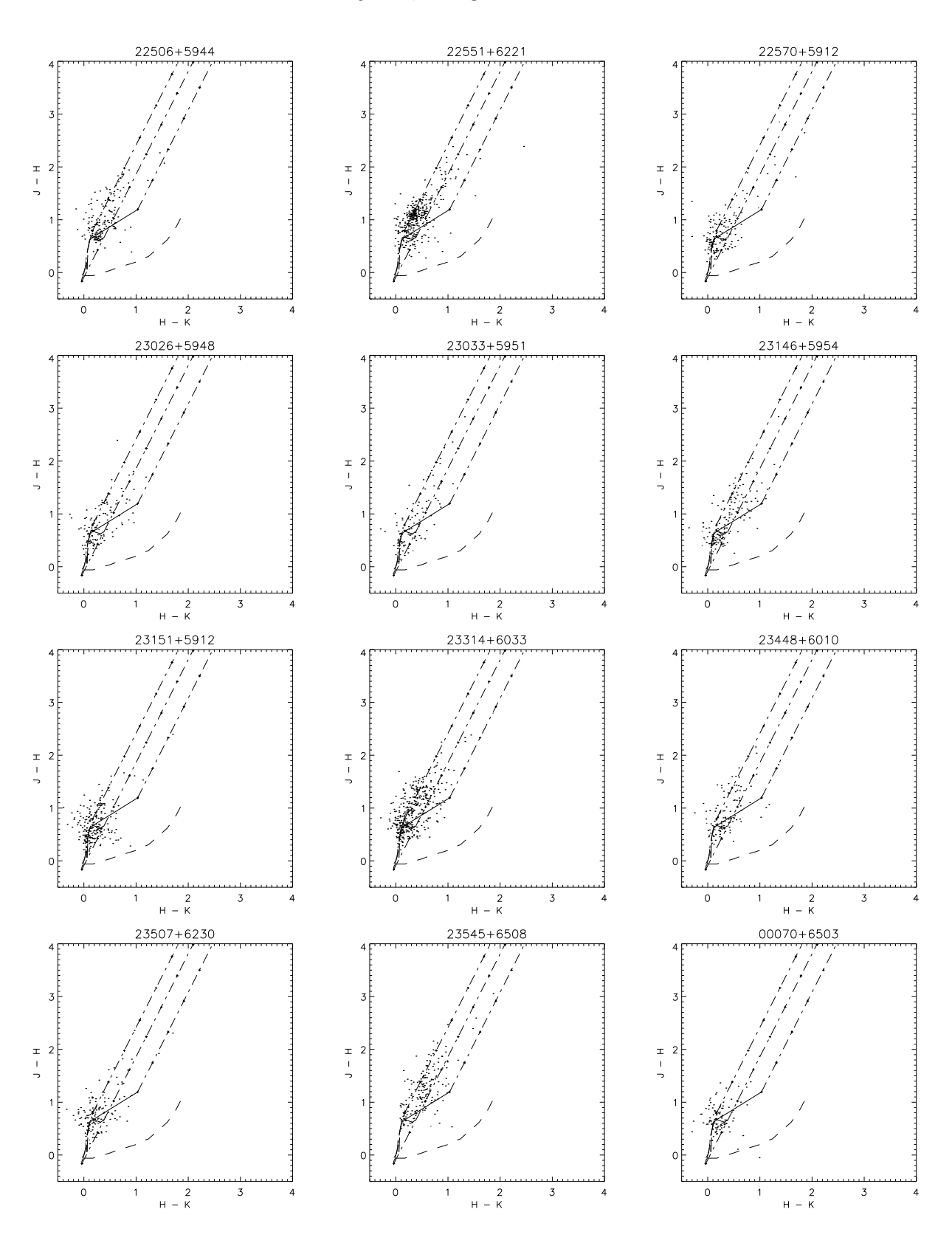


Figure 4.2: figure continued

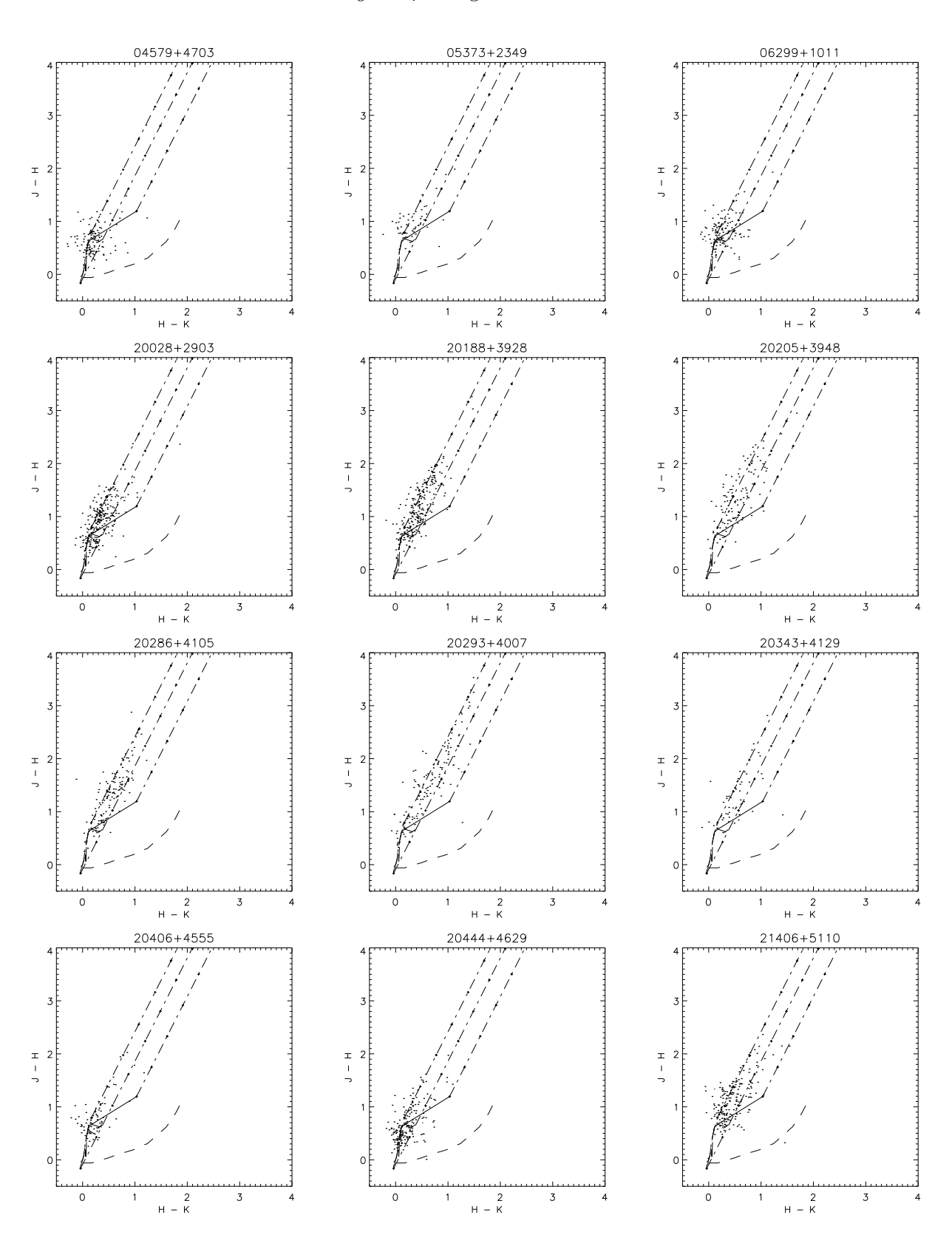
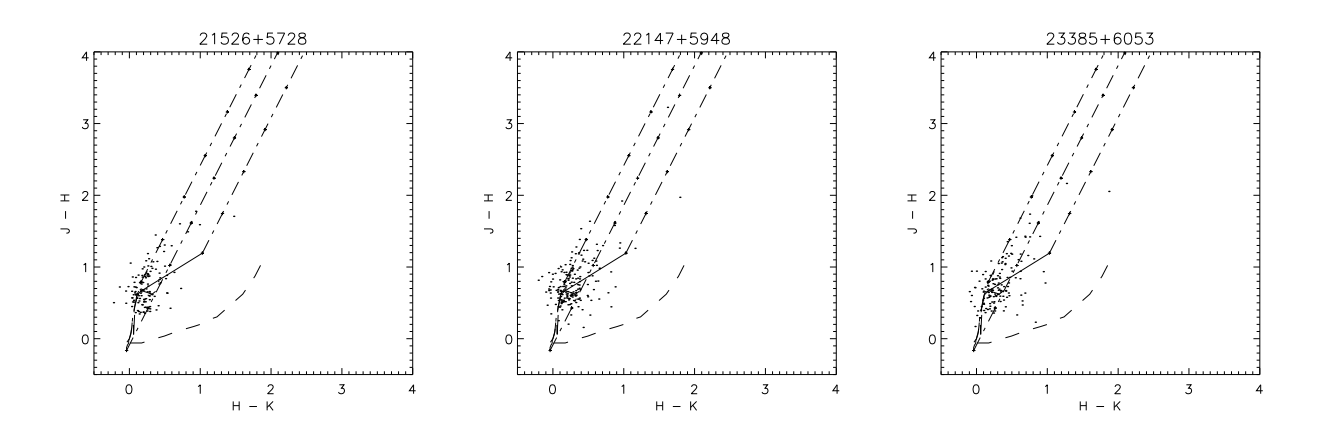


Figure 4.2: figure continued



had promising results removing much of the stars around the main sequence curves and display a clear beginning to cluster members at a height above the main sequence curve. This technique was not however applied for this thesis due to time constraints as well as difficulties resulting from such a high number of sample sources.

We selected stars which fell only within the $mode + 1\sigma$ contour by using the polygons formed as described in area estimation as in chapter 3. If the star position fell within these polygons, then we applied the additional photometric constraints which were already applied to the K band stars to both the J and H bands. We calculated the colours and converted them into the B&B photometric system and then plotted them in the cc-diagrams which can be seen at the end of this subsection.

Soares et al. (2002) plotted the magnitudes of the J, H, K bands as a function of their 2MASS data errors. Errors were all low in all bands up to 13.5mags were K band errors started to rise exponentially, followed by H at 14mags and J at 14.5mags. K band error seemed to diverge from H at all magnitudes and likewise H with J. As their work was based on the first Incremental Release of 2MASS, an earlier database, they used this to determine a maximum magnitude of stars to minimise error in their analysis. For us and our cc-diagrams, this explains some of the artifacts that we see. For the y-axis, the (J-H) colour, uncertainties will increase as H increases, i.e when the colour is low. Similarly for (H-K), errors will be greatest when it is low. This seems to be consistent with the obvious artifacts lying to the left of the main sequence loci in most of the cc-diagrams.

The percentage of stars within the areas of infrared excess to those in the main sequence areas can be considered as a crude measure of age. Infrared excess is not the same as reddening of dust extinction, it results from the presence of circumstellar dust around the

stellar objects, a known property of young forming stars. A ratio of member stars with and without infrared excess would be a possible factor of the age of the cluster. It is too much to discuss each cc-diagram here, we bring the readers attention to the large variance in extinction on these diagrams, some clusters such as 20319+3958 extend objects over 20 A_v , while other clusters such as 04579+4703 contain all its members close to the main sequence curves and therefore of low extinction. All our clusters contain the majority of objects close to the main sequence. Clusters such as 23314+6033 seem to even map the normal main sequence curve as well as the massive curve. This cluster also has a weak but observable secondary group of objects a little above these stars. This may be the main sequence members of the group.

Some cc-diagram of these IRAS sources have appeared in earlier works, namely 20050+2720 in (Chen et al., 1997) and 22134+5834 in (Kumar, Ojha & Davis, 2003). The cc-diagram of both this thesis and Chen et al., 2003 compare quite well, even without transforming colours of the same system and noting that there is a difference in the power of the telescopes used. Both have similar sources that extend into the T-tauri zone and areas of AeBe stars, although its not easy to directly identify each source in these areas. The errors are largest for lower colours. At the top of the diagram were errors will be less, there is a clear one to one correspondence.

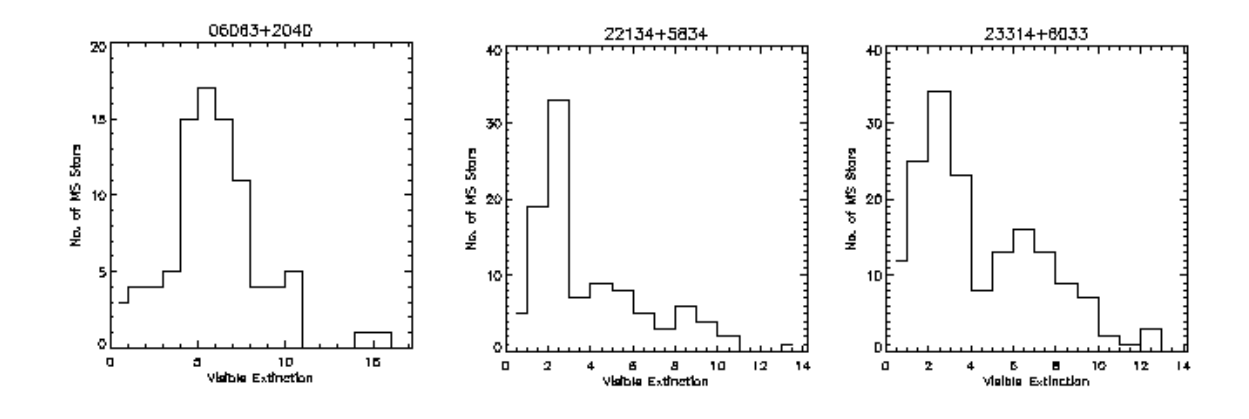
The cc-diagram of Kumar, Ojha & Davis (2003) on IRAS 22134+5834 has few similarities with the one of this thesis, even though they are both in the same B&B system. There may be many reasons for this, firstly it is possible that the studies focused on different regions, the Kumar, Ojha & Davis study focused on the inner 100 arcsecond area around the IRAS coordinate, while this region may of fell outside the region of greater stellar density (above the mode+ 1σ) contour level. Secondly there was substantial difference between the UKIRT telescope which they used (17 mags completeness limit) and the 2MASS telescopes. And finally they argue that IRAS 22134+5834 is a very special type of cluster which may be its quite possibly atypical of the others in this thesis. A characteristic feature in their diagram is an object of negative (J-H) colour. This does not appear on our diagrams and may fall outside the window of the cc-diagram figure, but nevertheless this characteristic object appears to be present in about 10% of the cc-diagrams of this thesis, while 50% have objects in the area expected of AeBe stars. Other cc-diagrams of our sample appear in (Carpenter et al., 1993)

4.1.2 A Measurement of the Dust Extinction

An estimate for dust extinction for each cluster in our sample can be made with the aid of cc-diagrams. Stars that fell inside the reddening zone (i.e are most likely MS stars) can be effectively de-reddened by transforming them parallel to the reddening vectors, till they intersect their respective positions on the main sequence curve. Unfortunately, this transformation is not injective, so the precise spectral type of a star cannot be uniquely determined by the use of cc-diagram analysis alone. Without ridding the degeneracy, we can approximately alleviate this problem for extinction quantification by drawing an imaginary straight line perpendicular to the reddening vectors which best fits the main sequence curve. Note also the existence of more lower mass types than higher, so the line should be biased in favour of the lower. We calculate the perpendicular distance, i.e parallel to the reddening vectors, of all the stars that fell inside the reddening zone to this imaginary line and convert these lengths into K band extinction by use of the B&B relations. We use this technique for all stars within the $mode + 1\sigma$ contour, as above and as per the diagrams at the end of the last subsection. This gives an extinction value for every main sequence star, whose RA and DEC fall within an area of high cluster probability. We constructed an histogram using these extinctions values, into bins of 1 mag of visible extinction and we assumed that the peak in this histogram was due to the cluster and a measurement for extinction to that cluster (see table 4.1).

The estimates for dust extinction was taken from the histograms, that can be seen pages figure 4.3 of this thesis. The mean visible extinction and standard deviation was written into the table directly from IDL code. The actual measurement for visible extinction was taken in a more haphazard way. Where a clear peak in the plots existed, we assumed that this was due to cluster members and therefore a measurement of extinction to the

Figure 4.3: Extinction histograms for three of the Clusters



cluster. Where two peaks of almost equal height we favoured the peak of most extinction, assuming that the first peak was due to foreground stars (with background stars shielded from vision by the molecular cloud).

 $Table\ 4.1:$ Extinction measurement from use of cc-diagram analysis

IRAS Name	$\begin{array}{c} \text{Visible} \\ \text{Extinction} \\ \text{A}_V \end{array}$	Mean Extinction	Standrad Deviation	Maximum Extinction	Extinction (K band) A_K
Groups Detec	cted				
00117+6412	2	3.23488	2.60429	12	0.3
00420 + 5530	5	4.03852	2.26433	8	0.6
03211 + 5446	5	5.16824	3.07853	14	0.6
04034 + 5116	2	3.18976	2.31916	10	0.3
05137 + 3919	2	2.19639	1.56696	8	0.3
05168 + 3634	3	2.90661	1.85640	8	0.4
05274 + 3345	4	3.61705	3.33032	15	0.5
05345 + 3157	5	4.48329	2.58090	11	0.6
05358 + 3543	4	4.99675	3.10962	16	0.5
05382 + 3547	7	5.55906	3.14974	15	0.8
05490 + 2658	5	5.66154	3.53663	14	0.6
05553 + 1631	3	4.38197	2.78409	12	0.4
06056 + 2131	7	5.15280	2.86011	14	0.8
06061 + 2151	9	5.57285	4.17349	17	1.0
06063 + 2040	6	5.93780	2.78658	15	0.7
06068 + 2030	5	4.68704	2.83566	10	0.6
06103 + 1523	2	3.07871	2.82656	9	0.3
06104 + 1524	2	2.96789	2.67487	9	0.3
06105 + 1756	9	5.04506	2.94215	13	1.0
06155 + 2319	5	5.83025	3.30349	13	0.6
06291 + 0421	4	5.60965	3.26634	12	0.5
06308 + 0402	5	7.32657	5.06220	24	0.6
06382 + 0939	4	4.72838	2.64467	11	0.5
06584 - 0852	3	3.30581	2.66020	12	0.4
20050 + 2720	6	5.82345	2.74356	12	0.7
20081 + 2720	9	6.06823	4.32452	15	1.0
20216 + 4107	8	7.87820	4.00426	17	0.9
20293 + 3952	7	6.46988	2.89241	11	0.8
20319 + 3958	9	8.54386	4.28583	19	1.0
21078 + 5211	5	6.66500	3.52032	16	0.6
21202 + 5157	4	4.03637	2.17129	10	0.5
21548 + 5747	2	2.80868	1.73661	6	0.3
22134 + 5834	3	3.97332	2.68705	13	0.4

22172 + 5549	2	2.66639	1.79174	7	0.3
22272 + 6358	3	3.83729	1.88758	8	0.4
22305 + 5803	3	2.95862	2.48943	11	0.4
22506 + 5944	4	4.93277	2.45103	13	0.5
22551 + 6221	7	5.75278	2.40879	14	0.8
22570 + 5912	2	2.99462	2.19835	9	0.3
23026 + 5948	2	3.11750	2.31427	9	0.3
23033 + 5951	2	3.49947	3.26972	17	0.3
23146 + 5954	2	3.95023	3.43033	22	0.3
23151 + 5912	3	2.48346	1.93114	11	0.4
23314 + 6033	5	4.38698	2.88318	13	0.6
23448 + 6010	4	4.23500	2.86033	14	0.5
23507 + 6230	3	3.13971	2.03288	9	0.4
23545 + 6508	6	6.71089	3.17927	14	0.7
Possible Groups	s Detecte	ed			
00070 + 6503	3	2.91291	1.60303	8	0.4
04579 + 4703	3	2.35153	1.56409	7	0.4
05373 + 2349	4	5.09812	2.20694	11	0.5
06299 + 1011	3	3.69492	2.08091	10	0.4
20028 + 2903	6	4.17592	2.38241	10	0.7
20188 + 3928	5	5.63234	3.40400	23	0.6
20205 + 3948	5	6.91745	3.26578	15	0.6
20286 + 4105	7	6.64386	3.38893	15	0.8
20293 + 4007	5	7.65541	4.97972	23	0.6
20343 + 4129	6	7.63105	3.43905	14	0.7
20406 + 4555	4	3.54713	2.09826	9	0.5
20444 + 4629	2	2.43959	1.97881	9	0.3
21406 + 5110	5	5.95133	2.77648	15	0.6
21526 + 5728	3	3.25976	2.03697	10	0.4
22147 + 5948	3	3.41061	1.67894	8	0.4
23385+6053	4	3.82950	2.46978	12	0.5

The usefulness of quantifying extinction for very young stellar clusters in this way is questionable. Most of the members of the groupings are in a pre-main sequence phase and therefore cannot be de-reddened to the main sequence curve. In fact, most of the main sequence stars that go into making these histograms are probably not stellar members of the clusters at all. We are therefore trying to get an extinction estimate from a very modest number of main sequence cluster members. It would of been possible also to attempted to improve extinction estimates for embedded clusters by de-reddening objects that are inside the expected T-Tauri reddening zone to the T-Tauri loci, such as in (Carpenter et al., 1997). We however did not do this, as we believed, it would not improve or

estimate. Our clusters are in regions defined as containing UCHII regions whose colours are presently not well defined and may inhabit the region of the T-Tauri reddening zone. Other higher mass stellar objects such as Herbig AeBe stars are know to inhabit these regions. Considering the completeness limitations of the 2MASS database, we do not expect that a high enough ratio of T-tauri stars to Herbig AeBe stars(and others) will be detected to justify the usefulness of including such a method.

The average extinction estimates on table 4.1 range from 2 A_v to almost 10. The (Kumar, Ojha & Davis, 2003) paper measured a dust extinction estimate for IRAS 22134+5834 using similar cc-diagram analysis, except that their main sequence best-fit line was not intentionally biased in favour of low mass stars as ours was. Their estimate was 5 A_v compared to our $3A_v$. Although the small difference of $2A_v$ would be easily accounted for by the position of the main sequence best fit line, in addition to this, they used a more powerful telescope which detected bright stars with extinction between 20-40 A_v . A few of these bright stars would easily shift their average extinction estimate higher than ours. We included on table 4.1 a measurement of the highest extincted star detected for each cluster. In the case of IRAS 22134+5834, the highest extinction measured was 13 A_v . The maximum extinction estimates range from 7 A_v to the mid-twenties for all the 63 clusters.

4.1.3 The Colours of Massive Protostars

We have already seen a selection process(section 1.2) that used the colours of an object to select a sample. The colours of UCHII regions are known in the FIR(Wood and Churchwell, 1989) and both Srid and Palla et al., 1991 used IRAS colours to identify candidates. They did so because using colours is a cheap and simple way to find a particular object and It would be very desirable to find a set of colour constraints in the NIR typical of young massive protostar. With it we could locate a very illusive object using simple analysis and near infrared all-sky surveys such as 2MASS or DENIS.

Massive protostars may inhabit a closed tidy region of the cc-diagram but as (Menton & Reid, 1995) massive protostars will spew out very little NIR energy, it is likely that the ratios of the magnitudes that produce colours will have more uncertainty and thus form a less bounded and more dispersed area of the JHK cc-diagram than in the FIR cc-diagrams. Some theoretical work has been done into this question. The already mentioned paper (Lada & Adams, 1994) modelled the locations of Herbig AeBe stars with centrally holed circumstellar disks. These being in a region of high infrared excess, one might assume that the massive counterparts of these intermediate high mass stars to be

located in their vicinity. In the color-color diagrams on figure 4.2. Two-Thirds of these diagrams contain object that are close to the Lada & Adams Curve. This is consistent with the existence of intermediate high mass stars. About 10 of these diagrams contained objects below this curve, which is outside the possible regions expected for AeBe stars with centrally holed circumstellar disks. Massive stars form in dense region of alot of stellar and photometric confusion and may not appear as point sources. Therefore, the color-color diagrams of the last section may not contain the massive protostar, due to our selection of photometric quality conditions.

It was speculated that Srid, followed by Mol-L and then Mol-H are statistically the youngest to oldest in that order before commencing this research and we have many times mentioned this and supported it, to an extent, in chapters 2 and 3 with new data. We separated the 217 IRAS sources of our original sample into a younger and older group. MolIII selected sources from the original MolI list that had circumstellar disks, a sign of youth. Beut and MolIII used 1.2 and 1.3 mm continuum emissions to calculate positional offsets from the central IRAS coordinates to the peaks in molecular cloud density. We will consider these as the younger set(group A) of our sample. MolII looked at 67 IRAS sources using the VLA radio continuum free-free emissions representing the sources associated with HII regions. These are therefore considered to be the older group B. We calculated the exact RA and DEC coordinates using the positional offsets in Beut, MolII and MolIII and then went back to the GATOR database to obtain point sources data within 5 arcsecs from (PSC) and extended sources within 10 arcsecs from (XSC) around these sources. A cc-diagram of group A and B can be seen figure 4.4.

We represented points sources as open circles and extended sources as open stars. The difference between these two cc-diagram is striking. In group B, the older all objects are confined to the defined areas of the reddening zones of both main sequence and T-Tauri stars and above in Lada & Adams' curve. We also see a concentration of the objects around the giant main sequence curve. Group A contains a massive spread of stellar objects into areas of infrared excess. It contains loads of objects which are below or outside the brow of the AeBe curve. The group A also contains objects that are further to the left of the diagrams. This may suggest an evolution of young massive protostar to the giant main sequence.

If the photometric constraints are applied to these diagrams almost all the points in the infrared excess disappear from both diagrams and the plots look almost identical. This perhaps adds some concern to our photometric selection (section 1.3). Although we are choosing real stars, for the embedded cluster detected, we may have excluded the massive

Figure 4.4: Colours of massive protostars for a younger and older group

protostar and this may in turn question the usefulness of the cc-diagrams of the previous subsection and also question whether we are excluding some low mass protostars particularly of infrared excess for both cluster detection and property determination. However, the numbers are likely to be low in this case as the photometric conditions were only applied to the K-band for the analysis of chapter 2 and 3 and the forthcoming chapter 5.

0

1

H-K

2

3

3

4.2 Color-Magnitude Diagrams

2

1

H-K

0

0

A color-magnitude diagram is a simpler form of the Hertzsprung-Russel (HR) diagram. In our near infrared study, it substitutes the required luminosity with that of the K magnitude and the temperature with the H-K colour. Since cm-diagram contain only photometric data from two bands, more of the original K band stars fulfil the photometric quality constraints and so a greater number of them are displayed on these diagrams compared to the cc-diagrams of the previous section. We will now discuss the cm-diagrams in relation to our clusters.

Our selection process for choosing which stellar objects to display on the cm-diagram is different to that of the cc-diagram. We split our 600 arcsecond squared area, into two areas of equal size, one an inner region and the other an outer. This makes an inner

box of length $200\sqrt{3}$ arcseconds long. We plot all the stars within this inner region that fulfils the normal photometric conditions in the H and K bands. By observing the cluster boundaries of the contour plots at the end of the chapter 3, this will predominately cover the clusters area in 95% of the cases. And therefore should contain almost all detectable cluster members for most clusters.

These graphs can be seen figure 4.5. The characteristic fan-shaped spread of the cmdiagram shows most massive members, located high in the diagrams, of low numerical K magnitude. Stellar objects of greater extinction are spread to the right of the diagram according to the B&B relation, $E(H-K) = 0.34A_v$. It is possible to draw a grid of spectral type using the B&B relations on these diagram. This is fitted in place by calculating the position of the grid according to the clusters distance and extinction. Due to errors in the distance, this grid sometimes appeared in the wrong location of the graphs. It also had the effect of obscuring some of the finer points of the diagrams. So we removed it in the final print. The effect of extinction on a source will decrease its K_{mag} by $A_k = \frac{34}{19} \times E(H-K)$.

Age estimation is one of the most difficult features of a cluster to quantify. Many clusters have been aged, by placing its members on a H-R diagram and determining the distance, its main sequence members have progressed along the main sequence curve (Testi et al., 1998). This however is not very practical, for very young, particularly embedded clusters ($\leq 3 \text{Myrs}$) as many of its members are in an evolutionary stage prior to the main sequence phase. This leaves some young cluster's ages being determined by only a handful of its members. Another method for estimating the ages of clusters is by the use of the cm-diagram. Many authors (Baraffe et al., 1998; D'Antona & Mazzitelli, 1994) determinate the pre main sequence evolution tracks for stellar structures from 2.5M_{\odot} down to 15 times the Jupiter mass. These can be used as age isochrones on cm-diagrams and used to estimate the age of clusters.

We used the outer field as a makeshift control field. Control fields should be normally chosen, just off the main molecular cloud, however in dealing with such a large number of sources, such efforts is not very feasible. As mentioned above, the inner region covers almost the entire cluster in almost all the case, therefore it should not be unreasonable to chose an off field surrounding the target region like this. Using a similar Nyquist sampling technique as in chapter 2, we form contour maps of cm-diagram positions of the target field and the off-field. We subtract the off-field from the inner field and these graphs are displayed at the end of the section table 4.3. These diagrams do not display a clear burst of star formation as in (Moitinho et al., 2002) on 5Myr open cluster NGC2362 as

displayed in LL03, our motivating example, however this is probably due to complications due to extinction of embedded clusters. Extinction on stellar members would have the effect of spreading to the left of the diagram, increasing the thickness any short burst of star formation on the diagrams. Even with this, some of our clusters do exhibit a thin elongation as in the example, such as 05490+2658, 05553+1631 and 06105+1756. One interesting case is 06061+2151 which seems to show three different stages in star formation in the region. Closer inspection of the morphology(figure 2.1) contours show at least 2 well defined cluster centres. (Porras, Cruz-Gonzalez & Salas, 2003) study looked at the IRAS 05358+3543, they measured the ages of the three different components, the South-West, the North-East and the field star contribution to be 3Myr, 1Myr and 7Myr respectively which they measure using theoretical luminosity functions from (Storm et al., 1993). The different probably position for the isochrones can be seen on the contour CMD of 05358+3543 on figure 4.4. The generally different regions mentioned in this paper are also clearly visible in figure 2.1.

The isochrone evolves from left to right, with age arises from the percentage of members that exhibit infrared excess in the cluster. Since our clusters are subjected to dust extinction this further deludes the usefulness of this method. It is decided that no useful estimate can been be easily obtained for a sizable number of our clusters. These diagrams however show certain details of star formation in the cluster and are incorporated in this thesis for that reason.

The bulge in around the area of normal stars is probably an artifact of our method from normal non-member stars in the target field being reddened by interstellar extinction while stars in the off-field not reddened and therefore not cancelled. Possibly this techniques needs to be better perfected, the control field could be for example be artificially extincted and this should eliminate this bulge but it would be not at all clear what effect this would have on the rest of the contours.

Figure 4.5:

CMD of target field the inner region along with a contour plot of the difference between the inner and outer regions as described in the text

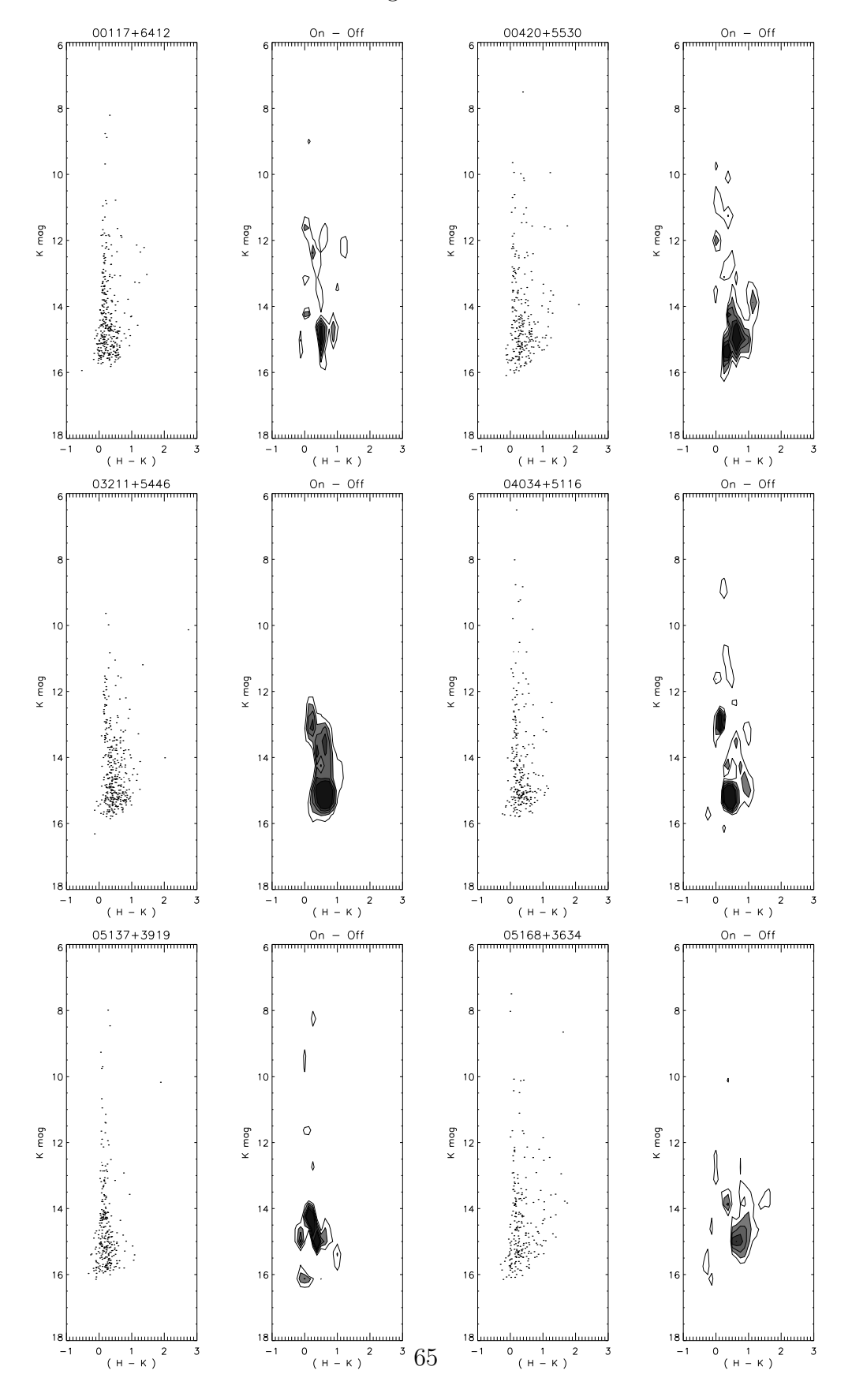


Figure 4.5: figure continued

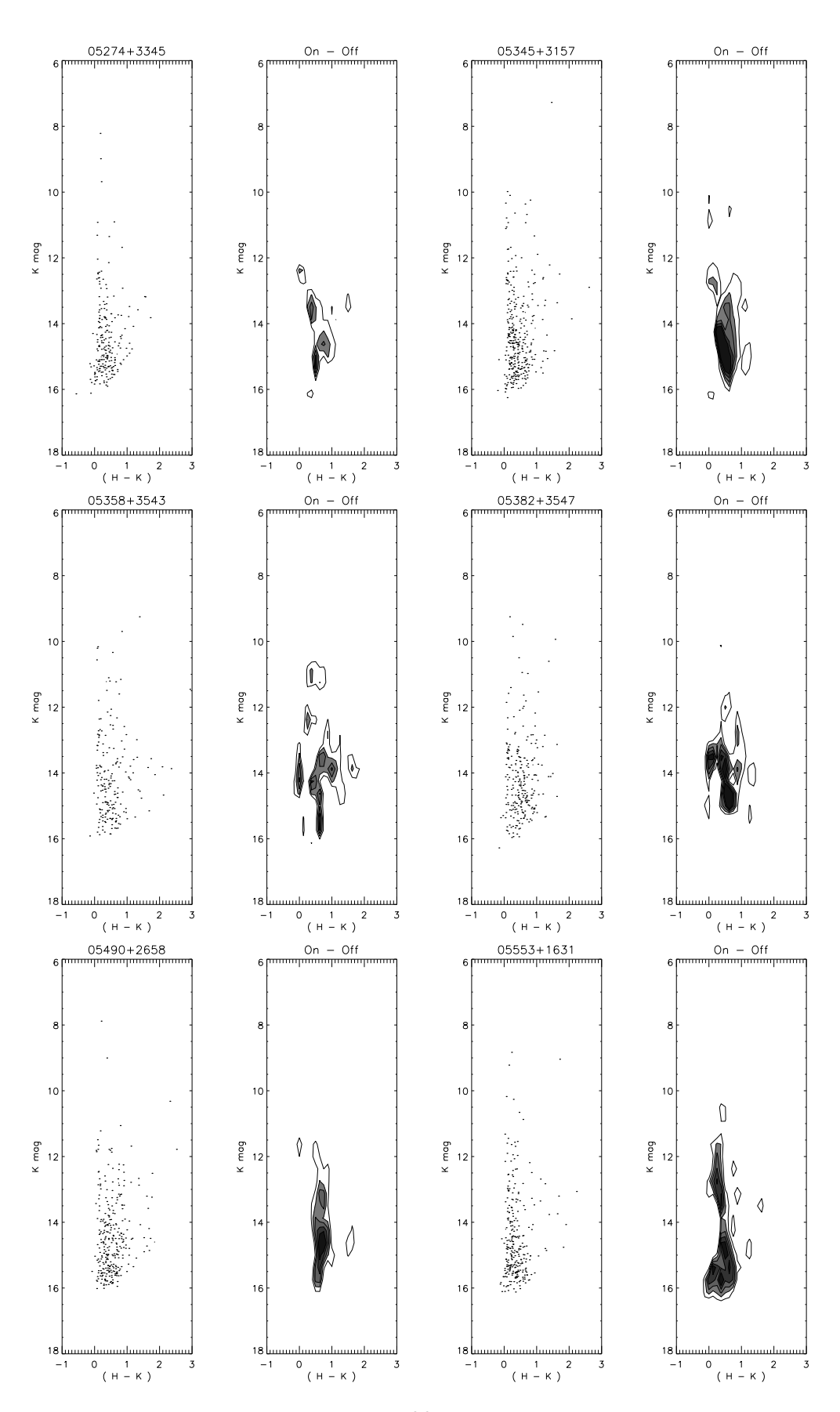


Figure 4.5: figure continued

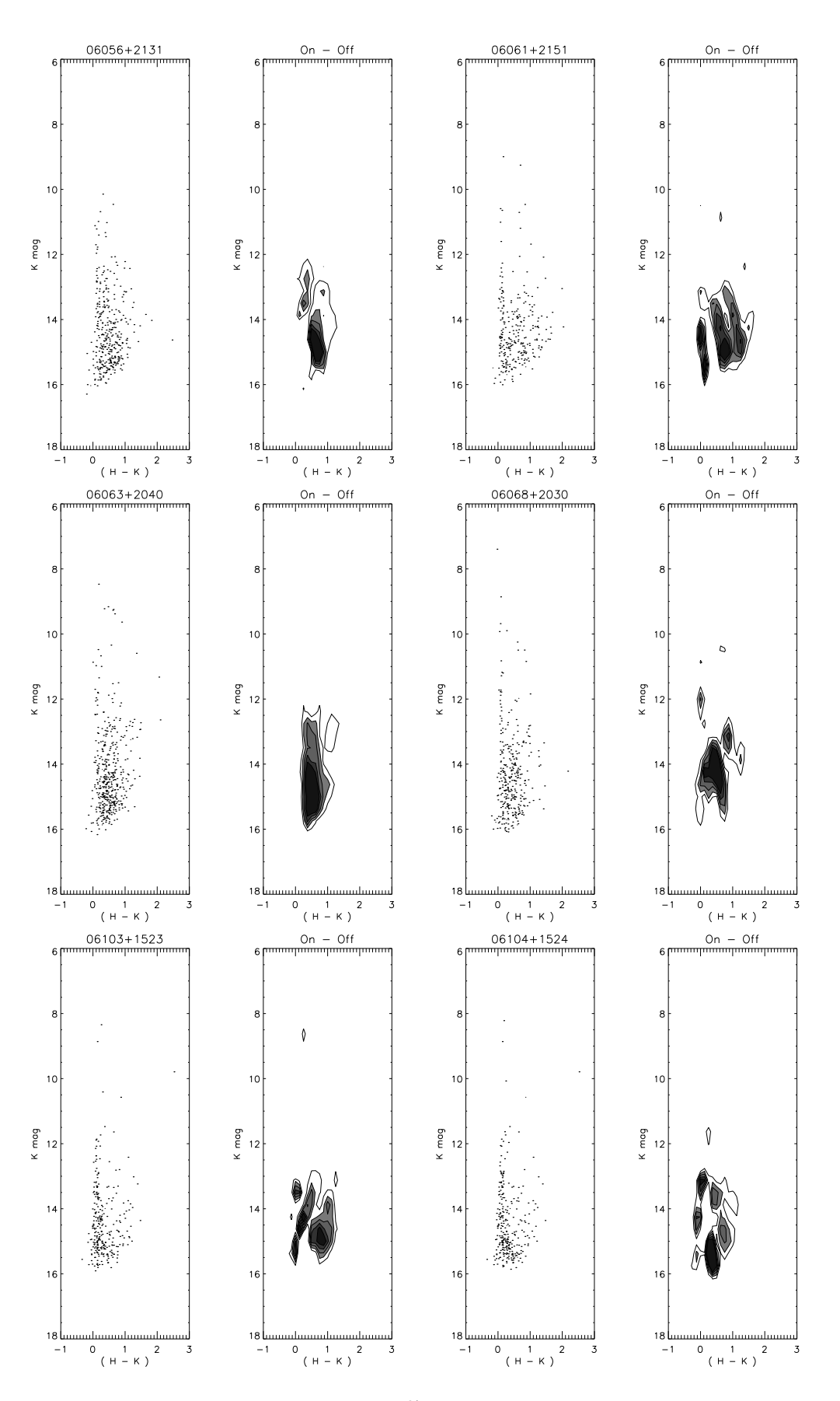


Figure 4.5: figure continued

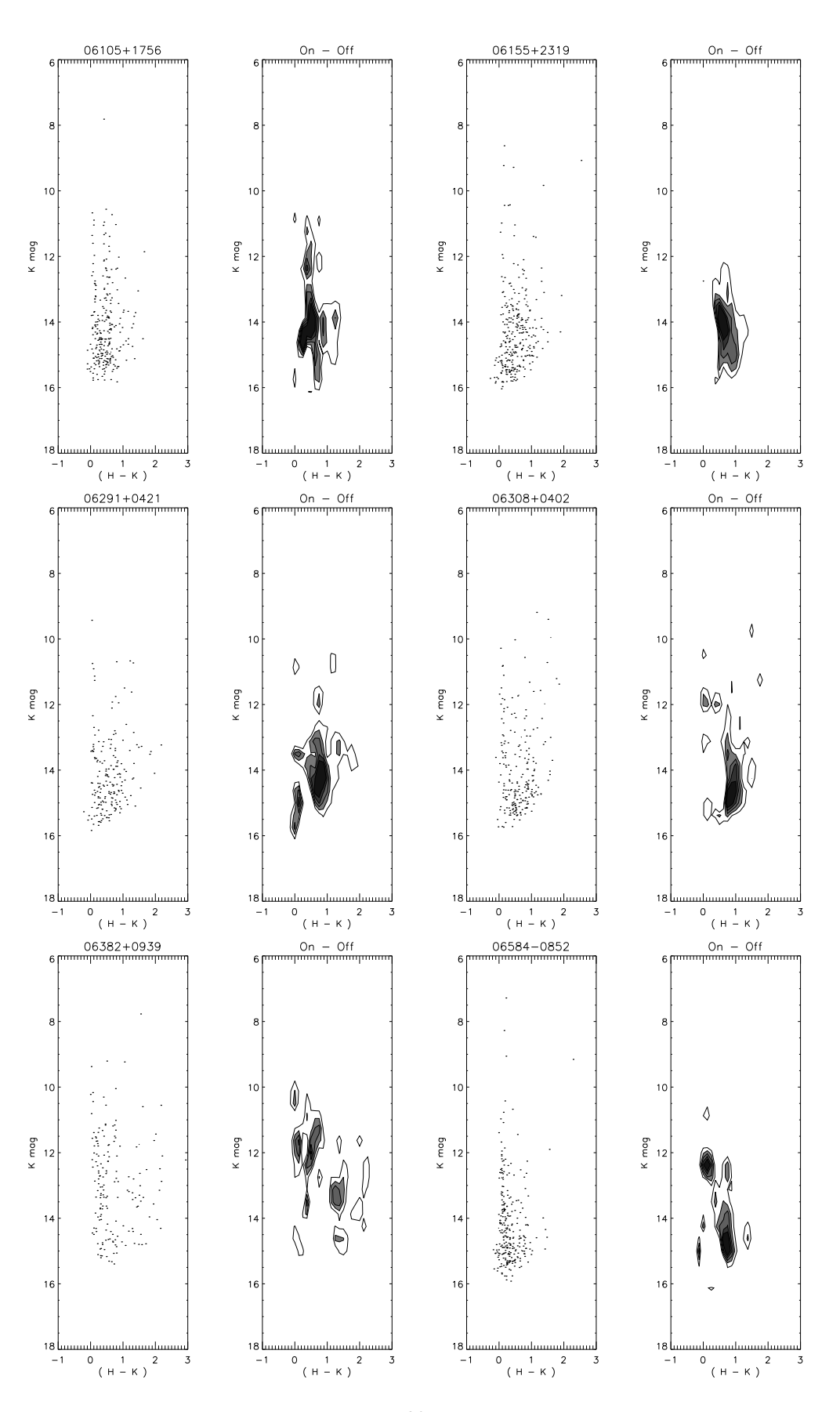


Figure 4.5: figure continued

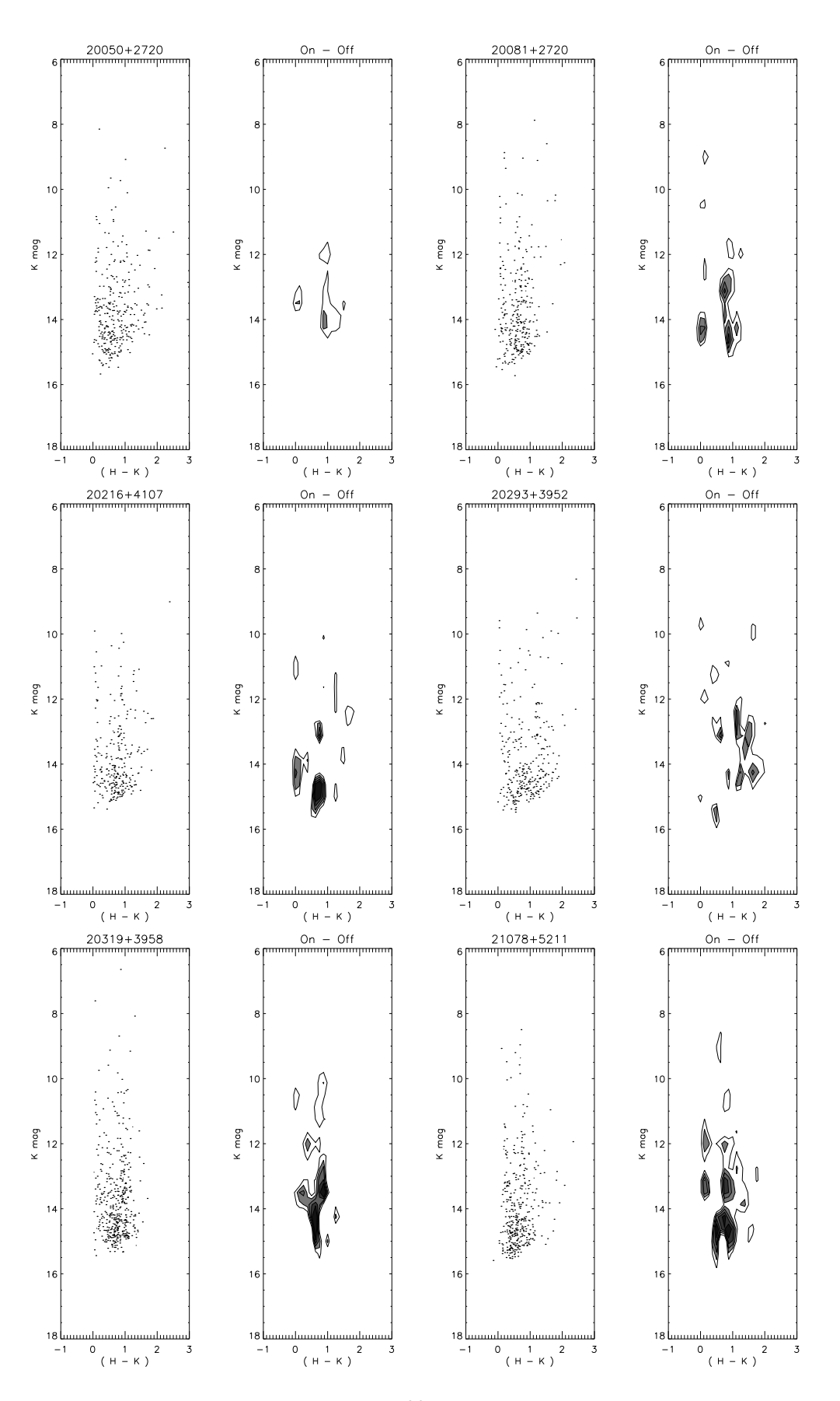


Figure 4.5: figure continued

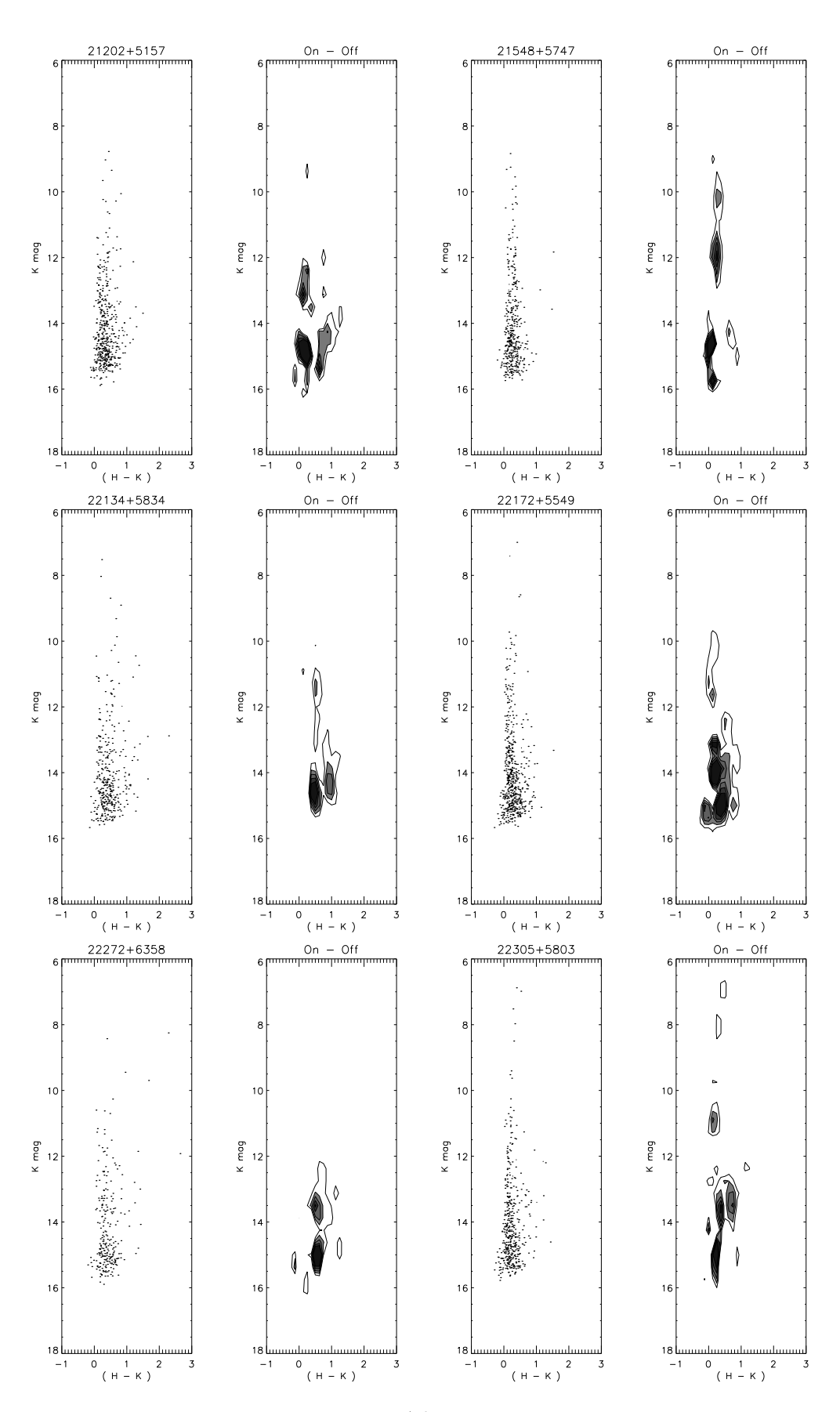


Figure 4.5: figure continued

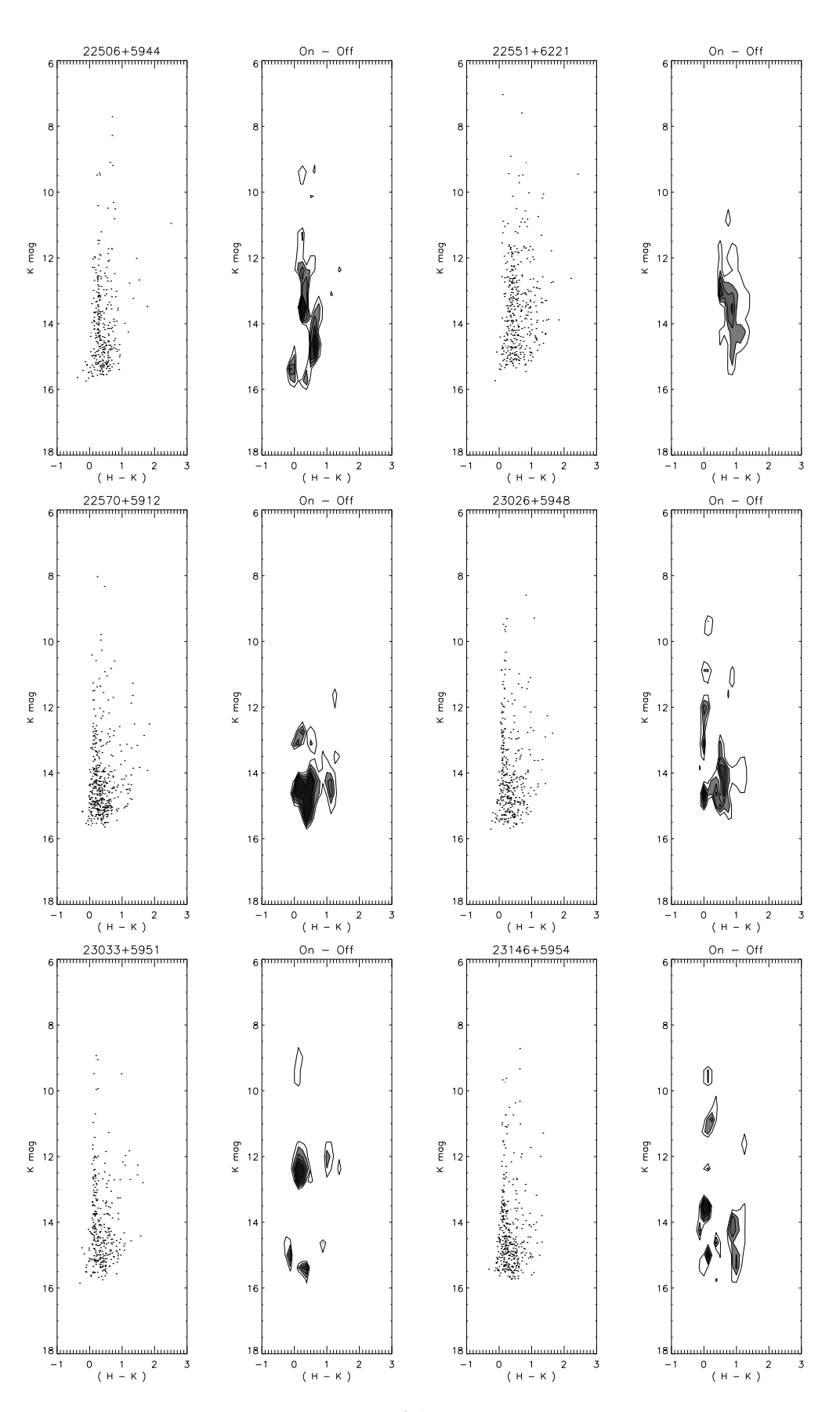


Figure 4.5: figure continued

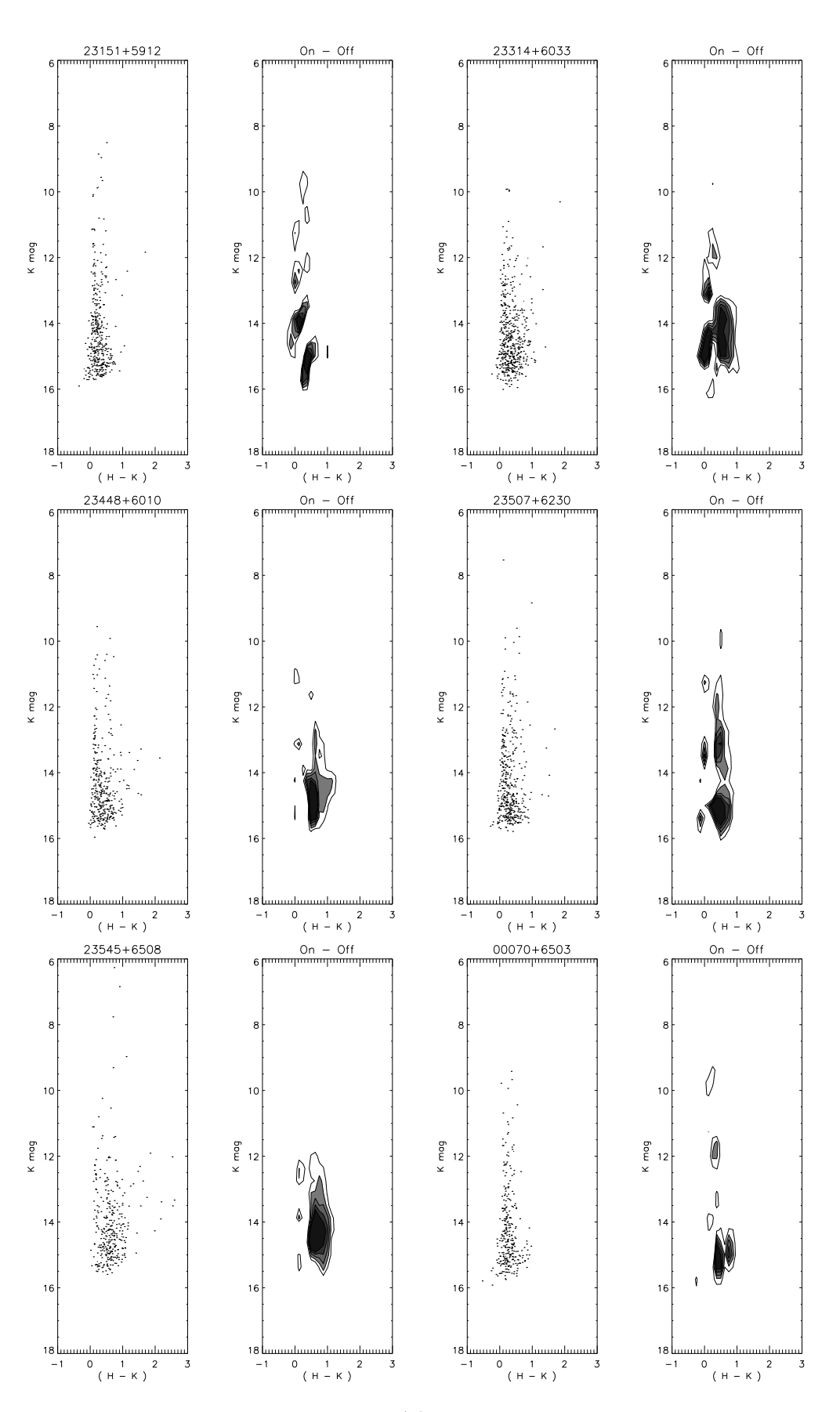


Figure 4.5: figure continued

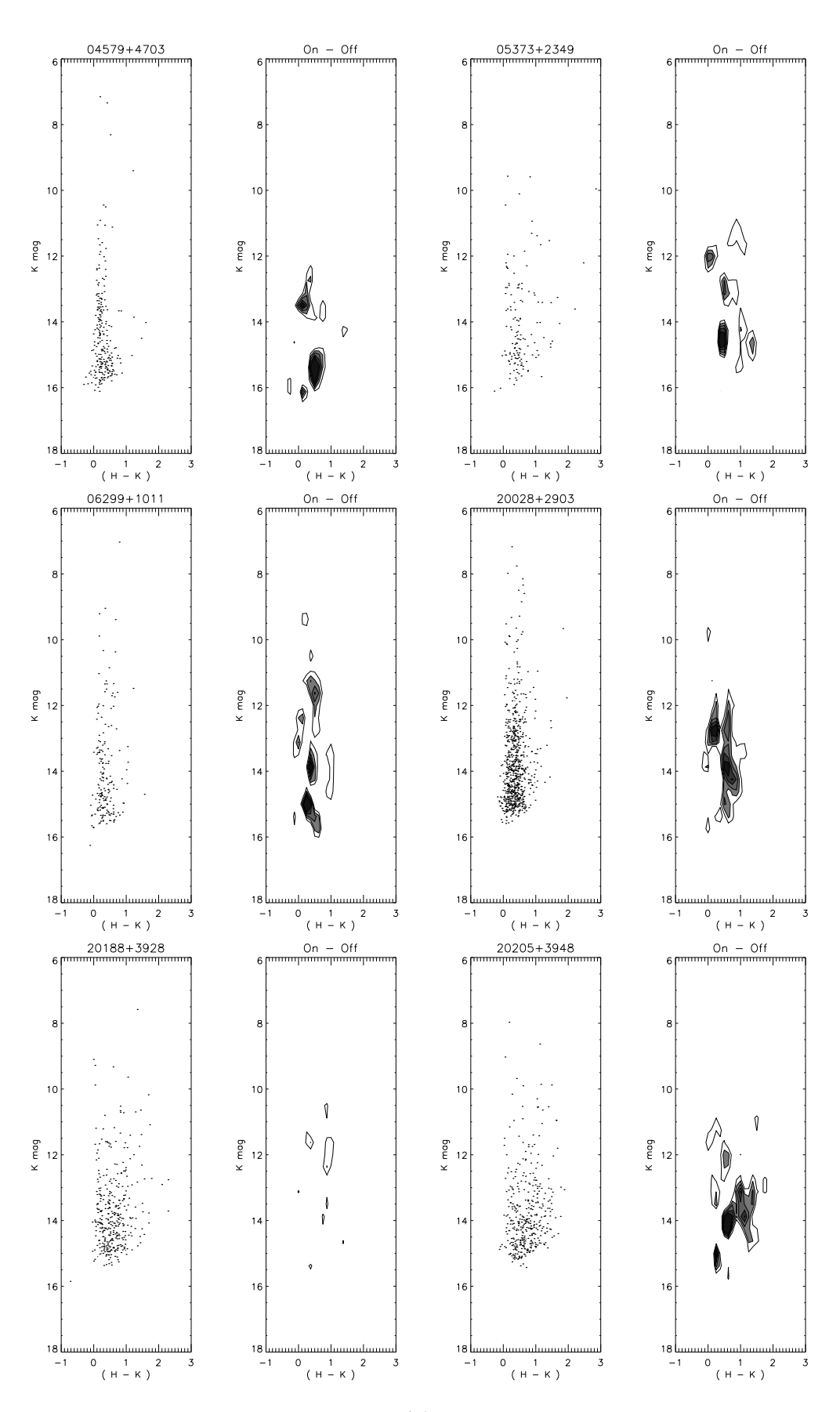


Figure 4.5: figure continued

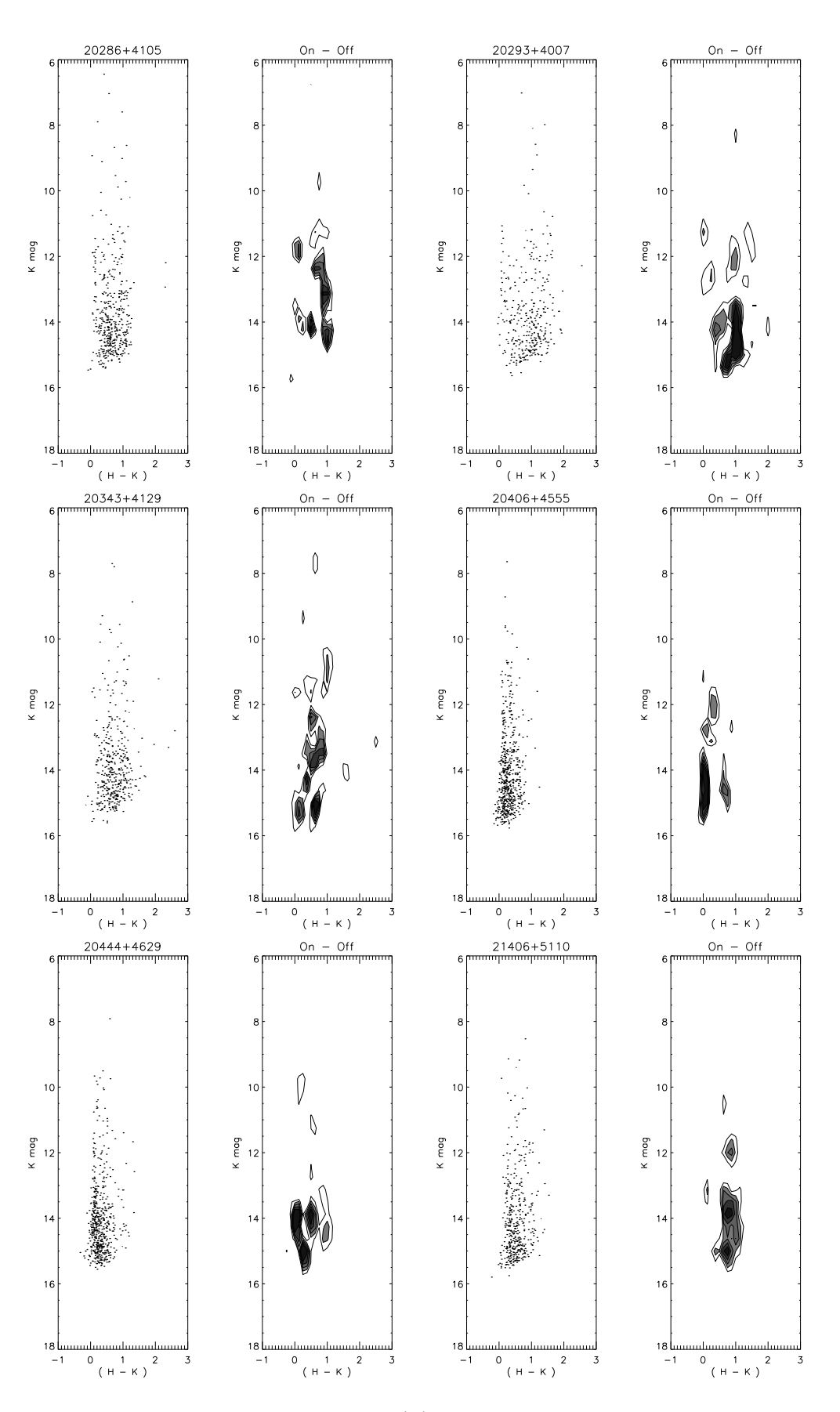
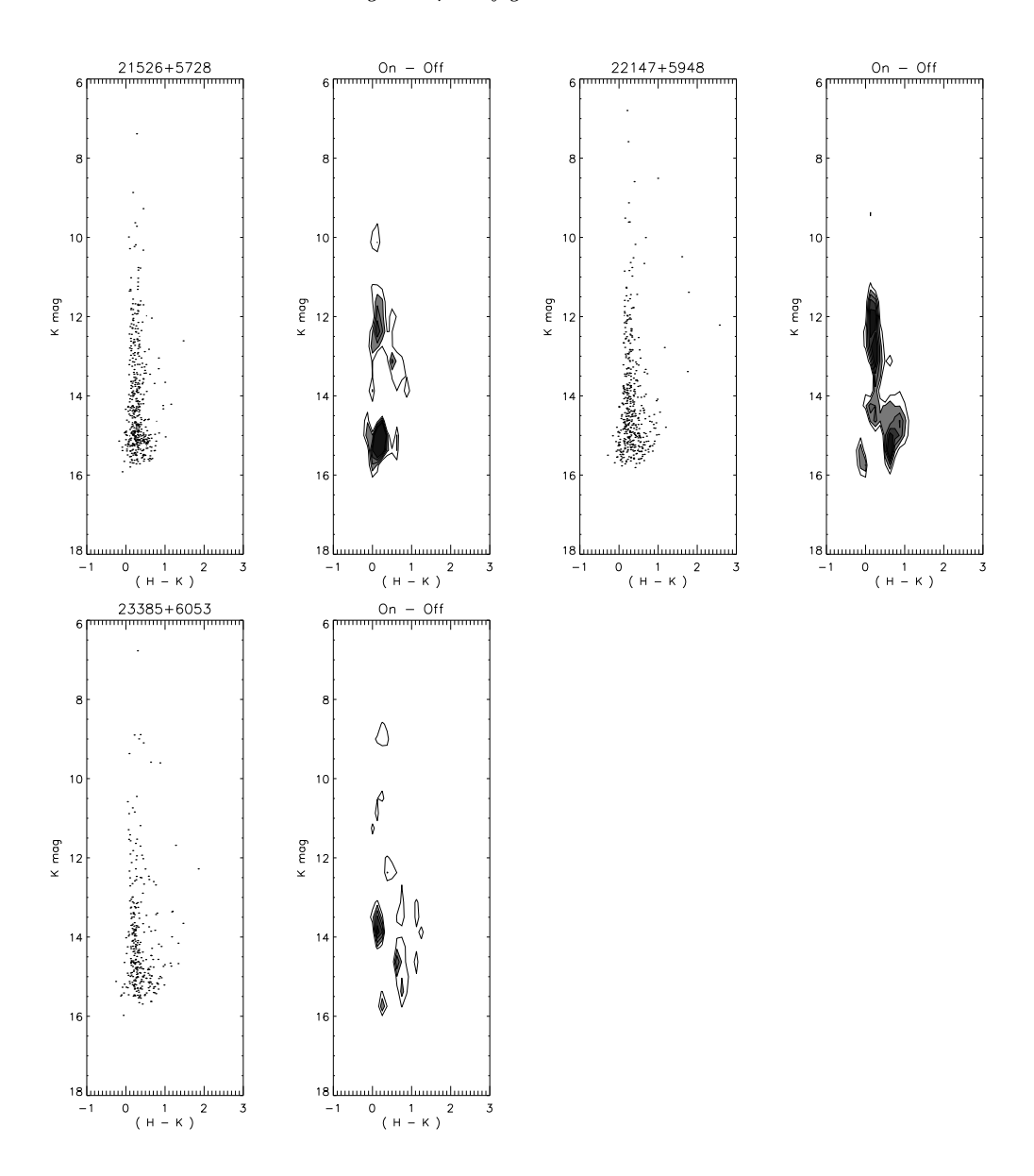


Figure 4.5: figure continued



Chapter 5

KLF, IMF and Mass Estimation

5.1 The Initial Mass Function

The entire history and evolution of a stellar object is dependent on one parameter above all others, its mass. Therefore, with knowledge of the distribution of masses at birth, the Initial Mass Function (**IMF**), one can predict the future of any stellar cluster, which in turn answers important galactic and cosmological questions.

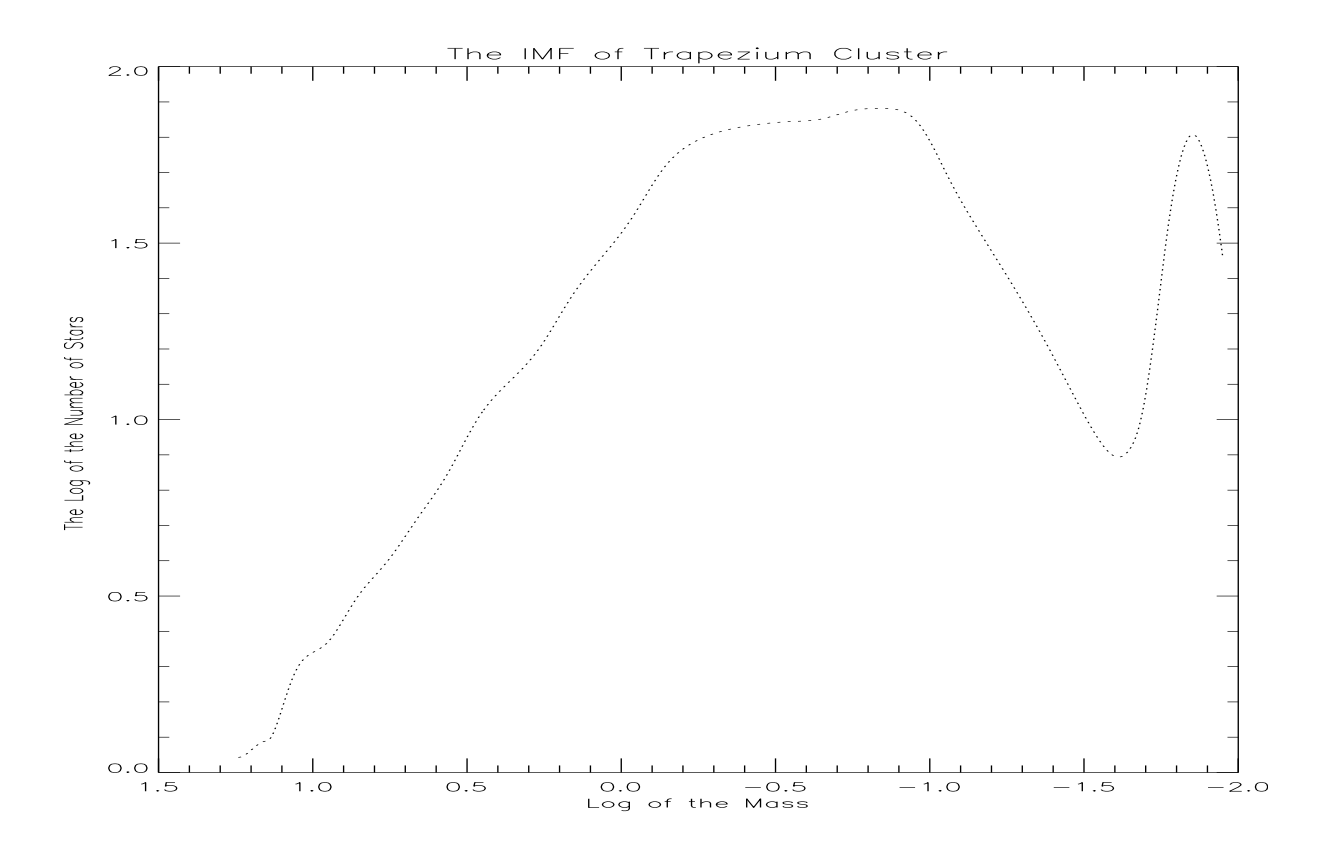
The IMF has, in the past, been estimated using the Present Day Mass Function (**PDMF**) of field stars. This estimate suffers from errors at both the high and the low mass extremes. Massive stars burn out alot quicker than low mass stars giving a reduction in their number while extreme low mass stars close to the brown dwarf limit are faint and alot harder to detect. There is still much debate in Astronomy, whether the IMF rises, falls or remains constant for low mass stars.

Embedded clusters are ideal places for the study into the IMF. They are continuing or have very recently ceased star formation processes, therefore the PDMF is the IMF. Massive stars haven't had time to burn out. Also extreme low mass stars appear brighter at birth than at any other time in their evolution, making them easier to detect. All this makes, embedded clusters as one of the best locations for estimates into the IMF. One such, detailed study has been carried out by Muench et al., (2002) on the well-known Trapezium Cluster.

The Trapezium cluster gets its name from the four bright OB stars arranged at its centre in the shape of a trapezium. Due to its fame and proximity, the trapezium cluster has been best studied of all embedded clusters.

In the aforementioned paper, (Meunch et al., 2002), the IMF of the Trapezium has been

Figure 5.1: The Initial Mass function of the Trapezium Embedded Cluster as per (Meunch et al., 2002). A cubic spline has been fitted to the points to form a continuous function



calculated down to just above the deuterium burning limit, about 17 times the mass of Jupiter. The paper used a Monte Carlo simulation technique to generate an underlining mass function that best matched the observed KLF. This lead to an IMF that initially raised with decreasing mass to $0.6 M_{\odot}$, where it flattens into a broad peak after which it decreases after the Hydrogen burning limit, and then sharply rises in the sub-stellar range.(see eqn 5.1 and fig 5.1)

$$\frac{dN}{dlogM}=M^{\Gamma}$$

$$\text{where } \Gamma = \left\{ \begin{array}{ll} -1.21, & M_{\star} > 0.600 M_{\odot}, \\ -0.15, & 0.600 M_{\odot} > M_{\star} > 0.120 M_{\odot}, \\ 0.73, & 0.120 M_{\odot} > M_{\star} > 0.025 M_{\odot}, \\ -5.00, & 0.120 M_{\odot} > M_{\star} > 0.025 M_{\odot}, \\ M = 0 & \text{if } M_{\star} < 0.017 M_{\odot}. \end{array} \right.$$

However, the IMF is believed to pretty much universal among embedded clusters, and so we can assume a trapezium IMF for our clusters and use this to generate some interesting

data along the same lines as was previously done by Lada & Lada, (2003).

5.2 The K-Luminosity Function

By using the IMF derived by Meunch et al., (2002), we generated theoretical KLFs for typical(trapezium like) embedded clusters of different ages. In the LL03 paper, the authors gather together several mass luminosity relations for clusters of varying ages from various sources. These include (Barrafe et al., 1998), (D'Antona & Mazzitelli 1994; 1998), (Burrows et al., 1997) as well as others. Most of whom modelled the mass luminosity relations for low to intermediate mass stars, less than $2.5 \rm M_{\odot}$. These relations are in relative agreement for stellar masses from roughly $0.03 \rm M_{\odot}$ to a solar mass although they diverge a little at the low extremity and mass above $2.5 \rm M_{\odot}$, especially in the case for a very young cluster less than 1Myr. They best fit the relations from various authors and we assume this as our mass-luminosity relation. Points we scanned into IDL and a cubic spline was fitted to provide a continuous function.

$$\frac{dN}{dlogM} = M^{\Gamma} = \frac{dN}{dK} \times \frac{dK}{dlogM}$$
 (5.1)

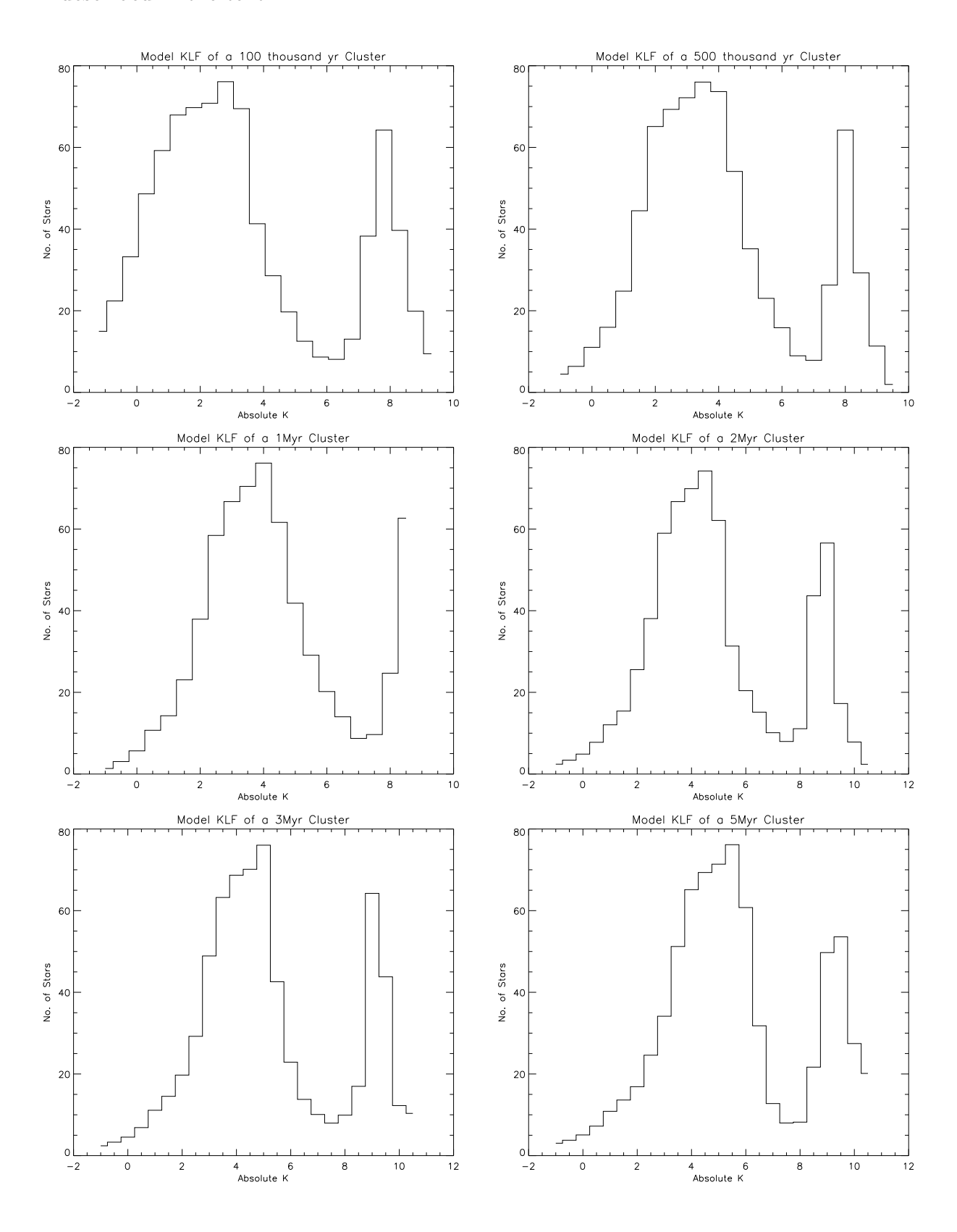
The initial mass function of a cluster is given above Eqn 5.2 can be split using the chain rule into the far right. Inverting this gives.

$$dN = \int_{-\infty}^{k} \left(M^{\Gamma} \times \frac{dlogM}{dK} \right) dK$$

For solving this integral, we use the simple Riemann method which leaves the solution to our integral as essentially a series of Riemannian rectangles. For each k step of a Riemann rectangle, we determine the corresponding mass using the mass-luminosity relations and in turn determine the value of Γ from the IMF(Eqn 4.1). We thus get 6 functions of stellar counts in terms of K for each mass-luminosity relation. These are binned into histograms to mimic the way the data would be collected in an observed cluster KLF. See figure (5.2).

All the KLFs show two characteristic peaks in stellar counts stemming from the underlying IMF. The first is due to intermediately low mass stars. The second in the extreme sub-stellar region, close to the deuterium burning limit, this is again from the IMF of Meunch et al.,(2002). The KLFs generally seem to spread out with increasing age, especially in the case of the secondary peak which is consistent with the already mentioned fact that extreme low mass stars appear brighter at birth than at any other time in their

Figure 5.2: The 6 model KLF generated from the IMF of Meunch et al.,(2002), as described in the text



evolution. With this model KLF, we will look at the KLF of the clusters to see if any more details of our clusters can be gathered.

The KLFs of our 63 possible embedded clusters was made using a similar method that was adopted for the cc and cm-diagrams. All the stellar objects that fell within the mode+ σ contour were plotted in the diagrams giving participant K Band stars a higher probability of being cluster members. Any additional information gathered about our clusters is rather limited from the K-Luminosity Function. It probably best emphasises how poorly sampled our clusters are and that there is much room for improved more detailed study using larger telescopes. For most of the clusters, the stellar counts increases with higher K magnitude till the completeness limit, (marked with a dotted line on the diagram) where it falls off sharply.(fig 5.3)

Sadly as one can see, that are embedded clusters are comparatively far away compared to other known examples. They are badly sampled and any derived IMF would be relatively meaningless in comparison to those of closer embedded clusters using a better telescope. For example the IMF of the Trapezium cluster at 450pc was estimated using a sophisticated method using a telescope with completeness limit of 18 magnitudes. The 2MASS telescope has a completeness limit of 15.3 mags in the K-band, and our clusters are typically 2,3 or 4 Kpc away.

Our KLF are consistent with seeing only the initial first slope of the model KLFs. If our clusters where better sampled, i.e to at least the drop off of the first peak, it would be possible to get an age estimation of our clusters by measuring the width of the spread and comparing it to the model KLFs. For the sake of completeness we display all the 63 KLF in figure 5.3.

Figure 5.3:

KLF of K band detected stars that within the mode + σ contours. They are in the same order as in table 2.2

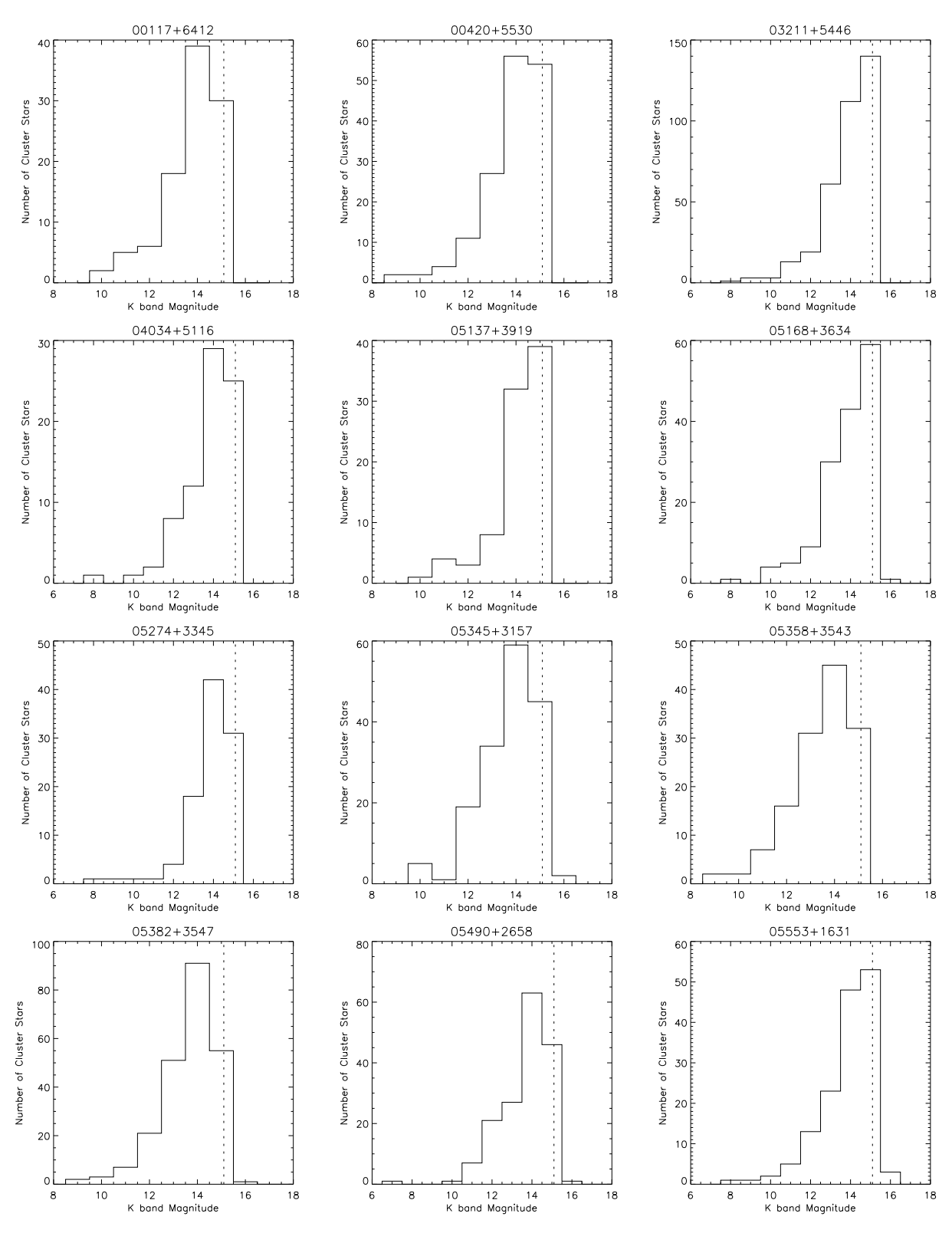


Figure 5.3:

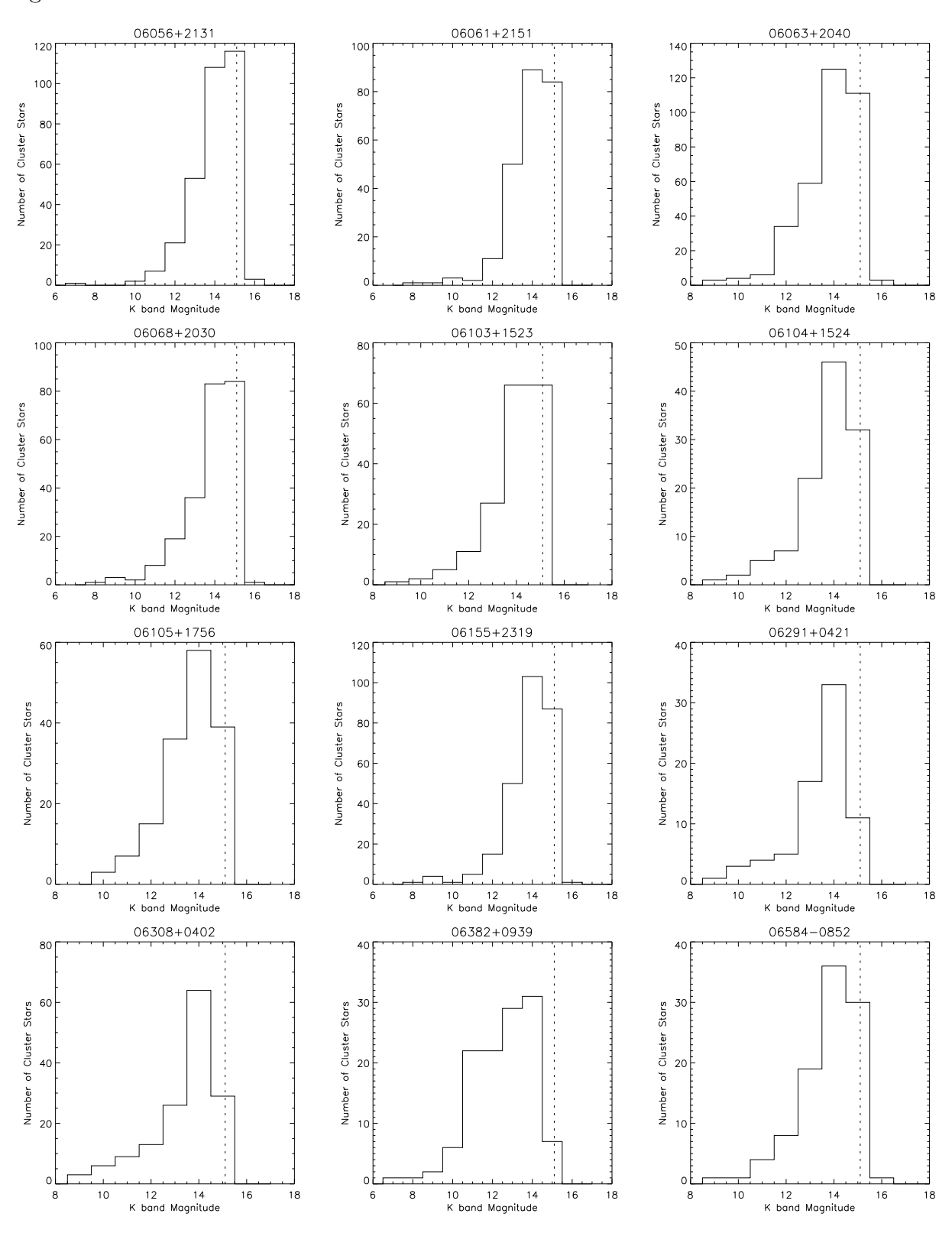


Figure 5.3:

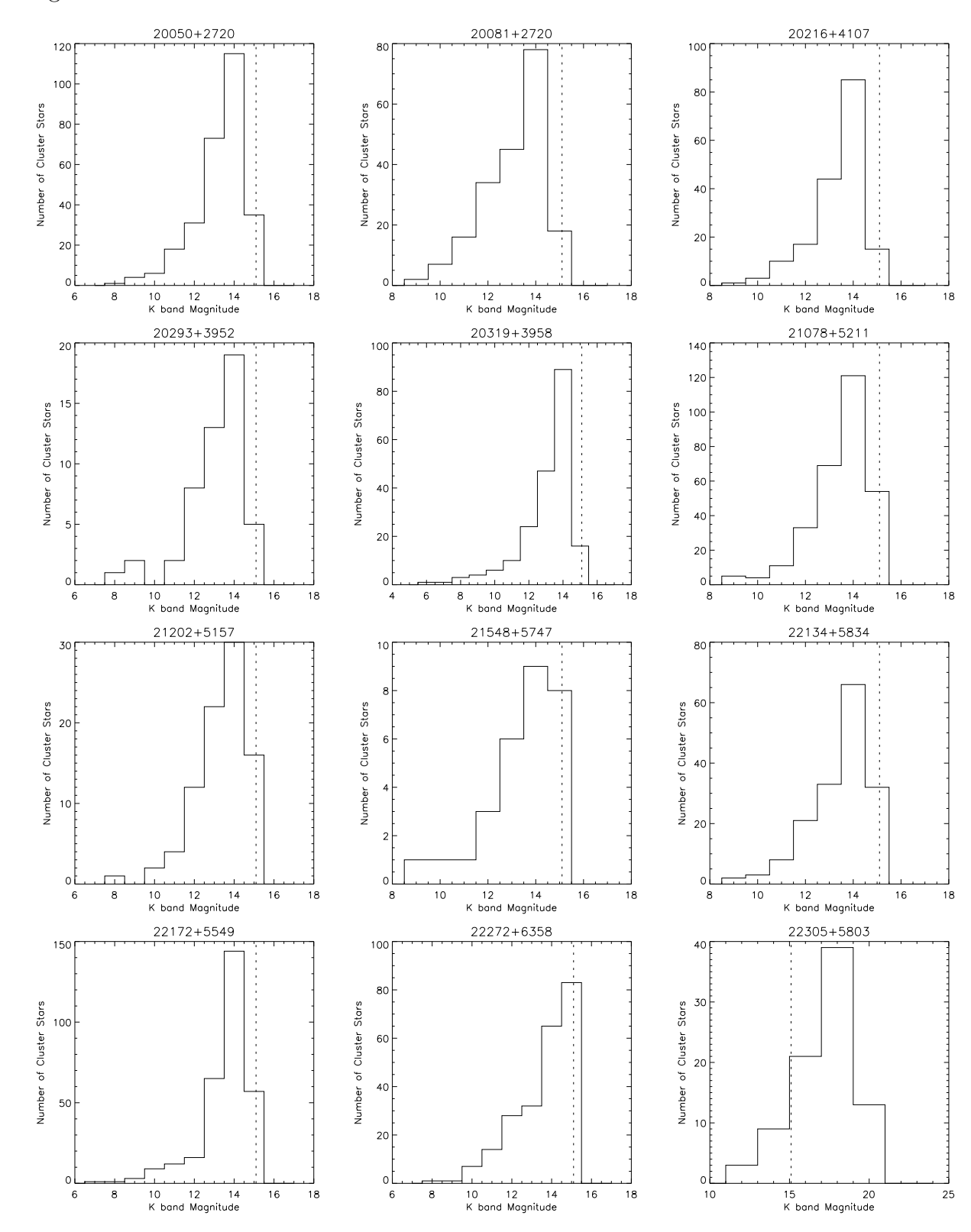


Figure 5.3:

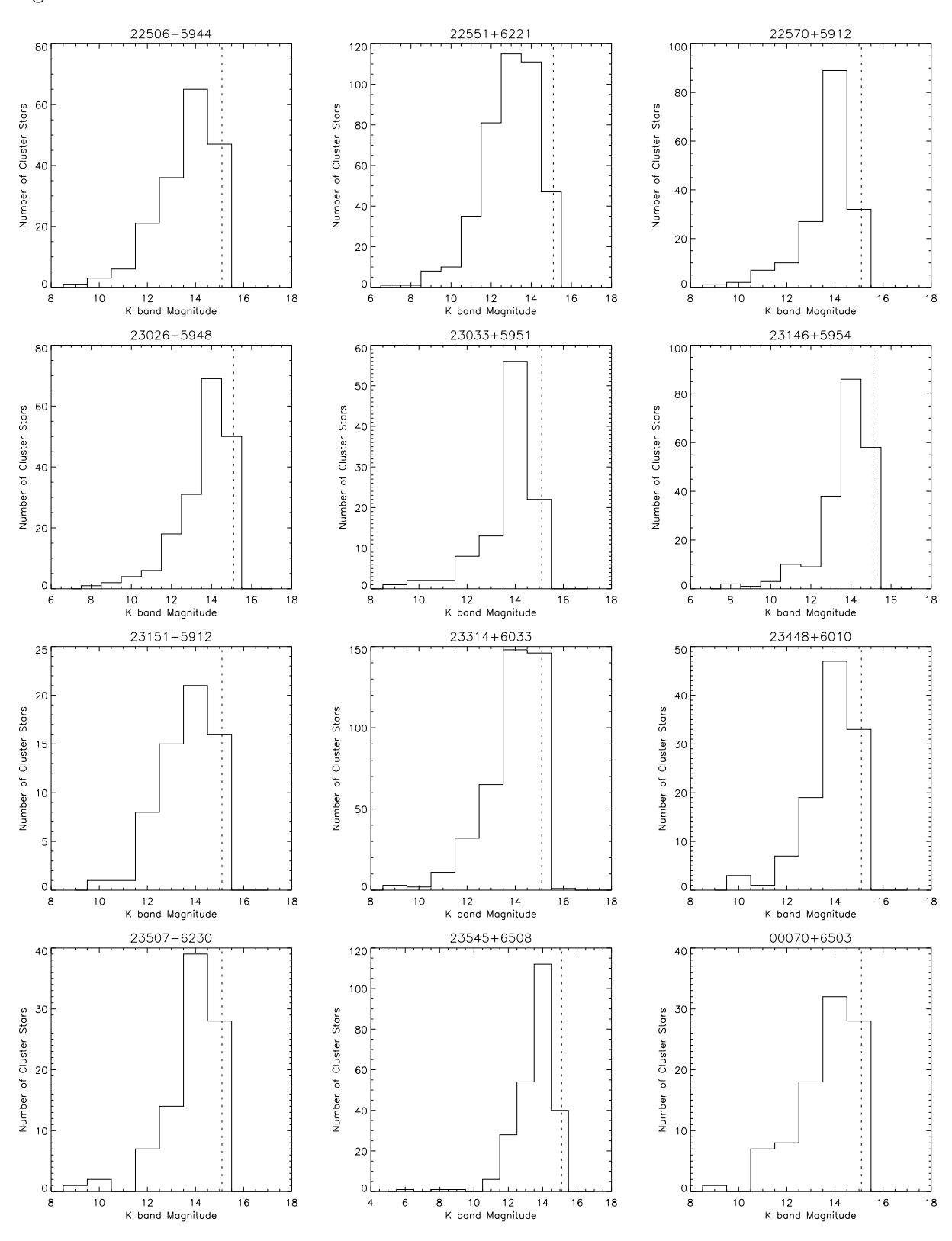


Figure 5.3:

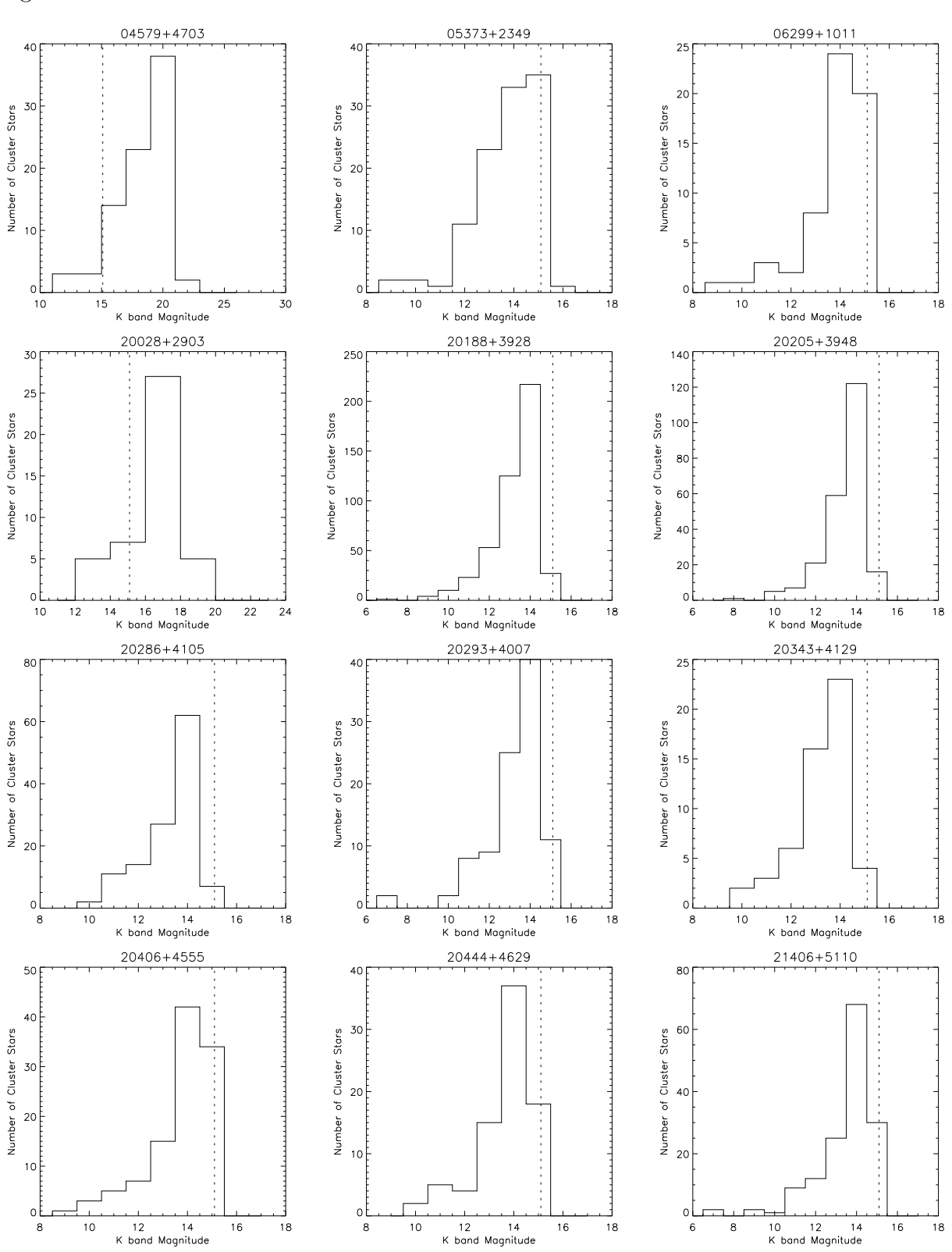
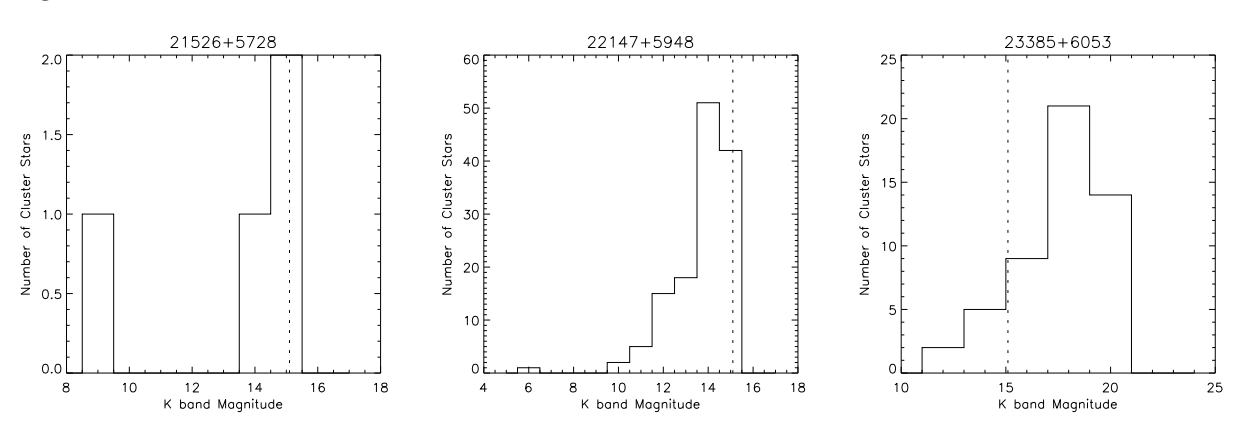


Figure 5.3:

figure continued



5.3 Mass Estimation

The Theoretical KLF derived in the last section provide an opportunity to approximate the total Mass of the stellar objects in our clusters. If we were to place the Trapezium cluster at the same distance as one of our clusters and subject it to the same dust extinction, how many of it 780 members are we likely to see? This question can be trivially answered using

$$M_k = K_{mag} - 5 + 5Log(distance) - A_k$$

knowing that the completeness limit of 2MASS data is 15.3 mag and the model KLFs of the previous section. Thus the observed number of members, along with the expected number if this cluster was the Trapezium personified, gives a ratio of the size of the cluster to that of the Trapezium. The Mass of the Trapezium Cluster is known to be 413 ${\rm M}_{\odot}$ from Meunch et al., (2002). Using this ratio can give a mass estimate for a particular cluster. Hence with knowledge of the stellar counts of a particular cluster, along with a distance, one can estimate the stellar mass of the cluster. Lada & Lada, (2003) used this method to compile a list of 76 embedded clusters within 2Kpc of the Sun. They assumed an average extinction of 0.5 in the K-band and an age of 1.5Myr for all cluster.

As we have an extinction estimate available to us, we instead used this. We also decided to chose an average age of 1.25Myrs. Assuming a posteriori that our clusters are slightly younger than that of Lada & Ladas'. This was achieved by averaging the estimate from the 0.5 and 2Myr KLFs. We calculated the mass of each of our 63 clusters using the distance estimates from their respective papers and the extinction determined in the last chapter. The data can be seen on the table below 5.1

 $Table\ 5.1:$ Mass estimated by use of the IMF from (Muench et al., 2000). Mass of the cloud from Beut.

EC No.	IRAS Name	Dist. Kpc	Cluster Members	Extinc. K band	$ m M_{\it stellar} \ m M_{\odot}$	${ m M}_{stellar}~{ m pc}^{-3} \ { m M}_{\odot}~{ m pc}^{-3}$	${ m M}_{cloud}$ ${ m M}_{\odot}$	SFE
48	00070+6503	6.83	15	0.4	1642	40.0		
1	00117 + 6412	1.80	16	0.3	21	26.9		
2	00420 + 5530	7.72	28	0.6	-	-		
3	03211 + 5446	4.54	33	0.6	379	8.38		
4	04034 + 5116	3.98	23	0.3	123	2.9		
49	04579 + 4703	2.47	12	0.4	26	13.6		
5	05137 + 3919	10.80	17	0.3	-	-		
6	05168 + 3634	6.08	14	0.4	378	2.36		
7	05274 + 3345	1.55	32	0.5	39	20.42		
8	05345 + 3157	1.80	38	0.6	57	3.45		
9	05358 + 3543	1.8	24	0.5	34	5.6	813	0.04
50	05373 + 2349	1.17	7	0.5	7	3.8		
10	05382 + 3547	25.41	31	0.8	-	-		
11	05490 + 2658	2.1	36	0.6	68	8.7	360	0.16
12	05553 + 1631	2.5	14	0.4	30	3.75	197	0.13
13	06056 + 2131	1.50	57	0.8	77	21.5		
14	06061 + 2151	0.10	39	1.0	21	-		
15	06063 + 2040	4.52	71	0.7	943	12.23		
16	06068 + 2030	4.44	36	0.6	385	278.99		
17	06103 + 1523	4.63	37	0.3	291	3.78		
18	06104 + 1524	4.68	24	0.3	195	2.10		
19	06105 + 1756	3.38	30	1.0	241	8.80		
20	06155 + 2319	0.10	46	0.6	24	5.39		
21	06291 + 0421	1.96	21	0.5	33	6.4		
51	06299 + 1011	0.35	6	0.4	4	133		
22	06308 + 0402	2.02	22	0.6	39	11.2		
23	06382 + 0939	0.76	27	0.5	20	48.8		
24	06584 - 0852	4.48	29	0.4	238	4.5		
52	20028 + 2903	1.55	9	0.7	12	18.18		
25	20050 + 2720	0.73	24	0.7	18	85.7		
26	20081 + 2720	0.7	12	1.0	9	128.6	11	0.45
53	20188 + 3928	0.31	18	0.6	11	1100		
54	20205 + 3948	4.5	10	0.6	112	6.4	730	0.13
27	20216 + 4107	1.7	7	0.9	12	5.6	171	0.07
55	20286 + 4105	3.72	6	0.8	49	10.4		
28	20293 + 3952	2.0	15	0.8	30	83.3	538	0.05
56	20293 + 4007	3.41	12	0.6	61	2.8		
29	20319 + 3958	1.6	22	1.0	36	58.1	87	0.29
57	20343 + 4129	1.4	8	0.7	10	34.5	179	0.05

58	20406 + 4555	11.92	8	0.5	-	-		
59	20444 + 4629	2.42	6	0.3	11	8.7		
30	21078 + 5211	1.49	40	0.6	49	22.0		
31	21202 + 5157	6.78	13	0.5	8785	98.7		
60	21406 + 5110	0.59	15	0.6	10	166.7		
61	21526 + 5728	8.11	9	0.4	-	-		
32	21548 + 5747	7.10	3	0.3	273	29.7		
33	22134 + 5834	2.6	30	0.4	70	7.4	436	0.14
62	22147 + 5948	7.29	17	0.4	-	-		
34	22172 + 5549	2.87	37	0.3	96	4.35		
35	22272 + 6358	1.23	10	0.4	9	25.0		
36	22305 + 5803	5.40	10	0.4	154	3.7		
37	22506 + 5944	5.70	28	0.5	680	12.5		
38	22551 + 6221	0.7	44	0.8	33	58.9	33	0.5
39	22570 + 5912	5.1	18	0.3	192	5.6	2902	0.06
40	23026 + 5948	5.76	16	0.3	264	4.6		
41	23033 + 5951	3.5	9	0.3	35	4.2	2327	0.01
42	23146 + 5954	4.43	28	0.3	195	2.8		
43	23151 + 5912	5.7	12	0.4	231	2.8	1229	0.16
44	23314 + 6033	2.78	35	0.6	111	5.5		
63	23385 + 6053	6.94	2	0.5	690 +	7.2		
45	23448 + 6010	2.02	35	0.5	58	21.8		
46	23507 + 6230	4.28	6	0.4	43	1.7		
47	23545 + 6508	0.8	21	0.7	16	21.6	37	0.30

These values from the two KLFs were in good argument for the better sampled clusters, i.e clusters that are close to the solar neighbourhood and under relative low extinction. This method is very sensitive to distance errors. For some of our clusters, if the trapezium cluster is placed at that distance, it would have no observed members. This is likely due to distance errors and it occurs for only Molinari et al.s' (1996) sources. The paper is expected to have the least accurate distance estimate. The Masses of these clusters are appropriately left undetermined.

Stellar mass estimation for a cluster can be very difficult to determine directly. For most surveys and in these cases, the magnifying power of the telescope is not sufficient to detect all it's extreme low mass members. Even without precise knowledge of membership, this method gives an estimation to the mass. Lada & Lada, (2003) states that their values should be "accurate to an order of 2 for most clusters". Nevertheless, these estimates are interesting in an statistical sense. For most of the clusters, the method seems to give a reasonable estimate, except possibly 21202+5157 at the 8785 M_{\odot} . This is probably due to as before an error in distance determination, while this same distance error was also evident while fitting the spectral grid to its cm-diagram for this cluster. Where we

see a gloss overestimate for the distance, the trapezium KLF registers no members at the distance and therefore no mass estimate is obtainable such as IRAS05382+3543 at 25.41 Kpcs. The method however gives a value, for cluster distances that may be hugely underestimated, such as 06061+2151 at 100 pc. This means that its estimate of $21 \rm M_{\odot}$ is probably several times too small. Lada and Lada in LL03 used thus method for clusters less than 2 kpc. We include data on the table which appears reasonable however we voice an added caution for clusters at distances greater than 5 kpc.

Beuther et al.(2002) calculated a reliable measure for the cloud mass for the peaks in molecular cloud density for each of Sridharans' sources. This constitutes 15 of the clusters we detected. We summed the peaks for each cluster and we calculated the Star Formation Efficiency. The Star Formation Efficiency is given by (SFE = $M_{stellar}/(M_{gas} + M_{stellar})$). According to Lada & Ladas' (2003) review, the local SFE of embedded clusters range from 10 to 30%. Our clusters range approximately from 5% to 45% see figure 4.1. The average is 17% but the median is probably low around 10% or less. If star formation efficiency is dynamical with time, with gas being converted into stars, this is consistent with the assumption that our embedded clusters are very young examples.

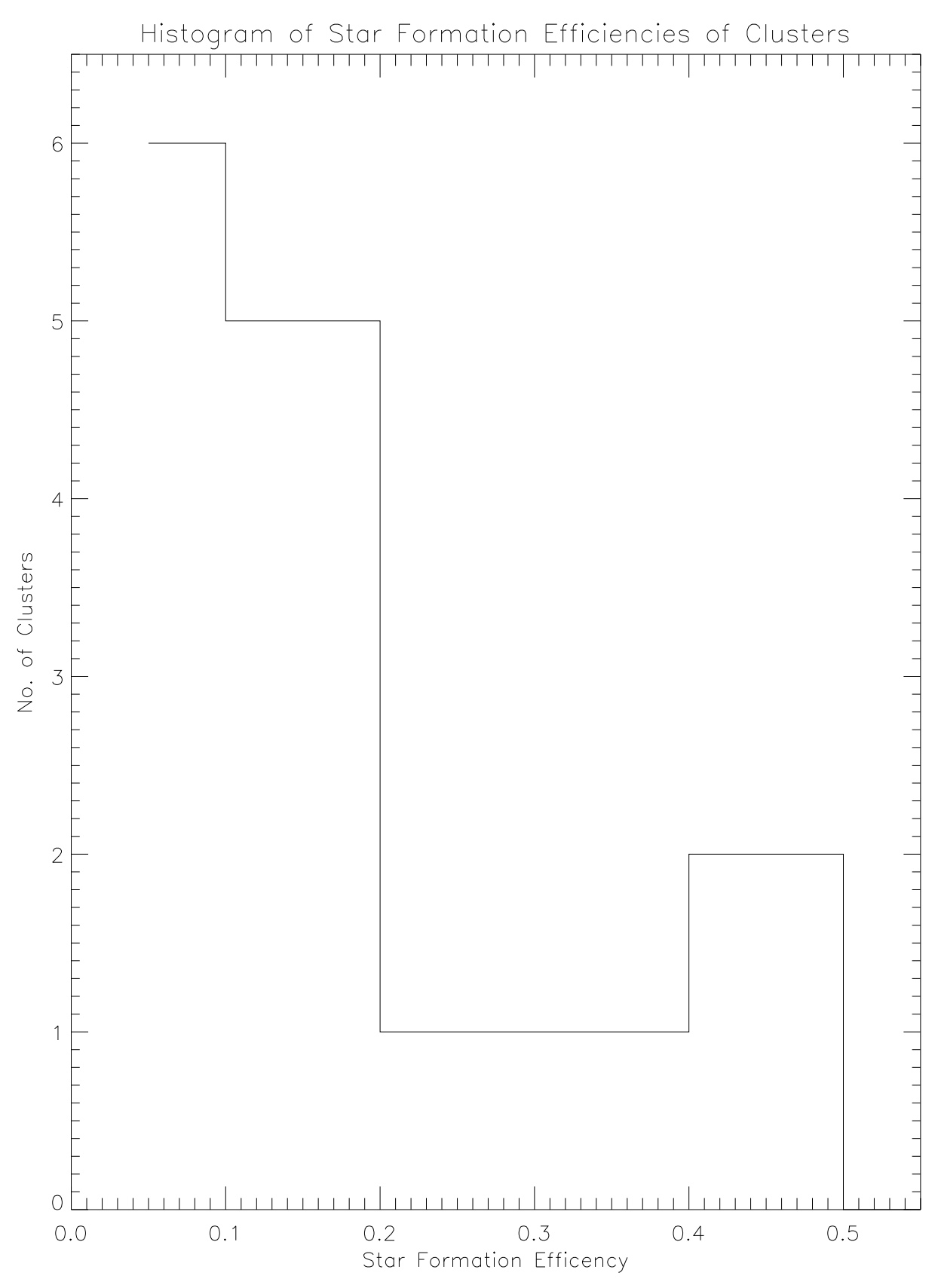
Table 5.2: The total expected number of stars and stellar density for each grouping.

					stellar	steallar		
EC	IRAS	Dist.	Area	Expec.	density	density	Lumin.	Spectral
Number	Name	Kpc	pc^2	*	$\star~{\rm pc}^{-2}$	$\star~{\rm pc}^{-3}$	${ m L}_{\odot}$	type
48	00070 + 6503	6.83	5.68	3685	648	89,8	19953	B0.5
1	00117 + 6412	1.8	1.03	42	40.8	53.8	1259	В3
2	00420 + 5530	7.72	40.72	-	-	-	12589	B0.5
3	03211 + 5446	4.54	15.48	898	58.0	19.8	31623	B0
4	04034 + 5116	3.98	14.76	281	19.0	6.7	15849	B0.5
49	04579 + 4703	2.47	3.95	54	13.7	28.3	1995	B2
5	05137 + 3919	10.80	116.19	-	-	-	39811	09.5
6	05168 + 3634	6.08	35.81	922	25.8	5.7	25119	B0
7	05274 + 3345	1.55	1.88	78	41.5	40.8	3981	B2
8	05345 + 3157	1.80	3.78	119	31.5	7.2	3981	B2
9	05358 + 3543	1.8	4.04	71	17.5	11.8	6310	B1
50	05373 + 2349	1.17	2.45	13	5.3	7.06	1995	В3
10	05382 + 3547	25.41	1105	-	-	-	501187	05.5
11	05490 + 2658	2.1	4.83	142	29.4	18.2	3162	B2
12	05553 + 1631	2.5	5.022	64	12.7	8.0	6310	B1
13	06056 + 2131	1.5	2.89	158	54.7	44.0	6310	B1
14	06061 + 2151	0.1	0.015	39	-	-	25	A1
15	06063 + 2040	4.52	21.99	2253	102.4	29.3	79433	08
16	06068 + 2030	4.44	1.54	908	589.6	658.0	50119	09

17	06103 + 1523	4.63	21.99	682	31.0	8.8	19953	B0.5
18	06104 + 1524	4.68	24.92	457	18.3	4.9	50119	Ο9
19	06105 + 1756	3.38	11.012	565	51.3	20.6	31623	B0
20	06155 + 2319	0.10	3.27	46	13.9	10.3	20	A2
21	06291 + 0421	1.96	3.61	69	19.11	13.4	3981	B2
51	06299 + 1011	0.35	3.3	7	2.12	233.3	63	В9
22	06308 + 0402	2.02	2.779	82	29.5	23.6	7943	B1
23	06382 + 0939	0.76	0.67	38	56.7	92.7	158	later
24	06584-0852	4.48	17.16	556	32.4	10.5	7943	B1
52	20028 + 2903	1.55	5,27	25	4.7	37.9	5012	B2
25	20050 + 2720	0.73	0.43	35	80.8	166.7	398	B5
26	20081 + 2720	0.7	0.22	18	81.8	257.2	316	B6
53	20188 + 3928	0.31	3.04	20	6.5	2000.0	316	B6
54	20205 + 3948	4.5	8.18	265	32.4	15.2	31623	B0
27	20216 + 4107	1.7	2.034	25	12.3	11.7	1995	В3
55	20286 + 4105	3.72	3.17	114	36.0	24.2	3981	B2
28	20293 + 3952	2.0	0.61	64	104.9	177.8	6310	B1
56	20293 + 4007	3.41	12.33	139	11.3	6.4	7943	B1
29	20319 + 3958	1.6	0.88	76	86.4	122.6	6310	B1
57	20343 + 4129	1.4	3.23	19	5.89	65.5	3162	B2
58	20406 + 4555	11.92	-	-	=	-	125892	07
59	20444 + 4629	2.42	2.95	24	8.1	19.0	3162	B2
30	21078 + 5211	1.49	2.109	99	46.9	44.4	12589	B0.5
31	21202 + 5157	6.78	24.148	17457	722.9	196.1	63096	08.5
60	21406 + 5110	0.59	3.01	19	6.3	316.7	251	B7
61	21526 + 5728	8.11	3.96	-	-	-	25119	B0
32	21548 + 5747	7.10	5.375	624	116.1	67.8	25119	B0
33	22134 + 5834	2.6	5.4	149	27.6	15.8	12589	B0.5
62	22147 + 5948	7.29	16.96	-	-	-	25119	B0
34	22172 + 5549	2.87	9.61	205	21.3	9.3	5012	B2
35	22272 + 6358	1.23	0.61	19	31.1	52.8	1995	В3
36	22305 + 5803	5.40	14.77	367	24.8	8.7	12589	B0.5
37	22506 + 5944	5.70	20.1	1654	82.3	30.4	19953	B0.5
38	22551 + 6221	0.7	0.84	63	71.3	112.5	1585	В3
39	22570 + 5912	5.1	12.78	454	35.5	13.3	50119	09
40	23026 + 5948	5.76	18.01	634	35.2	11.1	15849	B0.5
41	23033 + 5951	3.5	5.02	78	15.6	9.3	10000	B1
42	23146 + 5954	4.43	20.56	456	22.2	6.6	25119	B0
43	23151 + 5912	5.7	22.80	555	24.3	6.8	100000	07
44	23314 + 6033	2.78	9.04	244	26.9	12.1	1000	B1
63	23385 + 6053	6.94	12.15	-	-	-	63096	08.5
45	23448 + 6010	2.02	2.37	121	51.1	45.5	2512	В3
46	23507 + 6230	4.28	10.41	101	9.7	4.1	12589	B0.5
47	23545 + 6508	0.8	1.00	32	32.0	43.2	1000	В3

Previous estimates of the total number within the cluster is limited to the seeing power of the 2MASS survey. Therefore its both dependant on the distance to the cluster and the average extinction of the members and thus comparisons between the number of members detected in each cluster and the same cluster of various studies can be therefore precarious. The 2MASS surveys, sees the number of members in a cluster depending on the cluster distance and extinction. We also used the relative size of the cluster to that of the Trapezium to estimate the total number of cluster members down to deuterium burning limit. (see table page 93) This is essentially the same method as that of mass estimation. It is dependent on the same accuracy decreasing inversely to the distance. It is very useful to have a number which is an estimate of the total number of the cluster. It allows us to calculate the total stellar number per pc² in the region, independent of the position and properties of the cluster. If the cluster survival is only dependent on the strength of the gravitational forces that bind it, it is ipso facto the mass per pc³ and thus total stars per pc². Lada & Lada (2003) states that between 4-7% of embedded clusters survive to become classically open clusters. If our clusters are typical, this means that between 2 to 4 of the 55 with total number estimates are likely to survive. This is very roughly in the range of 110 $\star pc^{-2}$. Cluster with a lower stellar density and not likely to emerge from it molecular cloud.

 $\label{eq:Figure 5.4:} Figure~5.4:$ The Star formation efficiencies of our clusters, plotted from the table 5.1.



Chapter 6

Summary & Conclusions

During the past 7 years, two major efforts have been made to search for and identify the precursors to UCHII regions, written on 5 papers (MoII, MoIII, MoIIII, Srid, Beut) and they examined these sources using far-infrared, radio continuum, 1.2 and 1.3 mm continuum emissions and many spectral lines and masers observed (H₂O, NH₃, CH₃OOH). The papers combined constituted a selection of 217 bright IRAS sources, which were predominately UCHII but also a believed handful of precursor to UCHII regions. This selection could be separated into three groups (Srid, Mol-L, Mol-H) of 69, 83 and 80 sources respectively where each group was statistically expected to be of different age. The Mol-H satisfied many of the requirements of UCHII regions while the Mol-L had a slightly redder FIR colour than normal UCHII regions (Wood and Churchwell, 1989), a known indicator of youth. The Srid group was compiled from a selection process of Ramesh and Sridharan (1997) and was expected to be the youngest. In the research we several times back up this fact and used it to reveal some general properties of starformation.

We added a near-infrared study using 2MASS into these sources to the already impressive list of wavelengths. As all the sources were associated with dense molecular dust and gas (Beut) and probable massive star formation, we wanted an automated technique of detecting the possible presence of embedded clusters around them. So, we devised a technique of Nyquist binning stellar counts to detect the presence of local enhancements in stellar density which almost certainly in almost all cases is an embedded cluster or group. Although it remains a possibility, as with most embedded cluster surveys, that perhaps some may be due to spurious clusterings from patchy absorption of the cloud (Clarke, Bonnell & Hillenbrand, 1999). We found 63 of these enhancements of stellar density around the (pre) UCHII sample, of which 50 should be newly discovered embedded clusters. Our detections showed a pronounced evolution of cluster detection between the source type and thus the age of the underlying (pre) UCHII region.

We conducted a short study into the sensitivity of our detection technique and showed that it relied on the distance to the cluster but also more heavily on the background counts. The percentage of (pre) UCHII regions detected with clusters decreased with increasing distance but our diagrams also showed a reduction of cluster detected around the closest (pre) UCHII regions. This may be due to the closest clusters subtending a very large angles of view and thus registering very small increases in stellar density per arcsecond. As our detection system was entirely automated, we could minimise the two factors mentioned above and statistically conclude that roughly 85% of the 217 sources should have clusters surrounding them. This in itself is not surprising as other studies confirm that 90% of stars forming today are forming as part of an embedded cluster(Carpenter et al., 2000). But what is surprising is that all the sources with no clusters detected that went into forming these statistics were from the MolI study. The MolI study is more likely to both have distance miss-estimates as well as the possibility of some of their sources neither being precursors to UCHII regions nor UCHII regions themselves. Thus the percentage of (pre) UCHII in the sample which are members of embedded clusters is likely to be even much higher. Which would be necessary, if theories such as Bonnell, Vine & Bates (2004) are correct that the cluster are nurtured by the presence of an embedded cluster.

Using the stellar density contour maps we examined the morphology of our clusters. We discussed these in relation to the predominance of hierarchical star formation (Elmegreen (1993)) and the numerical simulations of Bonnell, Bates & Vine (2003) which suggest subclusters of a hierarchical-form cluster will emerge into a centrally-condensed cluster through mutual gravitational attraction. We find an equality between the ratio of centrally-condensed clusters and hierarchical clusters (H/C = $0.9 \approx 1$) and this appears to be conserved between Srid, Mol-L and Mol-H type sources. One mite expect there to be more centrally-condensed-form in Mol-H and less in Srid, but there is no evidence for this. The scenario proposed by Elmegreen (1993) suggests a sort of balance between the turbulence and gravity in a molecular cloud and this should be loosely extended to the more intermediate scale of starformation of an embedded cluster. The members of a centrally-condensed type are probably bound together by gravitational forces more so that hierarchical type were turbulence possibly plays a stronger role. The basic equality observed may be testament to this. But also on the intermediate scale turbulence is expected dissipate and decay and gravity is needed to pump energy into it. This may account for the slightly more centrally-condensed clusters.

The contours also revealed that $\frac{2}{3}$ of candidate (pre) UCHII regions occupy the centre of the cluster or of a subcluster of hierarchical-form, despite possible inaccuracies of the exact IRAS coordinate. We know from the selection process of the sample that starformation is actively occurring at these regions and it is very unlikely that this mass segregation can be explained through a purely dynamical evolution of members (Bonnell and Davis, 1998). Only 10% of the central coordinates could be described as being well outside the outline of the cluster boundary. This makes it quite conceivable that the massive protostars are being nurtured as part of an embedded cluster (Bonnell, Vines & Bates, 2004) whether that be through competitive accretion or accretion induced collisions of low mass members. In chapter 3, we also estimated the area, the effective radius and the volume of the 63 potential clusters. Their median is 0.5 pc in radii and they range from 0.2 to 2.5 pc, which is roughly equivalent to those in the embedded cluster catalogue of Lada and Lada, (2003). One potential problem with our estimation of the volume for hierarchical-form cluster is that for simplicity we summed the areas of the subcluster instead of dealing with them individually. We then calculated the volume from their effective radius and this may of made us grossly overestimate the volume for hierarchical form cluster. It would of been more proper to sum the individual volumes at the end.

In chapter 4, we looked at the clusters or groups with the use of near-infrared colour analysis. We use a technique of minimising the number of background stars by selecting only regions of higher than normal stellar density and form color-color diagrams of them from which we get an average extinction estimate for each cluster. We also make a first test look at the colours of massive protostars in the NIR. We use the Beut, MolII and MolIII studies to select a younger and older group. We plot these on color-color diagrams and the difference is quite striking. We also used made color-magnitude diagrams using a different selection technique than the color-color diagrams, where we choose both an inner (on) field and control (off) field. We subtracted these from each other to form contour color-magnitude diagrams in preparation for age estimation, although we didn't proceed far enough to obtain an actual age for any of the cluster.

We statistically estimate the number of members in each cluster using three methods. the first involves the counting of the stellar counts inside the boundary lines of the stellar contour maps assuming foreground contribution to be low and background stars to be shielded from view by the molecular cloud. And the second was equivalent to the first with background and foreground estimates subtracted. As we have a large number of new clusters, it wasn't feasible to make individual decisions which of the two numbers suited

each particular case. But as other authors have done (Carpenter et al., 1993) we argue an upper and lower band to the total number of members detected using the 2MASS telescopes. These number estimates should not be compared between different clusters of the same study as both the distance and extinction will effect the number of stars detected. Even the number estimates of the same cluster of different studies is precarious as the different telescopes have different seeing powers. To alleviate this, we extend the background subtracted number estimate to almost the deuterium burning limit by assuming a universal IMF from Muench et al., 2002. This allows us to have a total number estimate for the cluster, which is independent of the seeing power of the telescope or the distance or average extinction of the cluster. This number may be not be accurate but it is important as a first estimate to the total number of stars in a cluster and can be compared between different studies. By this number and definitions from Porras et al., (2003), 29 of the clusters should be classified as large clusters (over 100 members), 18 as small cluster (35 - 99 members) and the rest as stellar groups (5 - 34 members inclusively). We use these number estimates to calculate the number density per the area and volume of the cluster, although we may of underestimated some of the hierarchical-form clusters by an order of magnitude due to the already mentioned overestimation of the volume of subclusters.

Finally we estimate the total of 57 clusters/group as above by assuming a universal IMF of the Trapezium cluster and comparing stellar counts to generated KLFs (technique from LLO3) and stellar counts as a function of differing limiting magnitude, average extinction and distance to the cluster. The Beut paper measured the mass of the cloud for 15 of the sources and so this immediately gave us a Star formation efficiency which range from 5% to 45% with an average of 17%.

Just as a final remark, we were quite lucky to have chosen a rich sample (Sridharan, Beuther, Molinari et al.) which already had loads of nice work done on them. In many ways we were spoilt and perhaps we therefore didn't do the sample its full justice. This was part of a Masters, and was completely a learning curve throughout and we simply ran out of time towards the end. It probably noticeable where we intended to go next with it. Possibly we would of done more work into star formation efficiency and discussed its upper limits and it effect on the cut-off of Star formation processes. Also it would of been nice to obtain a numerical age estimation, even if it was poor it would of given us alot more power to discuss the relation of massive star formation and the ages of the clusters. Also the work needed to be far better gelled back into the original work, before one could conclude that it was in anyway complete. In short these sources require alot

more work and have the potential to tell us alot more about the topic and mechanism that lead to massive star formation.

Bibliography

- [1] Adams FC., Myers P., 2001 Ap.J 533:744-53
- [2] Altenhoff WJ., Downes D., Pauls T., Schrami J., 1978 A&AS 35,23
- [3] Baraffe I., Chabrier G., Allard F., Hauschidt PH., 1998 Astron. Astrophys, 337, 403
 412
- [4] Beuther H., Schilike P., Menten KM., Motte F., Sridharan TK., Wyrowski F. 2002 ApJ 566: 945-965
- [5] Beuther H., Schilke P., Gueth F., 2004, ApJ...608..330B
- [6] Bica, E., Bonatto, C., Dutra CM., 2003A&A...405...991B
- [7] Bica E., Dutra CM., Barbuy B., 2003 A&A 397, 177-180
- [8] Bica E., Dutra CM., Soares J., Barbuy B., 2003 A&A 404 223B
- [9] Bok, 1934 BHar 895...1B
- [10] Bonnell, IA., Bate, MR., Zinecker, H., 1998, MNAS, 298, 93-102
- [11] Bonnell IA., Vine SG., Bate MR., 2004, MNAS 349, 735-741
- [12] Bonnel, IA., Davies, MD., 1998 Astron. Soc. 295, 691-698(1998)
- [13] Blitz L., 1990, Star forming giant molecular clouds, in Bloemen J.B.G.M.(ed) The interstellar Disk-Halo Connection in Galaxies IAU Symp. 144, Klumwer Acad, Publ. Dordrecht(Nethl), p41
- [14] Brand, J., Blitz, L., 1993 A&A 275,67
- [15] Bressel MS., Brett JM., 1988 PASP, 100, 1134
- [16] Bronfman, L., Casassus, S., May, J., & Nyman, LA, 2000 A&A, 358,521
- [17] Bronfman, L., Nyman, LA., & May., J 1996, A&AS, 115, 81-95

- [18] Burrows A., Marley M., Hubbard WB., Lunine JI., Guillot T., Saumon D., Freedman R., Sudarsky D., Sharp C., 1997 ApJ 491..856B
- [19] Carpenter JM, Snell RL., Schloerb, FP., Skrutskie MF., 1993 ApJ 407:657-679
- [20] Capenter JM., Snell RL., Schloerb FP. 1995. Ap. J. 450:201-16
- [21] Carpenter JM., Meyer MR., Dougados C., Storm SE., Hillenbrand LA., 1997 AJ 114...198C
- [22] Cesaroni R., Olmi L., Walmsley CM., Churchwell E., Hofner P., 1994, ApJ, 435,137
- [23] Cesaroni R., Felci M., Testi L., Walmsley CM., Olmi L., 1997 A&A 325,725
- [24] Churchwell E., Walmsley CM., Cesaroni R., 1990 A&A 83,119
- [25] Chen H., Tafalla M., Greene TP., Myers PC., Wilner DJ., 1997 ApJ 475:163-172
- [26] Clarke CJ., Bonnell IA., Hillenbrand LA., 2000 prpl.conf.151C
- [27] Cohen M., 1973 MNRAS 164,395
- [28] D'Antona F., Mazzitelli I., 1994 ApJ 90:467-500
- [29] D'Antona F., Mazzitelli I., 1997 MmSAI..68..807D
- [30] Dutra CM., Bica E., 2000 A&A 359, L9
- [31] Elmegreen BG., 1993, AphJ 419:L29-L32
- [32] Elmegreen BG., 2002, ApJ 577,206E
- [33] Grasdalen G, Storm SE., Storm KM., 1973 Ap.J. Lett. 184:L53-57
- [34] Gregory PC., Condon JJ., 1991, ApJS, 75, 1011
- [35] Griffith, MR., Wright, AE., Burke, BF., Ekers RD., 1994, ApJS, 90, 179
- [36] Haynes, RF., Caswell, JL., Simons LWJ., 1979 AuJPA 48...1H
- [37] Herbig GH., 1962 AdA&A...1...47H
- [38] Hodapp K., 1994 ApJS 94: 615-649
- [39] Hodapp K., 1994 iaan.conf..406H
- [40] Horner DJ., Lada EA., Lada CJ., 1997 AJ 113: 1788-1798

- [41] Hunter T., Neugebauer G., Benford DJ., Matthews K., Lis DC., Serabyn E., Phillips TG. 1998, ApJ 493,L97
- [42] Jijina J., Myers PC., Adams FC., 1999 ApJS 125:161-236
- [43] Jones TJ., Hyland AR., 1980 MNRAS, 192, 359
- [44] Kumar Nanda MS., Ojha DK., Davis CJ., 2003 ApJ...598.1077K
- [45] Lada CJ, Adams FC., 1992 393, 278-288
- [46] Lada EA., Lada CJ., 1995 ApJ 109, 1682
- [47] Lada E., 1999, osps.conf.441L
- [48] Lada CJ., Lada, EA., 2003, ARA&A..41...57L
- [49] Lynga G., 1985 IAUS...106...143L
- [50] Marsalkova P., 1974 Ap&SS 27,3
- [51] Menton KM., Reid MJ., 1995 ApJ 445, L157
- [52] Meyer MR., Calvet N., Hillenbrand L., 1997, AJ, 114,288
- [53] Mezger PG., Smith LF., 1977 IAUS...75...133M
- [54] Migenes V., Horunchi S., Slysh VI., Val'tts IE., Golubev VV., Edwards PG., Fomelat EB., Okaysym R., Diamond PJ., Umnate T., Shibata KM., Inoue M., 1999 ApJSS 123:487-513
- [55] Miller GE., Scalo, JM., 1979, ApJS 41,513
- [56] Molinari, S., Brand, J. Cesaroni, R, & Palla, F, 1996, A&A 308: 573-587
- [57] Molinari, S.; Brand, J.; Cesaroni, R.; Palla, F.; Palumbo, G. G. C., 1998 A&A 336 339M
- [58] Molinari, S.; Brand, J.; Cesaroni, R.; Palla, F., 2000 A&A 335 617M
- [59] Molinari, S., Testi, L., Zhang, Q., 2002 ApJ 570:758-778
- [60] Muench AM., Lada EA., Lada CJ., & Alves JF., 2002 ApJ 573: 366-393
- [61] Muench AA., Lada EA., Lada CJ., Elston RJ., Alves JF., Horrobin M., Huard TH., Levine JL., Raines SN., Roman-Zuniga C., 2003, AJ...125.2029H

- [62] Palla F., Cesonaroni R., Brand J., Castelli F., Comoretto G., Felli M., 1991 A&A 280, 599
- [63] Palla F., Stahler SW., 1993 ApJ 418,414
- [64] Porras A., Christopher M., Allen L., DiFranceso J., Megeath ST., Myers PC., 2003 AJ...126.1916P
- [65] Ramesh B., Sridharan TK., 1997, MNRAS 284, 1001
- [66] Richards PJ., Little LT., Toriseva M., Heaton BD., 1987 MNRAS 228,43
- [67] Shepherd DS., Watson A., Sargent A., Churchwell, E., 1998, ApJ, 507, 861
- [68] Shu FH., Adams FC., 1987 TAUS..122....7
- [69] Soares JB., Bica E., A&A 2002 388 172-178
- [70] Spitizer L(Jr)., 1958 ApJ..127..17S
- [71] Sridharan TK., Beuther H., Schilke P., Menten KM., Wyrowski F., 2002, AphJ 566:931-944
- [72] Testi L., Palla F., Nata A., 1998, A&ASS 133, 81-121
- [73] Wright EA., Griffith MR., Burke BF., Ekers RD., 1994, ApJS, 91, 111
- [74] Wood DOS., Churchwell E., 1989, ApJ 340, 265
- [75] Wouterloot JGA., Brand J., 1989, A&AS 80,149(WB)
- [76] Yamaguchi R., Mizuno N., Onishi T., Mizuno A., Fukui Y., 2001 ApJ 553,185

Supplemental Figures

Figure 6.1: Extinciton Histograms of the 63 cluster sources

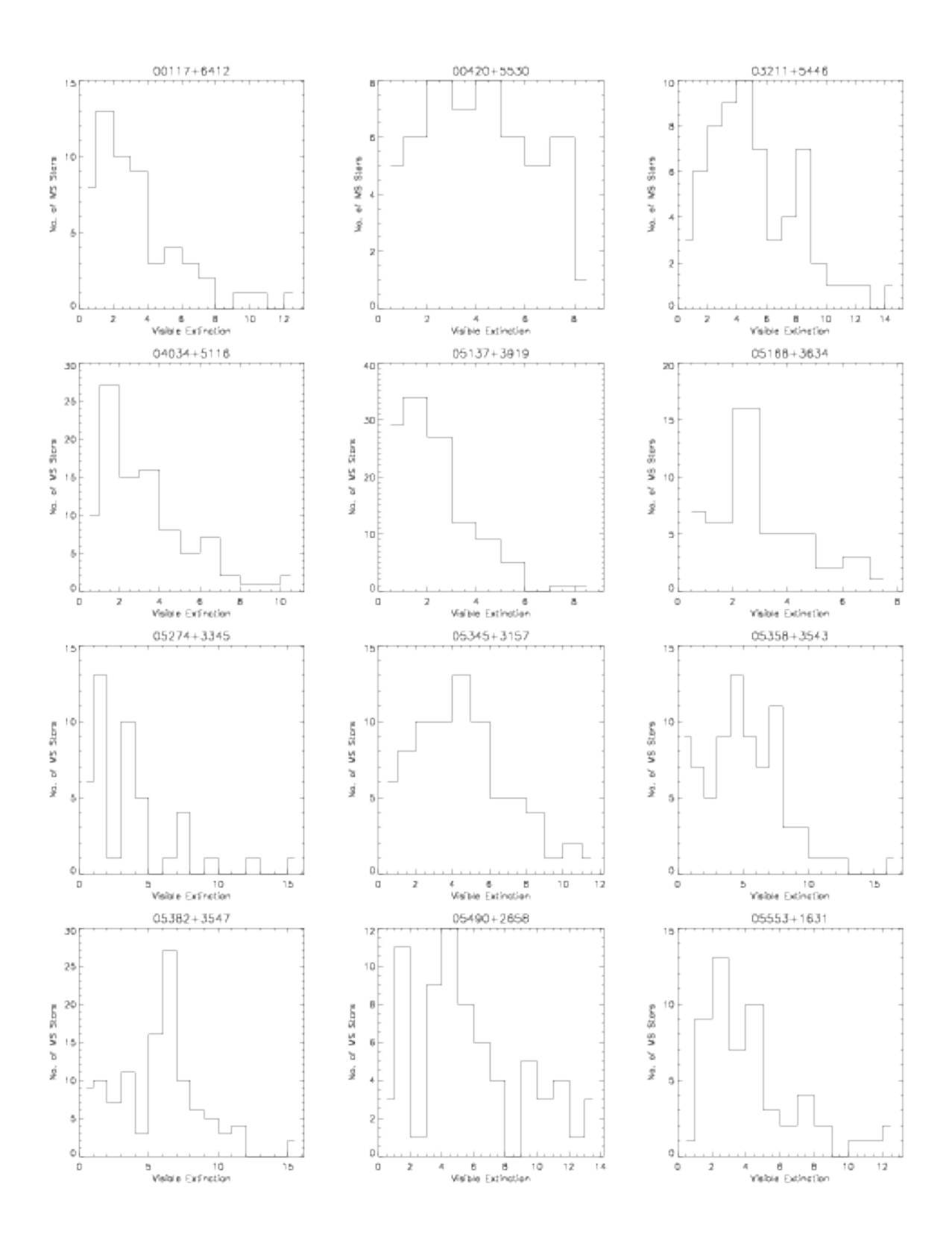


Figure 6.1: Extinction Histograms continued

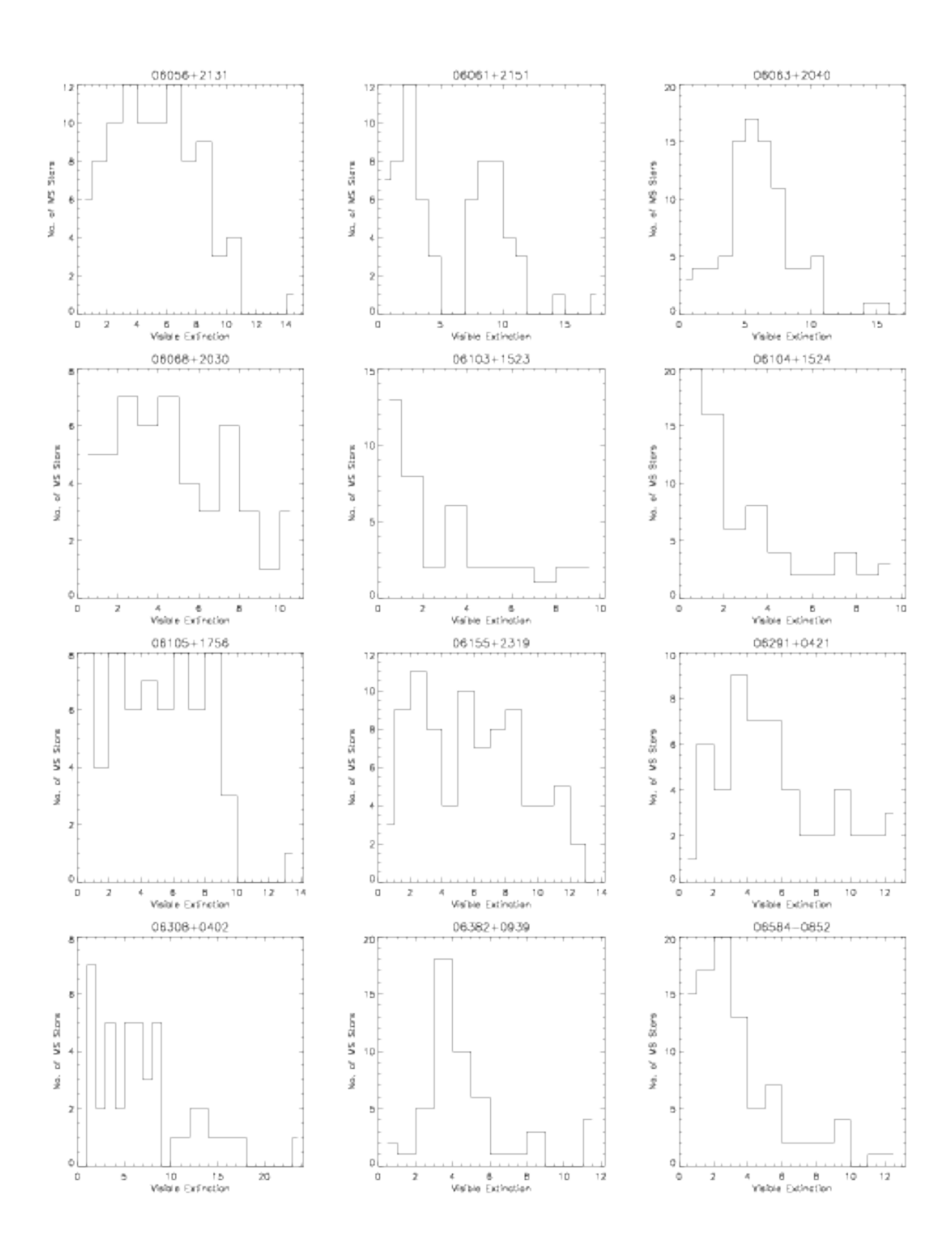


Figure 6.1: Extinction Histograms continued

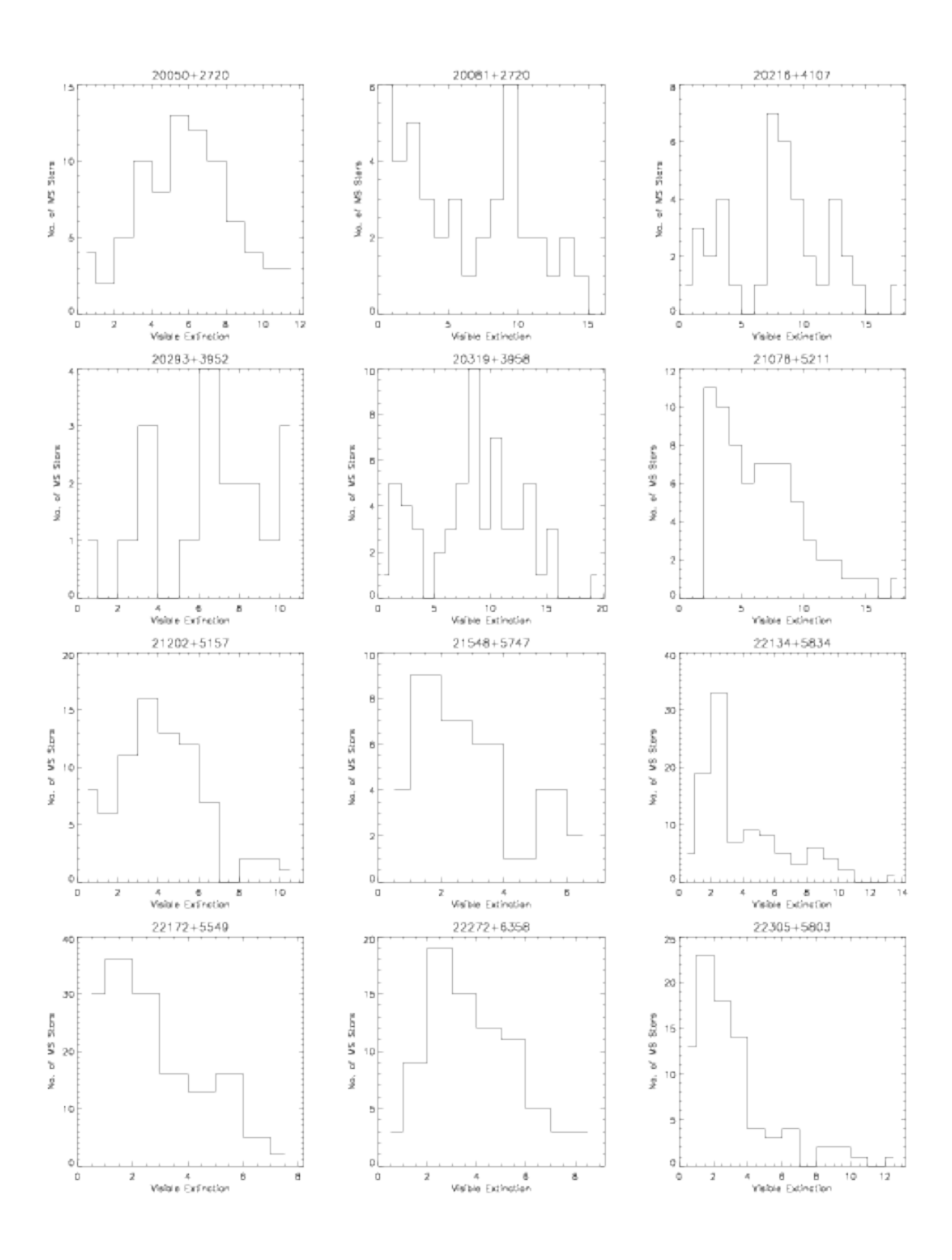


Figure 6.1: Extinction Histograms continued

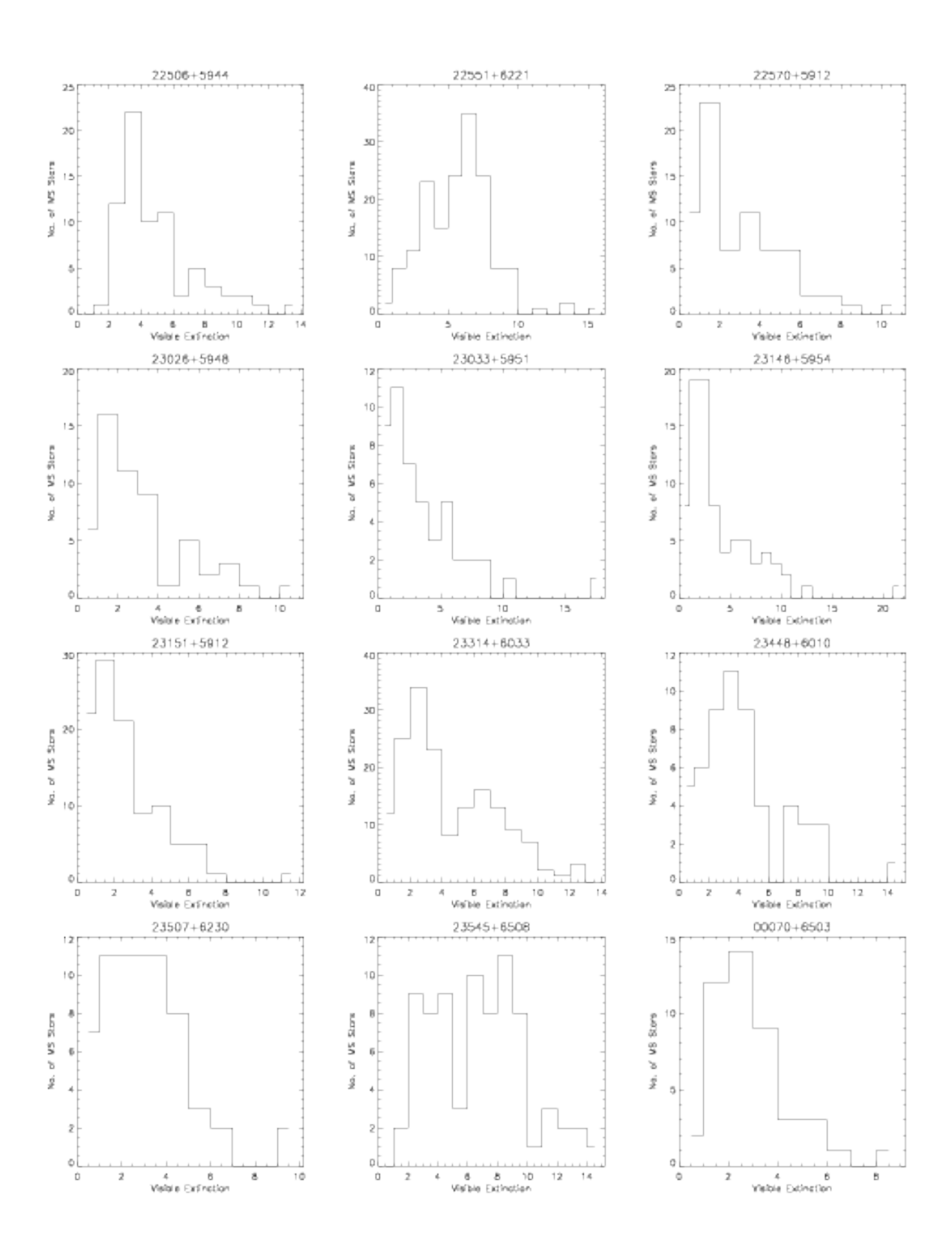
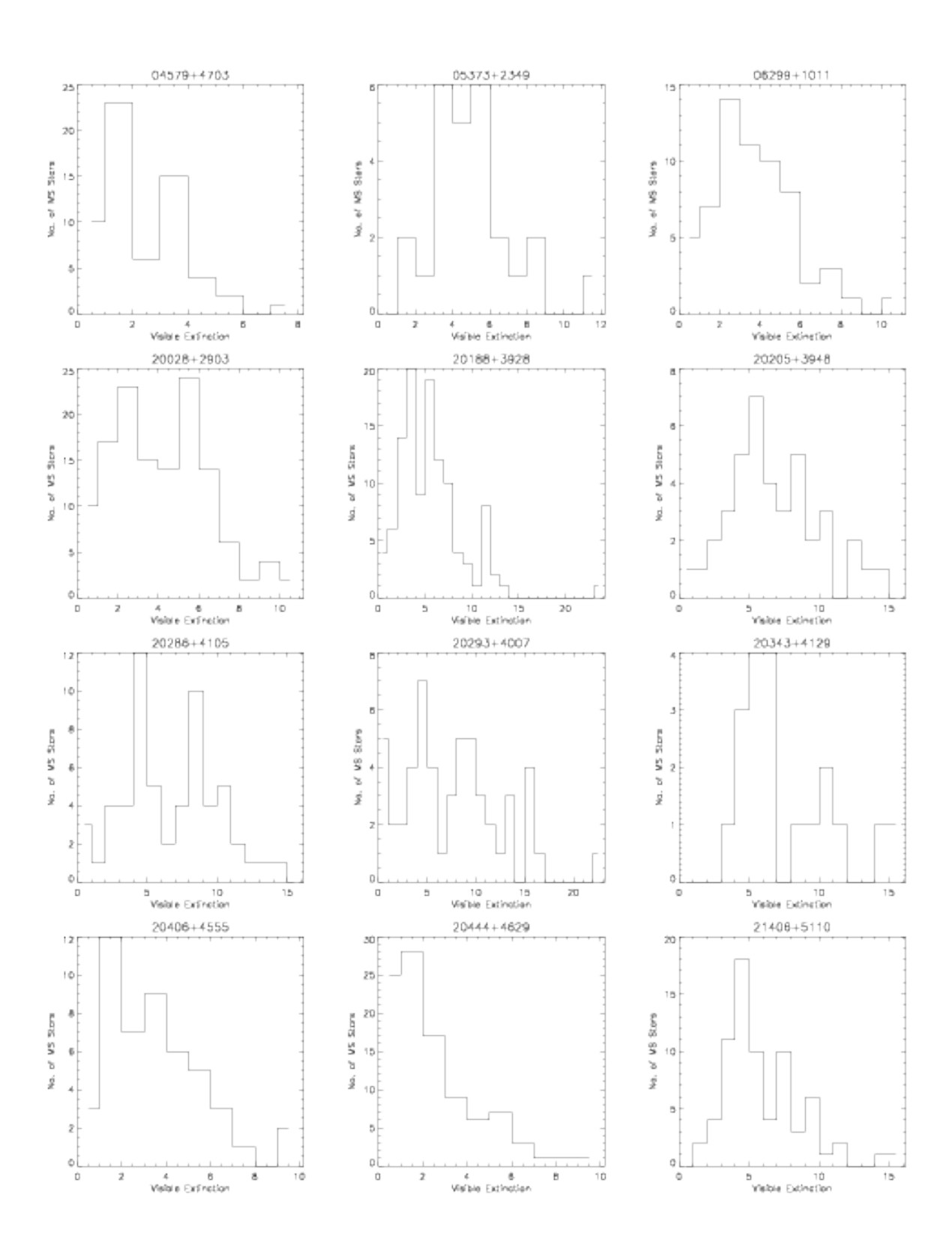


Figure 6.1: Extinction Histograms continued



Figure~6.1:~Extinction~Histograms~continued

